**TECHNISCHE UNIVERSITÄT MÜNCHEN**

TUM School of Life Sciences

# Mapping differences in C99 cleavage efficiency and specificity exhibited by presenilin 1 and presenilin 2 to structural subdomains

**Fabian Christopher Schmidt**

Vollständiger Abdruck der von der TUM School of Life Sciences der Technischen Universität München zur Erlangung des akademischen Grades eines

**Doktors der Naturwissenschaften (Dr. rer. nat.)**

genehmigten Dissertation.

**Vorsitzender:** apl. Prof. Dr. Michael W. Pfaffl

**Prüfer der Dissertation:**

1. Prof. Dr. Dieter Langosch
2. Prof. Dr. Harald Steiner

Die Dissertation wurde am 29.03.2022 bei der Technischen Universität München eingereicht und durch die TUM School of Life Sciences am 09.08.2022 angenommen.

# Zusammenfassung

Bei der Intramembranproteolyse von C99, dem carboxyterminalen Fragment des Amyloidvorläuferproteins (APP, engl. *amyloid precursor protein*), durch die γ-Sekretase, entsteht Amyloid β (Aβ), ein pathogenes Molekül, das bei der Entstehung der Alzheimer-Erkrankung beteiligt ist. Obwohl Fortschritte bezüglich der Strukturinformationen des Enzym-Komplexes und dessen schrittweiser Interaktion mit C99 gemacht wurden, konnte noch nicht eindeutig gezeigt werden, welche Regionen von Präsenilin (PS), der enzymatischen Untereinheit, hauptsächlich die Spalteffizienz oder –spezifität beeinflussen.

Im Rahmen dieser Arbeit wurde besonderes Augenmerk auf die beiden Homologe von PS (PS1 und PS2) gelegt, welche von menschlichen Zellen exprimiert werden. Unter Verwendung von Detergens-solubilisierter γ-Sekretase konnte eine höhere *in vitro* Spaltungseffizienz von PS1 bestätigt werden, welche zuvor kontrovers diskutiert wurde. Bei der Analyse chimärer PS-Varianten bestätigte die Quantifizierung von generierten Spaltprodukten, der intrazellulären Domäne von APP (AICD, engl. *APP intracellular domain*) oder Aβ–Peptiden, vorhergehende Studien, welche auf einen größeren Einfluss des PS1 N-terminalen Fragments (NTF) für die Spaltungsaktivität hindeuten. Die Ergebnisse dieser Arbeit zeigen zum ersten Mal, dass die membranumgebenen, hydrophoben Domänen maßgeblich zum höheren Substratumsatz von PS1 gegenüber PS2 beitragen. Auf dem Niveau einzelner Transmembrandomänen (TMDs) nehmen TMD6, TMD8, TMD9 und die Kombination aus TMD3 und TMD4 wesentlichen Einfluss auf die PS Spaltungseffizienz.

Des Weiteren konnten massenspektrometrische Analysen von immunoprezipitierten Spaltprodukten zeigen, dass die zuvor beschriebene geringere Aβ38 Produktion von PS2 mit einem gegenläufigen Anstieg von Aβ37 *in cellulo* und *in vitro* einhergeht. Außerdem konnte dargelegt werden, dass die PS-Homologe unterschiedliche Spezifitäten gegenüber der initialen Spaltstelle aufweisen, wobei im Fall von PS2 eine deutliche Verschiebung von AICDε48 zu AICDε51 erkennbar war. Da dies jedoch nicht die Unterschiede in Aβ37 und Aβ38 Produktion erklären kann, unterscheiden sich die beiden Homologe

zusätzlich in ihrer carboxyterminalen Prozessierung der Aβ-Peptide. Auch hier tragen die hydrophoben Domänen im PS NTF maßgeblich zur unterschiedlichen Prozessierung bei. TMD3 von PS agiert dabei als Hauptmodulator der initialen Spaltung, nimmt jedoch keinen Einfluss auf die anschließende schrittweise Prozessierung der Aβ-Peptide.

Insgesamt zeigen diese Daten potenziell wichtige Rollen einzelner PS Unterdomänen für die Spezifität und Effizienz der C99 Spaltung, welche zur Pathogenese der Alzheimer-Erkrankung beitragen können.

# Abstract

Intramembrane proteolysis of C99, the carboxy-terminal fragment of the amyloid precursor protein (APP), by γ-secretase generates amyloid β-peptide (Aβ), a pathogenic molecule in Alzheimer's disease. Despite recent progress on the structure of the enzyme complex and its stepwise interaction with C99, it remains largely unclear which regions of presenilin (PS), the enzymatic subunit, mainly determine cleavage efficiency and specificity.

In this study, we focused on the two homologs of PS (PS1 and PS2) that are present in human cells. Using a detergent-solubilized γ-secretase system, we confirmed the higher *in vitro* activity of PS1 which had been controversially discussed before. The investigation of chimeric PS1/PS2 molecules via quantitative analysis of the cleavage products APP intracellular domain (AICD) and Aβ on immunoblots, supported previous findings indicating a stronger influence of the PS1 N-terminal fragment (NTF) on the cleavage efficiency. Our results show, for the first time, that the membrane-embedded, hydrophobic domains account for the enhanced substrate turnover of PS1 relative to PS2. At a level of individual transmembrane domains (TMDs), the cleavage efficiency of PS is mainly determined by TMD6, TMD8, TMD9, and the combination of TMD3 and TMD4.

Mass spectrometric analysis of immunoprecipitated cleavage products revealed that the previously described lower Aβ38 generation by PS2 is accompanied by a reciprocal increase in Aβ37 production *in cellulo* and *in vitro*. Furthermore, we demonstrate that the PS homologs differ in their initial cleavage site specificity, with an apparent shift from AICDε48 to AICDε51 in case of PS2 compared to PS1. However, as these findings cannot explain the differences in Aβ37 and Aβ38 production, both homologs must also differ in their carboxy-terminal processing of Aβ peptides. After revealing the importance of the hydrophobic domains in the PS NTF for cleavage specificity, TMD3 was identified as a major modulator of initial cleavage, which however did not affect the subsequent carboxy-terminal trimming of Aβ peptides.

Collectively, these data reveal important roles of different PS subdomains for the

efficiency and specificity of C99 cleavage that can contribute to AD pathogenesis.

# Acknowledgements

I would like to thank Prof. Dr. Dieter Langosch for providing me the opportunity to carry out this project and write my doctoral thesis at the Chair of Biopolymer Chemistry. He supported and encouraged me throughout the entire project and helped me clear all hurdles, both formal and practical. By this, I was able to get an insight in the fascinating world of science and the interesting field of AD.

Special thanks to Prof. Dr. Harald Steiner for all the valuable input for my project and examination of my thesis. I would also like to thank Prof. Dr. Michael Pfaffl for being the chair of the examination committee and Prof. Dr. Matthias Feige who acted as my doctoral mentor.

Next, I thank Johannes Trambauer for answering any of my theoretical questions and for critical reading of my thesis. I also thank Gabriele Basset who patiently taught me everything about the finesses of protein analysis, as well as Lukas Feilen and Nadine Werner for the fruitful discussions and all the time they spent while waiting for me to acquire the optimal mass spectrometric data.

From our lab, I want to thank Elke Holzer for the harmonic working together as well as Philipp Heckmeier for revising sections of my thesis. The next big thanks go to Doreen Tetzlaff and my students, especially Katja Fitz, for their contribution to my projects. To all my other present and past colleagues (Philipp, Katja, Ayse, Julie, Martin, Christoph, Mark, Martina, Walter, Markus, Barbara, Alex, Johanna, and Yao): Thank you for the help and the nice atmosphere during my work at the chair. Working in science can be frustrating and stressful. Nevertheless, almost no day went by, where I did not want to come to work and that’s thanks to you.

Of course, I want to thank my parents and my sister. Throughout my studies and my PhD thesis you trusted in my skills and supported me without any doubts. Thank you for always having my back!

And finally, I would like to thank Theresa Pauli. You supported me a lot during the last months and took care of my well-being and of all the things at home, so I didn’t get distracted. Thank you for all the time you spent while listening to my theories and for critical reading of my thesis.

# Content

# 1 Introduction

## 1.1 The pathogenesis of Alzheimer's disease

Alzheimer's disease (AD) is the leading cause of dementia, accounting for approximately 55-75% of all cases [1, 2]. By now, AD and other clinical subtypes of dementia have become the seventh leading cause of death among all diseases worldwide. An explanation for the dramatic increase in the number of deaths are improved longevity and population growth, paired with an increase in the prevalence of risk factors [3]. In 2020, over 50 million people worldwide lived with dementia with estimations for future developments predicting an almost doubling of this number every 20 years [4].

The neuropathology of AD is defined by two cardinal lesions in the brains of patients, amyloid plaques and neurofibrillary tangles (Figure 1) [5].

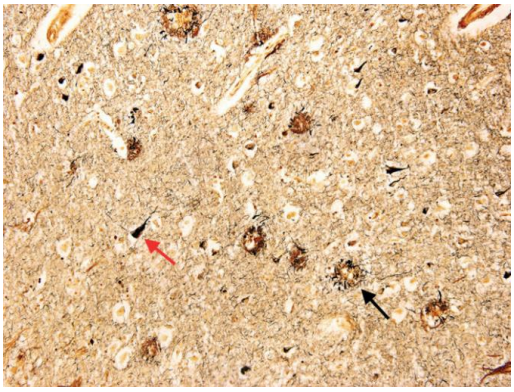

**Figure 1: Modified Bielschowski stain of the temporal cortex of a patient with AD**. The two cardinal lesions, neuritic plaques (black arrow) and neurofibrillary tangles (red arrow), are shown in numerous cases. (Image from [5]; license purchased from John Wiley and Sons).

These amyloid plaques (also called neuritic plaques) and neurofibrillary tangles have been first described by Alois Alzheimer when analyzing the brain of a patient with severe dementia [6]. By now, it has been shown that neurofibrillary tangles mainly consist of the microtubule associated tau protein. Under physiological conditions, tau stabilizes microtubules by crosslinking tubulin dimers via its microtubule-binding domains [7, 8]. In the neuropathology of AD patients, tau becomes hyperphosphorylated, dissociates from microtubules, and finally aggregates in neurofibrillary tangles [9, 10]. This reduces microtubule stability leading to defective microtubule assembly and axonal transport deficits in AD related disorders [11].

Amyloid plaques are formed by a central core of the 4 kDa Amyloid-β (Aβ) peptide, surrounded by disturbed neuronal processes or neurites [5]. While the phosphorylation of tau is believed to be important for its aggregation [12], Aβ can self-assemble during plaque formation. The plaques mainly exist in either diffuse or neuritic form in AD brains, with diffuse forms also being present in healthy subjects. In contrast to this, neuritic plaques are characteristic for the Alzheimer's pathology [13]. The 42 amino acid long Aβ42 was found to be the major component of the amyloid deposits [14]; however, also Aβ43 and other longer species are highly amyloidogenic [15]. Furthermore, different Aβ peptides, generated by the stepwise cleavage of the amyloid precursor protein (APP), can be found in plaques with length varying between 37-43 amino acids (Aβ37–Aβ43) [16-18].

## 1.2 APP and the amyloid hypothesis

### 1.2.1 The amyloid hypothesis

Due to the apparent importance for the development of AD, the role of Aβ peptides have been discussed in the context of the amyloid hypothesis over the last three decades. It focuses on Aβ accumulation as the cause of AD that triggers the other pathological processes like tau hyperphosphorylation, neuronal dysfunction, and selective neuronal loss [19, 20]. Being supported by an increasing number of studies, the hypothesis has developed into the central model of AD pathogenesis and is the basis for the development of potential therapeutics [21].

Numerous observations led to the formulation of the amyloid hypothesis or are supporting it to date. One of the first indicators was the discovery that the *APP* gene is located on chromosome 21 [22]. The recognition that duplications of the *APP* gene or the whole chromosome 21 in patients with trisomy 21 (Down syndrome) trigger the amyloid pathology and the development of AD-like symptoms [23-25] indicated a central role of Aβ accumulation in AD pathogenesis. In general, the progressive deposition of Aβ peptides is a common feature of AD that is followed by glial and neuritic cytopathology in brain regions

assigned to memory and cognition [21]. In contrast to sporadic AD (also called late-onset AD) which is mostly age-related, inherited mutations, so called familial AD (FAD) mutations, typically lead to an early-onset progression of AD. Strikingly, the majority of FAD forms are caused by mutations in either *APP* or gene loci encoding one of the Aβ-generating presenilin (PS) homologs (PS1 and PS2) [26-30], the catalytic subunits of the γ-secretase complex [31-36]. The strong association of these FAD mutations with Aβ generation suggests amyloid deposits as the main cause of AD. Besides this, apolipoprotein E (ApoE) is the main risk factor for the development of AD [37]. Human cells express three alleles of ApoE, ApoE ε2, ε3, and ε4, with ApoE ε4 being the major risk factor for AD [38]. Even though the exact effect mechanism of the different ApoE variants remain elusive, they presence of ApoE ε4 has been shown to correlate with a reduced Aβ clearance (ApoE ε4 < ApoE ε3 < ApoE ε2) [39]. As a consequence, humans expressing the ApoE ε4 variant develop more Aβ deposits and amyloid plaques compared to individuals expressing only ApoE ε3 [40].

With amyloid plaques and tau-containing neurofibrillary tangles being the most prominent neuropathological changes in AD brains, the question arose whether Aβ accumulation is a consequence of tau neuropathology or vice versa. Studies on patients with FAD mutations in the *APP* or *presenilin* (*PSEN*) genes reported Aβ deposition to precede the accumulation of tau-containing tangles [24, 41]. On the other hand, mutations in the gene encoding the tau protein lead to the development of frontotemporal dementia; however, without apparent deposition of Aβ [42, 43]. Hence, Aβ deposition can induce tau hyperphosphorylation and tangle formation, whereas tangle formation is insufficient for the amyloid plaque characteristic of AD. This strongly supports the amyloid hypothesis [44]. Besides tangle formation, the gradual deposition of Aβ42 is thought to induce microglial and astrocyte activation leading to neuroinflammation and oxidative injury [21]. Thus, while Aβ accumulation might initiate the pathological process, the main drivers of neurodegeneration may be the downstream processes like neuroinflammation and tau accumulation [45]. Even though many findings are in line with the amyloid hypothesis, a final prove for its correctness has not yet been shown.

Hence, alternative hypotheses have emerged, like the presenilin hypothesis which suggests a loss of γ-secretase function rather than increased Aβ42 production as the cause for developing AD [46]. Others indicate damages in the vascular system or an impaired glucose metabolism in the brain as the trigger of the disease [47]. Besides this, concerns with the amyloid hypothesis have been raised ever since. Among these are the observations that amyloid deposits also occur in non-demented brains; however, these studies have been shown to lack the distinction of neuritic and diffuse plaques [21]. In general, this and other concerns can be counter argued by an increasing number of evidence supporting the hypothesis [21, 44].

The interpretation of many findings is further complicated by the time scale of disease progression. During amyloid deposition, Aβ42 peptides accumulate earliest in the AD brain. However, the respective levels of free Aβ42 in the cerebrospinal fluid drop already 25 years before the onset of expected symptoms [41]. This demonstrates that once symptoms occur, the treatment options are limited. Thus, to counteract the development of AD, it is crucial to gain a better understanding of APP expression, cleavage and Aβ deposition.

### 1.2.2 The two pathways of APP processing

With Aβ-containing amyloid plaques being one of the hallmarks of AD, extensive research focused on the generation of Aβ peptides from its precursor APP. After expression from the human *APP* gene located on chromosome 21 [22], APP is synthesized in the endoplasmic reticulum (ER). The transmembrane protein with a type I topology contains a large extracellular domain, a transmembrane domain (TMD), and a cytosolic domain [48]. During its transport via the Golgi apparatus and the trans-Golgi network to the cell surface, post-translational modifications of APP include *N*- and *O*-linked glycosylation, ubiquitination, phosphorylation, and tyrosine sulfation [18, 49, 50]. Upon arrival at the plasma membrane, APP can be incorporated by endocytosis followed by either the delivery to endosomes or lysosomes, or its recycling back to the cell surface [18, 51]. By alternative splicing, APP isoforms of different lengths have been identified, with

$APP_{770}$, $APP_{751}$, and $APP_{695}$ being the major APP species. $APP_{695}$ is the predominant form present in the brain, while $APP_{770}$ and $APP_{751}$ are mostly found in non-neuronal cells [52, 53].

Processing of APP majorly occurs by two routes, the amyloidogenic and the non-amyloidogenic pathway (Figure 2). In the non-amyloidogenic pathway, APP gets cleaved by α-secretases within the Aβ region between the residues K16 and L17 (Aβ numbering). This results in the 83 amino acid long C-terminal fragment α (CTFα, also called C83) and the release of the soluble N-terminal fragment sAPPα (for "secreted APPα") [54, 55]. Several zinc metalloproteinases of the ADAM (for "a disintegrin and metalloproteinase") family can act as α-secretases with ADAM10 being most prominent in neurons [18, 56]. Subsequent cleavage of CTFα by γ-secretase releases the APP intracellular domain (AICD) and the extracellular p3, a truncated Aβ peptide that is pathologically irrelevant [57].

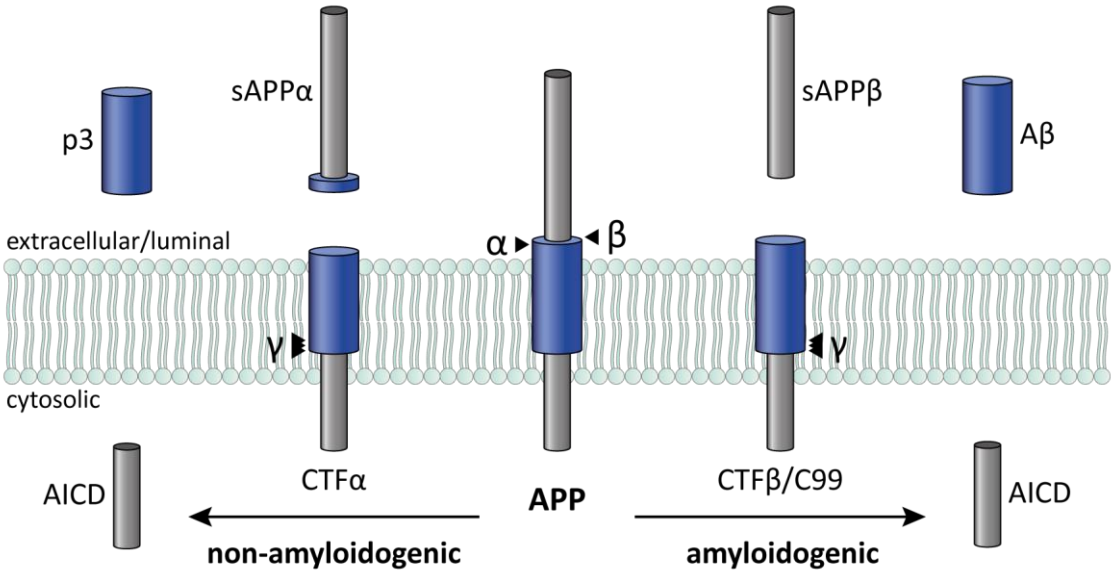


**Figure 2: The two pathways of APP processing.** The cleavage sites of α-, β-, and γ-secretases are exemplified by black arrowheads. In the non-amyloidogenic pathway (left), APP is cleaved by α-secretases within the Aβ region depicted in blue. The resulting sAPPα is released, whereas its counterpart CTFα is further processed by γ-secretase, leading to the generation of intracellular AICD and the extracellular p3 fragment that can be secreted. Cleavage at the β-site by BACE-1 releases the N-terminal sAPPβ in the amyloidogenic pathway (right). Sequential cleavage of the remaining CTFβ (also called C99) generates intracellular AICD and extracellular Aβ peptides of varying length.

On the other hand, APP can also be processed by the β-secretase BACE-1 (for "β-site APP cleaving enzyme-1") at the β-site in the amyloidogenic pathway (Figure 2). The active site of this membrane-bound aspartyl protease is located

in the extracellular space and cleaves APP before residue D1 (Aβ numbering, D672 of full length $APP_{770}$), generating sAPPβ and CTFβ (also called C99) [58-61]. While sAPPβ is released, CTFβ is further processed by the γ-secretase complex, generating 37-43 amino acid long secreted Aβ peptides (see also 1.4.3) [18, 62, 63]. Similar to γ-secretase cleavage of CTFα, intracellular AICD is also liberated from CTFβ. Even though AICDs are quickly degraded under physiological conditions [64], their involvement in cellular processes like nuclear signaling, transcriptional regulation or cell death has been described [65].

An alternative cleavage site of BACE-1, β', has been identified N-terminal of E11 (Aβ numbering). γ-Secretase cleavage of the resulting 89 amino acid long CTFβ' results in the formation of truncated $Aβ_{11-x}$ peptides that are not pathological [59]. While a whole set of proteases shows α-secretase activity [66], BACE-1 has been identified to be the sole β-secretase and its knock-out completely prevents Aβ generation [67, 68]. The shedding of APP by BACE-1 together with the consecutive processing by γ-secretase has been summarized under the term "regulated intramembrane proteolysis" [18, 69].

The amyloidogenic and the non-amyloidogenic pathway compete with each other [70, 71]; however, amyloidogenic processing seems to be predominant in neurons because of higher expression levels of BACE-1 in these cells. In contrast to this, non-amyloidogenic processing of APP is favored in all other cell types [18]. A recent study analyzed the expression levels of APP, BACE-1 and other complex partners during cortical neuronal differentiation of induced pluripotent stem cells (iPSC). Interestingly, APP and BACE-1 levels were significantly elevated in mature neurons compared to their progenitor cells [72]. Since β-site cleavage was proposed to be the rate limiting step in Aβ production [73], this marks major neurons as the primary source of Aβ peptides.

## 1.3 The γ-secretase complex

### 1.3.1 The four subunits of γ-secretase

The aspartyl protease that cleaves the APP-CTF within the membrane is γ-secretase [62]. Over the last three decades the four subunits PS, Nicastrin (NCT), APH-1 (for "anterior pharynx-defective phenotype"), and PEN-2 (for "presenilin enhancer") could be identified. Since no other stable complex partners were discovered in genetic screens [74] or purification of the γ-secretase complex [75-77], the four subunits build the core of the intramembrane protease. Being present in a 1:1:1:1 stoichiometry [78, 79] all four subunits have been shown to be required for γ-secretase activity [78, 80, 81].

The two human homologs of PS, PS1 and PS2, were the first subunits to be identified, when analysis of families with inherited forms of AD revealed mutations in the genes *PSEN1* (chromosome 14q24.3) [28, 82] and *PSEN2* (chromosome 1q42.2) [29, 30]. Later identified as the catalytic subunit of γ-secretase [31-35, 83], PS was thus marked as an important target for AD therapy. With a $N_{in}$-topology and containing nine TMDs [84, 85], PS contains two functional aspartic residues being located on TMD6 and TMD7 of the protein close to the cytosolic border [32, 83]. During complex maturation in the ER, the presenilins undergo autocatalytic endoproteolysis within the large cytosolic loop between TMD6 and TMD7 [32, 86, 87]. The resulting N-terminal fragment (NTF) and C-terminal fragment (CTF) remain in the complex as a heterodimer in a 1:1 stoichiometry [88].

The second complex partner NCT was identified by co-isolation experiments with PS [89]. The 130 kDa large type-I transmembrane protein consists of a single TMD and a large extracellular domain that becomes glycosylated during complex maturation [89-91]. After the formation of the complex in the ER the glycosylation of NCT is finalized after its transport to the Golgi [92, 93]. A small and a large lobe have been identified within the ectodomain of NCT that are considered to be involved in the substrate specificity of the γ-secretase complex. Important for this is the large lobe which is thought to act as a lid that can hinder large substrates to enter the enzyme complex [94, 95]. Recent computational studies identified F287 of NCT as a potential hinge between the two lobes that

enables movement of the large lobe [96]. Furthermore, NCT may act as a substrate receptor of active γ-secretase [97-99] and is important for the stability of PS [92].

With 12 kDa, PEN-2 is the smallest of the four subunits comprising three membrane-embedded domains, of which the first two traverse only half of the lipid bilayer [74, 100, 101]. After assembly of the subunits, PEN-2 regulates maturation of NCT and autoproteolysis of the PS subunit [81, 102, 103]. Furthermore, it is thought to regulate γ-secretase activity [104] and might exhibit a substrate-sorting function, as reported by computational studies comparing binding modes of different substrates and non-substrates [105].

APH-1 is a 30 kDa large, seven TMDs comprising subunit of γ-secretase [78, 80, 81, 106]. Similar to PS, two variants of APH-1, namely APH-1a and APH-1b, are expressed in human cells [107]. Concerning APH-1a, two splice variants are present in the human body, with the longer APH-1aL comprising 265 residues and APH-1aS consisting of 247 residues, respectively. All three variants can be incorporated into the γ-secretase complex; however, their expression varies depending on the cell type and differentiation state of the cells [72, 108, 109]. The choice of APH-1 variants might be directly connected to the development of AD, since some studies observed the generation of higher Aβ42/Aβ40 ratios for APH-1b-containing γ-secretase complexes than ones containing APH-1a [110-112]. However, other studies obtained contradictory results [113, 114]. Apart from this, the subunit influences the stability and trafficking of the γ-secretase complex as APH-1 depletion leads to impaired trafficking of NCT and decreased PS processing [81, 106, 115].

### 1.3.2 Assembly and maturation of the γ-secretase complex

Besides the identification of the individual γ-secretase complex partners, major progress has been made in understanding the interactions between the subunits during complex assembly. After translation, an initial ~140 kDa subcomplex of NCT and APH-1 is formed in the ER in a 1:1 stoichiometry [116], with multiple TMDs of APH-1 being involved in the interaction with NCT [117]. The NCT-

APH-1 complex subsequently binds to PS by interaction with the PS CTF [118-120]. PEN-2 binds to PS independently from the other two subunits via interaction with the conserved WNF motif located on TMD4 of PS [102, 121, 122]. This interaction has been shown to be highly stable [121-123]. Furthermore, the binding of PEN-2 is crucial for the stability of PS, since the unbound PS holoprotein is degraded quickly and PEN-2 mediates the PS endoproteolysis into the more stable PS heterodimer in the γ-secretase complex [74, 88, 124-126]. During translation, the ectodomain of NCT becomes rapidly *N*-glycosylated in the ER resulting in a ~110 kDa immature NCT form ($NCT_{im}$). While $NCT_{im}$ only shows a short half-life of <6 h, its stability increases after further glycosylation upon translocation to the Golgi, forming the highly stable mature NCT ($NCT_m$, ~130 kDa) [92, 127, 128]. Experiments with a mouse embryonic fibroblast (MEF) cell line lacking endogenous PS1 and PS2 expression have shown that the glycosylation of NCT is PS dependent [92, 129]. For this process the endoproteolysis of PS is not crucial; however, $NCT_m$ levels were increased when the PS is present in its heterodimeric form [102].

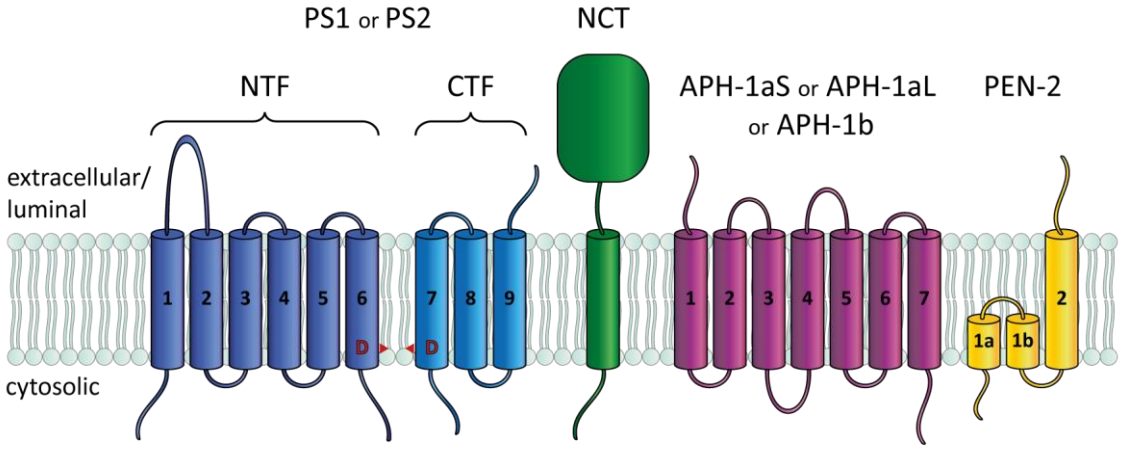


**Figure 3: Schematic representation of γ-secretase and its subunits.** PS1 and PS2 are depicted in blue as the heterodimer consisting of the NTF (dark blue) and CTF (light blue). The catalytic aspartates are displayed in red on TMD6 and TMD7, respectively. NCT is displayed in green, APH-1 in magenta, and PEN-2 in yellow.

Even though correct complex assembly and trafficking have been shown to be important for NCT maturation, it remains controversially discussed, whether a fully glycosylated NCT is necessary for γ-secretase activity, or if a less glycosylated state is sufficient [128, 130-133]. After the translocation of the γ-secretase complex to the Golgi and the subsequent completion of NCT-

glycosylation, the assembly and maturation of the complex is finished (Figure 3). Afterwards, γ-secretase is ready for being transported to other organelles of the cell.

### 1.3.3 The structure of γ-secretase

Given the hydrophobic environment of the membrane-spanning protease, resolving the structure of the protein has been challenging. Meanwhile, progress on the cryo-electron microscopy (cryo-EM) technology [134] mainly enabled the determination of high-resolution structures of large complexes. In parallel, structural information on single subunits became available, as seen for NCT [135] or a (stand-alone) archaeal PS homolog, PSH [136]. The first complete structure of γ-secretase was published in 2014. At a 4.5 Å resolution, the horseshoe-shaped architecture of the complex with a total of 19 resolved TMDs and the large NCT ectodomain was shown [137]. Follow-up studies by the same group could enhance the resolution first to 4.3 Å [101] and then to 3.4 Å [138]. These structures helped to assign the TMDs to the individual subunits and showed that the catalytic residues were located on the convex side of the horseshoe [101]. Furthermore, TMD2 of PS1 was added to the structure, which could not have been shown before due to its high mobility. With PEN-2 having three instead of the predicted two TMDs, the total number of TMDs in the enzyme complex increased to 20.

Using an image classification procedure, the authors later could identify three distinct conformations in their sample of the 3.4 Å structure [139]. In one of these, a so far unidentified rod-shaped density was observed close to TMD2 of PS1 that resembled the one of a transmembrane helix. Even though the analysis of co-purifying proteins revealed no previously known substrate, the observed density indicated where substrates might bind to the complex.

Most recently, two substrate-bound structures of γ-secretase, with either recombinant Notch [140] or APP [141], have become available. Based on the findings of the co-purified protein [139], the authors crosslinked the substrates to loop1 of a catalytically inactive PS1 (PS1 D385A). For both substrates, helix unwinding and extensions of substrate and enzyme TMDs accompanied the

substrate binding to the active site which revealed important insights for the complex mechanism of enzyme-substrate interaction [140, 141].

## 1.4 Substrate processing by γ-secretase

### 1.4.1 The substrate requirements of γ-secretase

Given the central role of γ-secretase and its substrates for the development of AD and other physiological processes [142], the underlying mechanisms of substrate recognition and cleavage is of fundamental importance. However, understanding substrate recognition and selectivity of γ-secretase remains challenging. In comparison to most soluble proteases, so far, no consensus motif or other reliable substrate markers could be identified by which the enzyme distinguishes between a substrate and a non-substrate. APP and Notch1 are the most prominent and intensely studied γ-secretase substrates. Besides this, around 150 substrates have been identified, to date, with relevant functions in embryonic development, adult tissue homeostasis, protein degradation, and signal transduction [143]. In general, γ-secretase cleavage usually generates an intracellular domain (ICD) which is released into the cytoplasm and short extracellular fragments that can be secreted from the cells. While for most of the cleavage products the physiological role remains to be determined, the ICD of some substrates was reported to translocate to the nucleus to modify gene transcription [144]. The ICD of Notch, being the best-understood example, is important for cell fate decisions and transcription regulation [145, 146]. Apart from that, the ICDs of CD44 and ErbB4 were shown to be involved in nuclear translocation, the regulation of signal transduction, and gene transcription [144].

Basic requirements for γ-secretase substrates are a type-1 transmembrane topology with only a short ectodomain [147]. Most substrate precursors contain a large ectodomain [143] that need to be cleaved off by sheddases, such as ADAM and BACE-1, prior to processing by γ-secretase [69]. The remaining ectodomains typically comprise 10-30 residues, whereby shorter lengths positively correlate with substrate cleavage efficiency [148, 149]. In agreement with this, substrates with naturally short ectodomains can be directly cleaved by

γ-secretase, as seen in case of the B-cell maturation antigen [147].

The high diversity of the substrates and the fact that multiple products are often generated during cleavage complicates prediction of novel, unidentified γ-secretase substrates. γ-Secretase has also been described to act with a "proteasome-like" activity within the membrane, by universally degrading remaining CTFs after ectodomain shedding [150]. The identification of substrate markers is also impeded by the fact that only few non-substrates have been identified so far. Among the few candidates for non-substrates are integrin β1 and telencephalin (TLN, also known as ICAM-5); both have been shown to interact with presenilin/γ-secretase without being cleaved [151, 152].

Besides these basic requirements, other determinants of substrate recognition and cleavage have been discussed. In case of C99 these include the flexibility of the substrate TMD [153, 154] and properties of the juxtamembrane regions [155, 156]. However, a set of markers reliably defining a γ-secretase substrate remains to be found.

### 1.4.2 Substrate recruitment and entry in case of C99

Intensive research was carried out to investigate the architecture of the γ-secretase complex, the substrate, or the interaction of both. In particular, the generation of Aβ peptides from APP was focused on as the central cause of AD (see 1.2.1). Thus, substrate binding and entry will be discussed below using the case of APP and its CTF C99 as an example.

Cryo-EM structures [139] revealed that the TMDs of γ-secretase adapt a horseshoe-shaped architecture in the membrane, with the active site being located at the external side (Figure 4). Crosslinking studies using the photocrosslinkable phenylalanine derivate Bpa (for "p-benzoyl-L-phenylalanine") at different positions of C99 identified substrate binding sites primarily on the PS NTF, but also on the PS CTF, NCT as well as PEN-2 [157]. The importance of PEN-2 and NCT for initial substrate recognition has also been proposed by other studies; however, the exact mechanism by which the interaction occurs remains a matter of debate [98, 99, 105, 158, 159]. The

observation that the initial binding site and active site are spatially distant [157, 160-162] led to a proposed multi-step model of C99 recruitment. In this model, the substrate initially binds to exosites on NCT and PEN-2, further translocates to the PS NTF, and finally enters the complex to arrive at the active site [26].

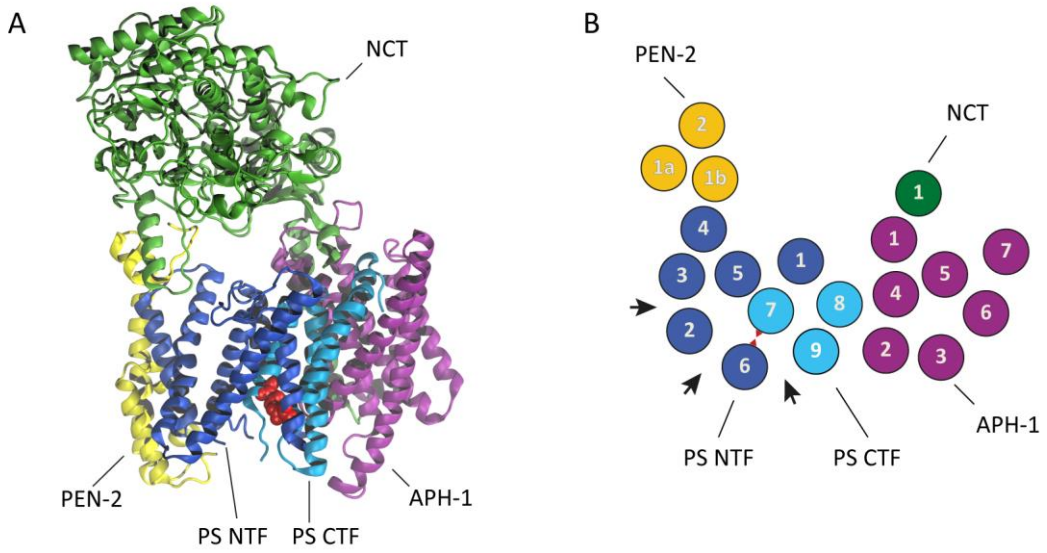


**Figure 4: The γ-secretase complex and putative substrate entry sites. A)** Structural model of mature γ-secretase containing the subunits NCT (green), PS NTF (dark blue), PS CTF (light blue), PEN-2 (yellow), and APH-1 (magenta). The catalytic aspartates on TMD6 and TMD7 are displayed in red (PDB 5FN3). **B)** Schematic top view on the horseshoe-shaped architecture of the γ-secretase complex. The catalytic aspartates are displayed by red arrowheads. Black arrows indicate putative substrate entry sites.

For PS1, initial substrate binding was shown to occur at the membrane/protein interface around TMD2, TMD6, and TMD9 [163-165] which are located on the same side of the horseshoe-shaped complex (Figure 4B). In particular the contribution of D450 of TMD9 to the formation of an initial binding site was previously reported [166] which is in line with observed salt bridge interactions between D450 and K28 of C99 during MD simulations [167]. Besides this, the process of substrate entry is still under debate. Entry sites between the TMDs 2 and 6 [26, 168-170] or TMDs 6 and 9 [136, 171] have been suggested. Furthermore, MD simulations analyzing different entry pathways recently hypothesized entry between TMD2 and TMD3 (Figure 4B) [165]. When testing different entry sites by pulling the substrate by an artificial force into the complex, the one between TMD2 and TMD3 was the only pathway by which the helix of C99 ended up in the substrate-binding cavity between TMDs 2, 3 and 5 that was identified by Shi and co-workers after solving the C83-bound γ-secretase structure (Figure 5) [141].

### 1.4.3 Substrate positioning, helical unwinding, and cleavage

Having entered the active site, C99 forms interactions with multiple TMDs of PS. Besides the catalytic aspartates-harboring TMD6 and TMD7 [32], also TMD2 [141], TMD3 [172], TMD4, TMD5 [173], and TMD9 [174] were reported to contribute to the formation of the active site of PS1. Contacts of the C-terminal part of APP at the active site include interactions with the highly conserved PAL motif located between TMD8 and TMD9 of PS [141, 174-176]. This interaction is critical as alterations of the PAL motif abolish γ-secretase activity [141, 176, 177]. Furthermore, the GxGD motif on TMD7 has been shown to be involved in substrate selection and cleavage [36, 178, 179].

The recent substrate-bound γ-secretase structure [141] gave new insights on enzyme-substrate interaction and helix unwinding within the active site. With the N-terminus of C83 being crosslinked to loop1, the substrate helix positions between TMD2 and TMD3. The binding mediated an extended conformation of the C-terminal end of the substrate helix that is accompanied by the formation of a β-strand (Figure 5). This β-strand interacts with the PAL motif of PS1 and forms an anti-parallel β-sheet with two induced β-strands on PS1 [141]. One of the β-strands, β1, is located C-terminal of TMD6 (residues 287-290), shortly before the endoproteolytic cleavage site of PS1 [87], while β2 starts N-terminal of TMD7 (residues 377-381) (Figure 5). Deletion of the PAL motif or the β1 and β2 forming residues led to impaired APP substrate cleavage [141]. Besides this, V44 of C99 was identified as one of the major interaction points involved in γ-secretase binding [157]. In the structure, this residue shows close interaction with W165 of PS1 TMD3 [26, 141], a domain whose importance in optimized substrate positioning has previously been hypothesized [172].

After substrate recognition and entry, γ-secretase mediated cleavage occurs close to the cytosolic border between the catalytic aspartic residues on TMD6 and TMD7 of PS [32, 83]. Importantly, initial endopeptidase cleavage of C99 does not occur at one specific site but rather in a cleavage region. This so called ε-cleavage happens predominantly after T48 or L49 of C99, generating Aβ48 or Aβ49 and releasing the intracellular AICDε48 or AICDε49, respectively [63, 180-185]. Also, initial cleavage at ε51 was observed to a minor extent [181, 186]. In

the C83-bound structure, β-sheet formation is accompanied by unwinding of the substrate helix at positions T48, L49, and V50, hence, facilitating the initial cleavage [141]. It is, however, worth mentioning that the structures have limitations due to the alanine substitution of one of the catalytic aspartates (D385A), the use of C83 instead of C99, as well as the restricted localization of the crosslinked substrates.

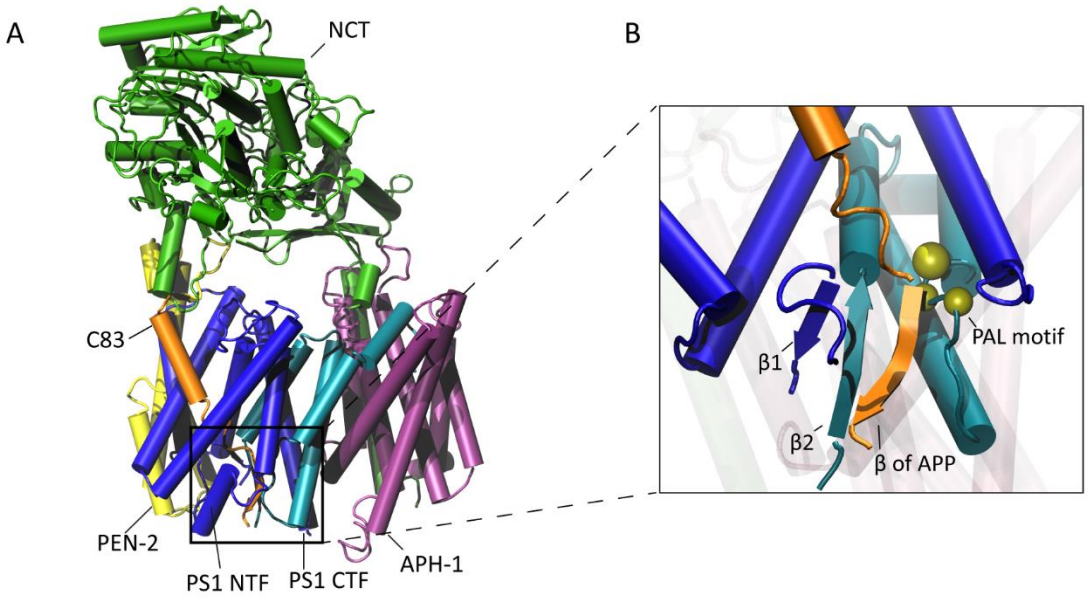


**Figure 5: Structure of the C83-bound γ-secretase complex. A)** Cartoon representation of the cryo-EM structure of γ-secretase with APP C83 at atomic resolution (PDB 6IYC). The four subunits are displayed: NCT (green), PS NTF (dark blue), PS CTF (light blue), PEN-2 (yellow), and APH-1 (magenta). The partially unwound substrate (orange) is located between TMD2, TMD3, TMD5, TMD6 and TMD7 of PS1. **B)** The close up shows the hybrid β-sheet formed by β1 and β2 of PS1 as well as the β-strand of APP, which also interacts with the PAL motif (yellow spheres).

After ε-cleavage, the resulting Aβ peptides undergo sequential exo-like proteolytic ζ- and γ-cleavage steps by γ-secretase in increments of three to four amino acids, which resembles approximately one turn of the α-helix [187]. The different ε-, ζ-, and γ-cleavage steps of C99 processing were reported to depend on the fit of substrate residues into postulated S1', S2', and S3' pockets at the active site of γ-secretase [165, 188]. Mutating the P2' position two amino acids upstream of the cleavage site of the substrate to a bulky, aromatic residue, prevents its positioning in the small S2' pocket and thereby altered or abolished substrate processing [188].

Two major processing pathways have been identified in C99 processing. The Aβ49 product line starts with Aβ49 and results in the predominant production of

Aβ40 and to some extent of Aβ37 (Aβ49 →Aβ46 →Aβ43 →Aβ40 →Aβ37). The second line starts at Aβ51 or Aβ48 (Aβ48 product line) and leads to the generation of Aβ42 and Aβ38 (Aβ51 →Aβ48 →Aβ45 →Aβ42 →Aβ38) (Figure 6) [63, 186]. It is worth mentioning that Aβ38 can originate from both product lines, either by the tetrapeptide release from Aβ42, or by pentapeptide cleavage from Aβ43. Other deviations from the tripeptide cleavage pattern include cleavage events leading to product line switching between the Aβ48 and Aβ49 lines (Figure 6) [63, 186, 189, 190].

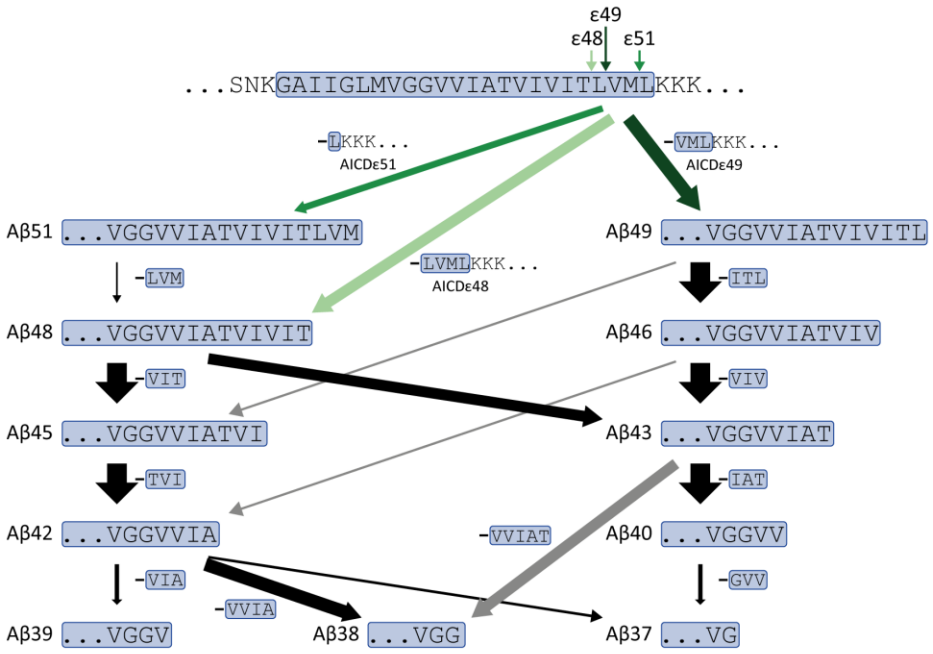


**Figure 6: Schematic overview of Aβ processing in the two major product lines.** ε-Cleavage of APP substrate TMD results in the generation of AICDε51 (green), AICDε49 (dark green), and AICDε48 (light green), as well as the associated counterparts Aβ51, Aβ49 and Aβ48, respectively. Stepwise Aβ processing is displayed in the two major pathways Aβ48 (left) and Aβ49 (right). Diagonal arrows represent cleavage events that do not follow the tripeptide-cleavage pattern and may lead to product line switching away from the Aβ48 line (black) or the Aβ49 line (grey). Aβ38 can originate from both product lines. Thickness of the arrows indicate the preference for the respective cleavage derived from MS data for Aβ [189].

In healthy human brains, Aβ40 is the most abundant species with Aβ42 being present only as a minor species. However, the aggregation prone Aβ42 is more neurotoxic, considered to be the main driver of AD, and the major form deposited in plaques [14, 187]. Since also most FAD mutations in the PS subunits and APP increase the Aβ42/Aβ40 ratio and thereby the risk of plaque formation [191], the prevention of Aβ42 production by changing the γ-secretase cleavage activity is a promising therapeutic target. Early studies on γ-secretase

inhibitors (GSI) showed promising results by reducing Aβ levels in cultured cells or in brains of mice [192]. However, longer treatments with GSI led to severe side effects in model organisms like *Drosophila* [193] and zebrafish [194]. Due to the lack of substrate specificity, the observed deficiencies in development and neurogenesis can be explained by inhibition of Notch signaling upon GSI treatment. Also, clinical trials on GSI were terminated before completion due to lack of efficiency or serious adverse events as seen for the inhibitors Semagacestat [195] or Avagacestat [196]. Therefore, recent approaches in AD therapy aim to modulate γ-secretase, such as to produce smaller Aβ peptides [197] without influencing processing of other substrates [45]. Even though these γ-secretase modulators (GSM) are thought to only influence the stepwise processing of APP after the initial cleavage [113, 198, 199], a potential impact of such compounds on ε-cleavage specificity has recently been reported, resulting in enhanced cleavage at position T48 at the expense of L49 [200]. A better understanding of how γ-secretase specifically interacts with C99 would be beneficial for manipulating its processing activity.

## 1.5 The catalytic homologs PS1 and PS2 – a detailed comparison

### 1.5.1 The localization of PS1 and PS2 and their contribution to AD

Extensive research has been conducted on the analysis of the homologous subunits PS1 and PS2. Comparing the two homologs is especially instructive, as it can give insights whether and how they interact differently with substrates during their specific roles in the cellular machinery and their contribution on AD progression. Furthermore, comparing subdomains within the homologs is highly interesting, with a view on the identification of their functional roles in the individual PS variant.

PS1 and PS2 were identified during the investigation of inherited forms of AD [28-30, 82]. Even though wildtype PS are present in >99% of the patients [21], analyzing inherited AD forms revealed the importance of PS for the disease. Most of the reported FAD mutations are located within *PSEN1* on chromosome 14, or within *PSEN2* on chromosome 1, with over 340 documented mutations in

*PSEN1* and over 80 in *PSEN2* [27]. However, FAD mutations within *PSEN2* demonstrate a smaller impact on AD neuropathology with the mean age of AD onset being over 10 years above that of *PSEN1* FAD mutations [201]. The exception from this is N141I, a FAD mutation of PS2, which leads to earlier mean onset of AD at 66 years and initially led to the discovery of this PS homolog [29].

The higher number of FAD mutations in *PSEN1* together with the earlier mean age of onset of disease indicates a higher importance of PS1-containing γ-secretase complexes for AD development compared to PS2. This also holds true for cellular homeostasis in general. While PS1-deficient mice show embryonic or perinatal mortality, most likely due to impaired Notch signaling [202, 203], PS2-deficiency revealed only very mild phenotypes in comparable mouse models [83, 204, 205]. Despite its seemingly lower impact, PS2 partly compensates absent PS1 activity, with PS2 mRNA upregulation being visible upon PS1 loss [72, 206-208].

The contribution of PS1 and PS2 on Aβ generation and cell differentiation depends on their distinct expression profiles. mRNA expression analysis during differentiation of iPSCs revealed that levels of PS1 gradually increased and were highest in mature neurons [72]. While NCT and APH-1b were expressed comparably at all states, PS2, APH-1a, PEN-2, BACE-1, and APP only showed high expression levels in mature neurons. This indicates that PS2 plays a minor role in cell differentiation and marks mature neurons rather than lesser differentiated cells as the most important source of Aβ production [72].

Functional differences of the PS homologs can possibly be explained by their subcellular localizations. While PS1-containing γ-secretase shows a broad distribution especially at the plasma membrane, complexes with PS2 are restricted to late endosomes (LE) and lysosomes (LYS) [72, 209, 210]. This PS2 localization has been shown to depend on its N-terminal $E_{16}RTSLM_{21}$ sorting motif [210]. Subcellular localization can influence the function of a γ-secretase complex. For example, the lipid compositions can alter γ-secretase activity in substrate processing [211-213]. Also, the lower pH of LE/LYS can influence C99 processing by reducing overall cleavage activity [214]. In addition to this, even though PS1 and PS2 probably exhibit overlapping substrate spectra [143], the

different subcellular localization of the homologs leads to the almost exclusive processing of co-localizing substrates. For example, the LE/LYS-localized premelanosome protein and tyrosine-related protein are barely cleaved by PS1, but mostly by PS2 [210]. On the other hand, N-cadherin is predominantly cleaved by PS1 as it is mainly found at the cell surface [72, 210].

The different localization of PS1 and PS2 also has implications on the processing of C99 and hence the development of AD. The pH of γ-secretase localization might affect Aβ generation, as a lower pH increases the Aβ42/Aβ40 ratio in case of PS1 [215]. However, even though PS1 and PS2 were reported to have the same pH optimum in studies with yeast microsomes [216], it remains to be shown whether lower pH values can also increase the Aβ42/Aβ40 ratios produced by PS2-containing γ-secretase complexes. With its cell surface localization, PS1 cleavage of C99 directly releases Aβ peptides in the extracellular milieu, where Aβ can aggregate in amyloid deposits. On the other hand, due to its localization in LE and LYS, PS2 is the main source of the intracellular Aβ pool [206, 210]. This is of importance as recent studies show that intracellular Aβ accumulation precedes the extracellular plaque formation and may be an early event in disease progression of AD [217, 218]. Hence, while most studies focused on PS1 as a main driver of AD, analysis of PS2 is gaining increasing attention more recently.

### 1.5.2 Structure and dynamics of the PS homologs

The γ-secretase structures resolved by cryo-EM have brought new insights on the architecture of the enzyme complex [138, 140, 141]. However, as these structures only represent snap shots of the molecule, molecular dynamics (MD) simulations [165, 172, 219, 220] as well as experimental studies (reviewed in [221]) were necessary to extend our knowledge on conformational dynamics of the different enzyme TMDs. In the past, these studies almost exclusively focused on PS1-containing γ-secretase complexes. Only recently, members of the Kepp group modelled the PS2 structure [222, 223] using the available PS1 cryo-EM

structures from 2015 [138, 139] as templates. This enabled the first comparison of the dynamics of PS1 and PS2.

During activation and acquisition of the active state, conformational rearrangements within PS1 occur in several TMDs of the NTF and the CTF [170, 219, 220]. For PS2, these changes were now shown to be mostly in line with the ones of PS1 [222, 223]. In both homologs, fast helix tilts of the TMDs 2, 3, 6, 7, and 9 control the distance between the catalytic aspartates. TMD6 and TMD7 show a two-state behavior in the different conformations of the proposed open, semi-open, and closed states of the enzyme. While a two-state behavior of TMD2 in PS1 is absent in PS2, the dynamic changes of TMD9 were more pronounced in PS2 compared to PS1 [222, 223]. As different TMD dynamics during the acquisition of the active state might change substrate binding, entry, or positioning, they might largely influence the activity of the homologs.

### 1.5.3 The catalytic homologs exhibit differences in substrate cleavage

The question of how different TMD dynamics affect the catalytic activity of the homologs and whether they differ in overall cleavage is still under debate. *In vitro* and *in cellulo* studies analyzing the total Aβ or AICD production as a measure of enzyme activity observed a higher proteolytic activity of PS1 compared to PS2 [112, 209, 224-227]. In contrast to this, others observed similar [206, 208] or even higher activity levels of PS2 [216], although the use of yeast microsomes in the latter study might complicate the interpretation of the data. While differences in expression levels, the *in cellulo* and *in vitro* setups, or the subcellular localization of γ-secretase might explain the different outcomes of the studies [72], the question remains whether PS1 and PS2 mediate different proteolytic activities. Besides the cleavage efficiency of the two homologs, their endo- and carboxypeptidase specificity has been a matter of discussion. Especially the production of the longer, more aggregation prone Aβ42 compared to Aβ40 by the individual γ-secretase complexes is a point of disagreement within the scientific community. The observation by some researchers that PS2 produces higher relative amounts of Aβ42 compared to PS1 [72, 228]

contradicts reports by others, showing similar Aβ42/Aβ40 ratios for PS1 and PS2 [209, 210]. In addition to this, PS2 shows a lower Aβ38 production compared to PS1 [112, 206]. Since these studies did not report a significant difference in ε-cleavage between the PS variants, a reduced carboxypeptidase activity in the Aβ48 product line was proposed for PS2, especially affecting the catalytic turnover of Aβ42 →Aβ38 [112].

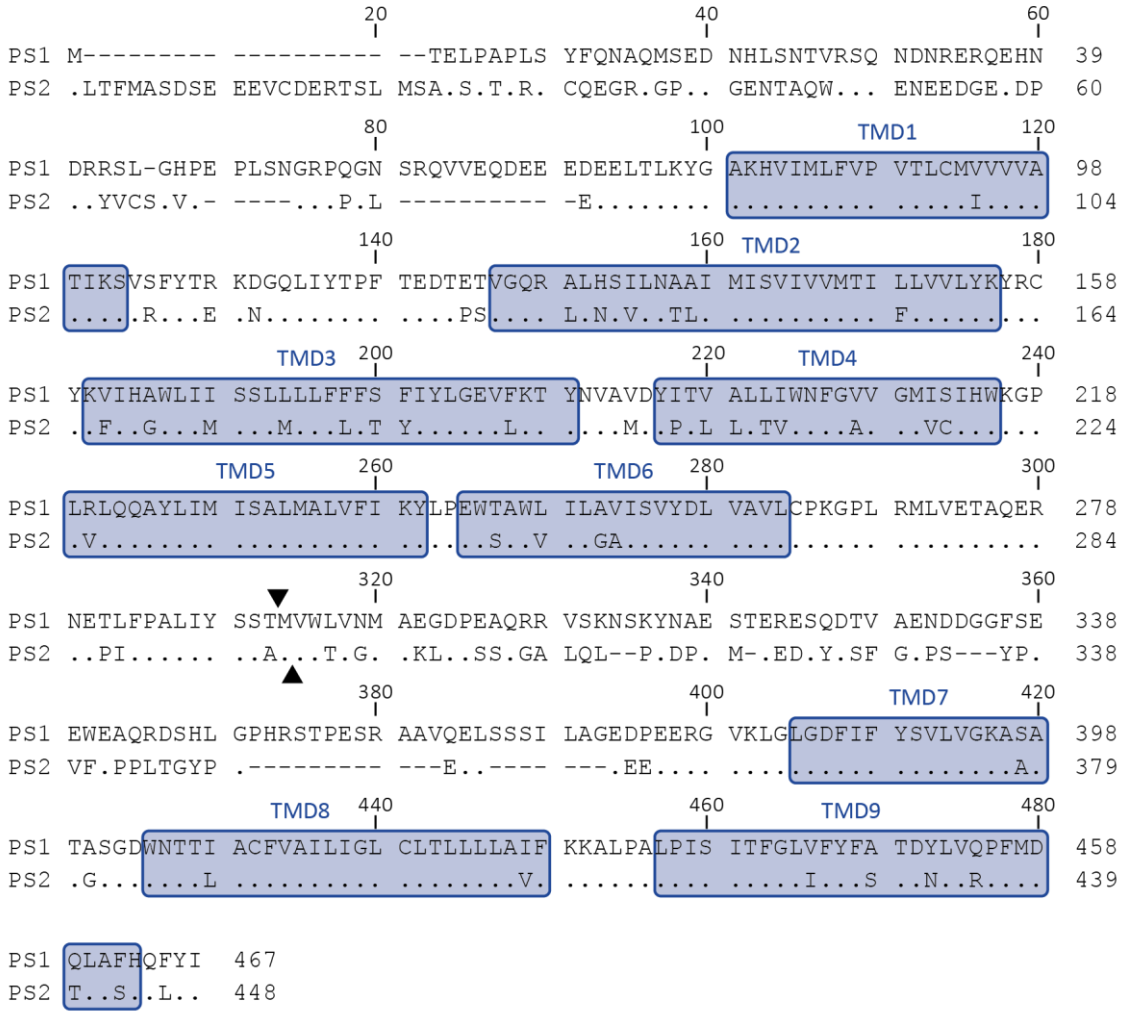


**Figure 7: Sequence alignment of PS1 and PS2.** The nine membrane-embedded TMDs are displayed in blue according to the cryo-EM structure of γ-secretase at atomic resolution (PDB 5FN3). Black arrowheads represent the endoproteolytic cleavage site between TMD6 and TMD7 for PS1 or PS2. Dots and dashes represent conserved residues or gap positions, respectively. Sequences originate from UniProt [229, 230].

The observation that PS1- and PS2-containing γ-secretase complexes can show differences in substrate processing raises the question of how the homologs achieve these differences and which PS subdomains are responsible for this. Both homologs share 67% identity at the amino acid level with the large hydrophilic loop between the TMDs 6 and 7 being the least conserved region

(Figure 7) [111]. Studies on chimeric PS constructs, containing either the PS1 NTF together with the PS2 CTF (PS1/2), or vice versa (PS2/1), demonstrated normal complex maturation and endoproteolysis of the PS variants [210, 226, 231]. Thus, chimeric PS constructs can be efficiently incorporated into the γ-secretase complex. Using a luciferase-based substrate cleavage assay, Strömberg *et al.* observed a higher *in cellulo* activity of PS1 compared to PS2. Testing their chimeric PS1/2 and PS2/1 constructs, the authors were able to show that the PS NTF was the main contributor to γ-secretase activity, however without statistical significance [226]. A smaller contribution could be assigned to the CTF, based on the rank order of cleavage efficiency (PS1 > PS1/2 > PS2/1 > PS2).

In line with the stronger impact of the NTF on substrate processing are observations from inhibitor tests with PS1 and PS2. Allosteric sulfonamide inhibitors, a class of GSIs, are 35x-51x more selective for PS1 compared to PS2 [231]. Using chimeric PS variants, the authors could identify two regions in the PS NTF (comprising TMD3 with its adjacent loop and the area C-terminal of TMD6, respectively) important for the binding of the inhibitors. This underlines the importance of the PS NTF in modulating substrate cleavage of C99. However, the mechanism by which the two homologs differ in their proteolytic activity could not be identified so far. PS1 and PS2 act differently upon application of GSI, GSM, or inverse GSM (iGSM) [200, 206, 207, 224, 232]. Hence, it is possible that PS1- or PS2-containing γ-secretase complexes differ in their regulation of substrate positioning and cleavage and therefore respond differently to inhibitors. Gaining a better understanding of how the two homologs differ and which parts of them mediate these differences is fundamental in understanding the complex machinery of substrate cleavage. The results might enable the development of PS1 and PS2 specific modulators.

# 2 Motivation

This study aimed to elucidate the functional roles of PS subdomains by systematically comparing the homologous subunits PS1 and PS2. Beside the wildtype homologs, a set of chimeric PS variants was designed and analyzed for differences in enzyme activity *in cellulo* and *in vitro*. As PS1 and PS2 had previously been shown to confer differences in the overall γ-secretase activity with a putative higher influence of the PS NTF, the first set of experiments aimed to analyze whether this can also be confirmed in a PS double knock-out (dKO) background or not. Further, partitioning the NTF and CTF into smaller non-conserved regions and single TMDs was envisioned to assess their contribution to the substrate turnover. Also, the impact of the membrane-embedded domains was to be compared to the one of the hydrophilic loops.

The second part of this study focused on investigating the specificity of substrate cleavage by the homologs. Most FAD mutations of PS show a shift in Aβ production towards longer, more aggregation prone variants like Aβ42 and Aβ43. Hence, it was envisioned that understanding which domains of PS can modulate cleavage site specificity is of fundamental importance. By analyzing cleavage products generated by chimeric PS variants *in cellulo* and *in vitro*, subdomains contributing to cleavage site specificity should be identified. Assigning the functional roles of these subdomains in cleavage efficiency and cleavage specificity was planned to expand our knowledge of γ-secretase function and to help identifying potential targets for future therapeutic treatments.

# 3 Materials and methods

All buffers and solutions were prepared using deionized water ($dH_2O$) (arium mini, Sartorius, Göttingen, Germany) if not stated differently. Detailed compositions are described in each relevant method section. Chemicals used for buffers were purchased from Sigma-Aldrich (St. Louis, MO, USA), Carl Roth (Karlsruhe, Germany), or AppliChem (Darmstadt, Germany) if not mentioned otherwise. DNA restriction enzymes came from Thermo Fisher Scientific (Waltham, MA, USA) or New England Biolabs (Ipswich, MA, USA). Consumable supplies for lab equipment were purchased from Thermo Fisher Scientific (Waltham, MA, USA) or Sarstedt (Nümbrecht, Germany).

## 3.1 Recombinant DNA techniques

### 3.1.1 Primers and template DNAs

Primers were purchased from Thermo Fisher Scientific (Synthesis scale: 25 nmole, desalted, dry) and resuspended at 100 µM with $dH_2O$ (Table 1, Table 2). Larger gene fragments were delivered by Twist Bioscience (San Francisco, CA, USA) cloned in the pTwistAmp cloning vector (Table 3).

**Table 1: Sequencing primers.**

| Primer | Name | Sequence |
|---|---|---|
| 938 | seqPrimer_PS1_TM2_fw | 5'-GAGCCCTGCACTCAATTCTG-3' |
| 939 | seqPrimer_PS2_TM2_fw | 5'-CCTCCTCAACTCCGTGCTG-3' |
| 944 | seqPS1_TM5_rev | 5'-TACTTGATAAACACCAGGG-3' |
| 945 | seqPS2_TM5_rev | 5'-GTACTTGATGAACACTAGGG-3' |
| 976 | seqPS1_TM5_fw | 5'-CCCTGGTGTTTATCAAGTA-3' |
| 977 | seqPS2_TM5_fw | 5'-CCCTAGTGTTCATCAAGTAC-3' |

**Table 2: Primers used for cloning.**

| Primer | Name | Sequence |
|---|---|---|
| 934 | PS2dTM3/4target_fw | 5'-AAGGGCCCTCTGGTGCTGCAGC-3' |
| 935 | PS2dTM3/4target_rev | 5'-GTAGCAGCGGTACTTGTAGAGCACCACCAAG-3' |
| 936 | PS2dTM3/4ins_fw | 5'-CTACAAGTACCGCTGCTACAAGGTCATCCATGCCTGGC-3' |
| 937 | PS2dTM3/4ins_rev | 5'-GCACCAGAGGGCCCTTCCAGTGAATGGAAATCATTCCC-3' |
| 1019 | PS1dTM7-9_insert_rev | 5'-CTCGAGGCAAATATGTCAGATGTAGAGCTGATGGGAGG-3' |
| 1020 | PS1dTM7-9_target_fw | 5'-CATATTTGCCTCGAGTCTAGAGGGC-3' |
| 1022 | PS2dTM1_2_insert_fw | 5'-CGATAAGGTACCAGGATCCATGACAGAGTTACCTGCACCGT-3' |
| 1023 | PS2dTM1_2_insert_rev | 5'-GCCATGGATGAACTTATAGCACCTGTATTTATACAGAACC-3' |
| 1024 | PS2dTM1_2_target_fw | 5'-AAGTTCATCCATGGCTGGTTGATC-3' |
| 1025 | PS2dTM1_2_target_rev | 5'-GGATCCTGGTACCTTATCGTC-3' |
| 1026 | PS2dTM2_target_rev | 5'-AGACTTGATGGTGGCTACCACC-3' |
| 1027 | PS2dTM2_insert_fw | 5'-GCCACCATCAAGTCTGTCAGCTTTTATACCCGGAAGG-3' |
| 1028 | PS2dTM6_insert_fw | 5'-GTGTTCATCAAGTACCTCCCTGAATGGACTGCG-3' |
| 1029 | PS2dTM6_target_rev | 5'-GTACTTGATGAACACTAGGGC-3' |
| 1033 | PS2dTM7-9_insert_rev | 5'-CCCTCTAGACTCGAGCTAGATATAAAATTGATGGAATG-3' |
| 1034 | PS2dTM7-9_target_fw | 5'-CTCGAGTCTAGAGGGCCCGTTT-3' |
| 1036 | PS2dTM9_target_rev | 5'-GAACACAGCAAGCAGCAGGAGG-3' |
| 1037 | PS2dTM9_insert_fw | 5'-GCTGCTTGCTGTGTTCAAGAAAGCATTGCCAGC-3' |
| 1038 | PS1dTM7-9n_insert_fw | 5'-CATTTACTCCTCAACAGTGTGGACGGTTGGCATGG-3' |
| 1039 | PS1dTM7-9neu_target_rev | 5'-TGTTGAGGAGTAAATGAGAGCTGG-3' |
| 1040 | PS2dTM7-9neu_insert_fw | 5'-CTCATCTGCCATGATGGTGTGGTTGGTGAATATGGC-3' |
| 1042 | PS2dTM7-9n_target_rev2 | 5'-CATGGCAGATGAGTATATCAGGGC-3' |
| 1063 | PS2dTM3_ins_rev | 5'-GCAAGAGGGTGGGGTAGTCCACAGCAACG-3' |
| 1064 | PS2dTM3_tar_fw | 5'-TACCCCACCCTCTTGCTGACTGTCTG-3' |
| 1065 | PS2dTM4_ins_fw | 5'-GGGAAGTGCTCAAGACCTACAACGTTGCTGTGG-3' |
| 1066 | PS2dTM4_tar_rev | 5'-GTAGGTCTTGAGCACTTCCCCAAGG-3' |
| 1067 | PS2dTM67_ins_rev | 5'-CCAGCGTGGTATTCCAGTCTCCACTGG-3' |
| 1068 | PS2dTM67_tar_fw | 5'-TGGAATACCACGCTGG-3' |
| 1069 | PS2dTM5_V226R_fw | 5'-GCCCTCTGAGGCTGCAGC-3' |
| 1070 | PS2dTM5_V226R_rev | 5'-GCTGCAGCCTCAGAGGGC-3' |
| 1085 | PS2TM8_L389I_fw | 5'-GGAATACCACGATCGCCTGC-3' |
| 1086 | PS2TM8_L389I_rev | 5'-GCAGGCGATCGTGGTATTCC-3' |
| 1087 | PS2TM8_V408I_fw | 5'-GCTGCTTGCTATCTTCAAGAAGG-3' |
| 1088 | PS2TM8_V408I_rev | 5'-CCTTCTTGAAGATAGCAAGCAGC-3' |
| 1091 | PS2_HindIIImut_fw | 5'-CGTTTAAACTTAAGCTCACCATGG-3' |
| 1092 | PS2_HindIIImut_rev | 5'-CCATGGTGAGCTTAAGTTTAAACG-3' |
| 1053 | PS2dTM6_ins_rev_n | 5'-GCCAACCGTCCACACTGTTGAGGAGTAAATGAG-3' |
| 1054 | PS2dTM6_target_fwd_n | 5'-GTGTGGACGGTTGGCATG-3' |

**Table 3: cDNA constructs purchased in the pTwistAmp cloning vector.**

| Name | Sequence |
|---|---|
| Twist_PS2_NTF_PS1 TMDpart | 5'-GCGGCCGCCAGGCCTGGAGGAAGAGCTGACCCTCAAATACGG AGCCAAGCATGTGATCATGCTCTTTGTCCCTGTGACTCTCTGCATG GTGGTGGTCGTGGCTACCATTAAGTCAGTGCGCTTCTACACAGAG AAGAATGGACAGCTCATCTACACGCCATTCACTGAGGACACACCC TCGGTGGGCCAGAGAGCCCTGCACTCAATTCTGAATGCTGCCATC ATGATCAGTGTCATTGTTGTCATGACTATCCTCCTGGTGGTTCTGT ATAAATACCGCTGCTACAAGGTCATCCATGCCTGGCTTATTATATC ATCTCTATTGTTGCTGTTCTTTTTTCATTCATTTACTTGGGGGAAGT GTTTAAAACCTATAATGTGGCCATGGACTACATTACTGTTGCACTC CTGATCTGGAATTTTGGTGTGGTGGGAATGATTTCCATTCACTGGA AGGGCCCTCTTCGACTCCAGCAGGCATATCTCATTATGATTAGTG CCCTCATGGCCCTGGTGTTTATCAAGTACCTCCCAGAATGGACTG CGTGGCTCATCTTGGCTGTGATTTCAGTATATGATTTAGTGGCTGT TTTGTGTCCCAAAGGGCCTCTGAGAATGCTGGTAGAAACTGCCCA GGAGAGAAATGAGCCCATATTCCCTGCCCTGATATACTCATCTGC CATGGTGTGGACGGTTGGCATGGCGAAGCTGGACCCCTCCTCTC AGGGTGCCCTCCAGCTCCCCTACGACCCGGAGATGGAAGACTCC TATGACAGTTTTGGGGAGCCTTCATACCCCGAAGTCTTTGAGCCT CCCTTGACTGGCTACCCAGGGGAGGAGCTGGAGGAAGAGGAGG AAAGGGGCGTGAAGCTT-3' |
| Twist_PS2_CTF_PS1 TMDpart | 5'-GAGGAGGAAAGGGGCGTGAAGCTTGGCTTGGGAGATTTCATTT TCTACAGTGTTCTGGTTGGTAAAGCCTCAGCAACGGGCAGCGGG GACTGGAACACAACCATAGCCTGTTTCGTAGCCATATTAATTGGTT TGTGCCTTACATTATTACTCCTTGCCATTTTCAAGAAGGCGCTGCC CGCCCTTCCAATCTCCATCACCTTTGGGCTTGTTTTCTACTTTGCC ACAGATTATCTTGTACAGCCTTTTATGGACCAATTAGCATTCCATCA GCTCTACATCTGACTCGAGTCTAGAGGG-3' |

### 3.1.2 Construct design of chimeric PS variants

All PS variants were based on the human wildtype PS1 and PS2. cDNA sequences of the homologs were obtained from UniProt choosing the respective human isoform 1 [229, 230]. For the chimeric PS variants, TMD substitutions almost exclusively included the neighboring loop region (Table 4). Exceptions from this are the PS2-All-PS1TMDs, PS2-NTF-PS1TMDs, and the PS2-CTF-PS1TMDs constructs. Also, the PS2ρTM8 construct still contained the G381 of PS2 instead of the respective A400 of PS1 in the loop between TMD7 and TMD8.

**Table 4: List of PS constructs.**

| PS variant | Origin of fragments |
|---|---|
| PS1 | 1-467 (PS1) |
| PS2 | 1-448 (PS2) |
| PS2ρTM2 | 1-108 (PS2), 103-159 (PS1), 166-448 (PS2) |
| PS2ρTM3 | 1-161 (PS2), 156-194 (PS1), 201-448 (PS2) |
| PS2ρTM4 | 1-195 (PS2), 190-218 (PS1), 225-448 (PS2) |
| PS2ρTM5 | 1-221 (PS2), 216-242 (PS1), 249-448 (PS2) |
| PS2ρTM6 | 1-246 (PS2), 241-291 (PS1), 299-448 (PS2) |
| PS2ρTM8 | 1-384 (PS2), 404-434 (PS1), 416-448 (PS2 |
| PS2ρTM9 | 1-409 (PS2), 429-467 (PS1) |
| PS2ρTM1-2 | 1-159 (PS1), 166-448 (PS2) |
| PS2ρTM3-4 | 1-161 (PS2), 156-218 (PS1), 225-448 (PS2) |
| PS2ρTM4-5 | 1-195 (PS2), 190-242(PS1), 249-448 (PS2) |
| PS2ρTM5-6 | 1-221 (PS2), 216-291 (PS1), 299-448 (PS2) |
| PS2ρTM6-7 | 1-246 (PS2), 241-403 (PS1), 385-448 (PS2) |
| PS2ρTM1-4 | 1-218 (PS1), 225-448 (PS2) |
| PS2ρTM3-6 | 1-161 (PS2), 156-291 (PS1), 299-448 (PS2) |
| PS2ρTM2/6 | 1-108 (PS2), 103-159 (PS1), 166-246 (PS2), 241-291 (PS1), 299-448 (PS2) |
| PS2ρTM6/9 | 1-246 (PS2), 241-291 (PS1), 299-409 (PS2); 429-467 (PS1) |
| PS2ρTM2/6/9 | 1-108 (PS2), 103-159 (PS1), 166-246 (PS2), 241-291 (PS1), 299-409 (PS2), 429-467 (PS1) |
| PS1/2 | 1-291 (PS1), 299-448 (PS2) |
| PS2/1 | 1-298 (PS2), 292-467 (PS1) |
| PS2-All-PS1TMDs | 1-84 (PS2), 79-105 (PS1), 109-130 (PS2), 125-155 (PS1), 162-165 (PS2), 160-189 (PS1), 196-200 (PS2), 195-215 (PS1), 222-224 (PS2), 219-240 (PS1), 247-248 (PS2), 243-252 (PS1), 259-363 (PS2), 383-398 (PS1), 380-384 (PS2), 404-428 (PS1), 410-415 (PS2), 435-463 (PS1), 445-448 (PS2) |
| PS2-NTF-PS1TMDs | 1-84 (PS2), 79-105 (PS1), 109-130 (PS2), 125-155 (PS1), 162-165 (PS2), 160-189 (PS1), 196-200 (PS2), 195-215 (PS1), 222-224 (PS2), 219-240 (PS1), 247-248 (PS2), 243-252 (PS1), 259-448 (PS2) |
| PS2-CTF-PS1TMDs | 1-363 (PS2), 383-398 (PS1), 380-384 (PS2), 404-428 (PS1), 410-415 (PS2), 435-463 (PS1), 445-448 (PS2) |

For each chimeric PS variant, the origin of the arrayed fragments is presented as the respective amino acid positions of PS1 or PS2. Annotations of membrane-spanning and hydrophilic domains of PS1 were obtained from the cryo-EM structure of γ-secretase at atomic resolution (PDB 5FN3). In accordance with that the domains of PS2 were annotated after sequence alignment of PS1 and PS2 (Figure 7).

### 3.1.3 Polymerase chain reaction

Polymerase chain reaction (PCR) was used to amplify cDNA fragments for cloning purposes like Gibson Assembly or QuikChange mutagenesis. Phusion High-fidelity DNA Polymerase (New England Biolabs) was used in all reactions. Due to the high GC content of the target sequences, the supplied GC buffer was chosen. Primers were designed with melting temperatures between 50°C and 70°C, preferably ending with G or C (Table 2). Annealing temperatures of each reaction were adjusted with respect to the applied primers.

| **Cloning PCR** | |
|---|---|
| Phusion GC buffer (5x) | 10 µL |
| dNTPs (10 mM) | 1 µL |
| DNA template | 10 ng |
| Forward primer (10 µM) | 2.5 µL |
| Reverse primer (10 µM) | 2.5 µL |
| Phusion polymerase (2 U) | 1 µL |
| $dH_2O$ | Add to 50 µL |

| **Amplification process** | | |
|---|---|---|
| 30 s | 98°C | |
| 10 s | 98°C | |
| 30 s | 60°C | 35x |
| 30 s/kb | 72°C | |
| 8 min | 72°C | |
| ∞ | 4°C | |

### 3.1.4 Cloning strategy for the individual PS variants

The constructs were designed as N-terminally hexahistidine-Xpress ($H_6X$) epitope-tagged PS variants. They were generated by cloning the respective cDNAs into the mammalian expression vector pcDNA4/HisC (Thermo Fisher Scientific). pcDNA4/HisC PS1 [233] and pcDNA4/HisC PS2 encoding the wildtype homologs of PS1 and PS2 were a kind gift by Prof. Dr. Harald Steiner (German Center for Neurodegenerative Diseases (DZNE), Munich, Germany) and served as main source for target and insert sequences. Plasmid DNA manipulation was conducted with Gibson assembly, QuikChange mutagenesis, or restriction-based cloning (Table 5) with suitable cloning primers (Table 2). Integrity of the generated plasmids was verified via sequencing at Eurofins (Eurofins, Luxembourg, Luxembourg) with appropriate sequencing primers (Table 1).

**Table 5: Cloning strategy for the respective PS variants.**

| Construct | Method | Backbone | Origin of insert | Target primers | Insert primers |
|---|---|---|---|---|---|
| $H_6$X-PS2_dHindIII | QC | pcDNA4/HisC PS2 | | 1091, 1092 | |
| $H_6$X-PS2ρTM2 | GA | pcDNA4/HisC PS2 | pcDNA4/HisC PS1 | 1026, 1024 | 1023, 1027 |
| $H_6$X-PS2ρTM3 | GA | pcDNA4/HisC PS2 | pcDNA4/HisC PS1 | 935, 1064 | 936 1063 |
| $H_6$X-PS2ρTM4 | GA | pcDNA4/HisC PS2 | pcDNA4/HisC PS1 | 934 1066 | 937, 1065 |
| $H_6$X-PS2ρTM5 | QC | pcDNA4/HisC PS2 | | 1069, 1070 | |
| $H_6$X-PS2ρTM6 | GA | pcDNA4/HisC PS2 | pcDNA4/HisC PS1 | 1029, 1054 | 1028, 1053 |
| $H_6$X-PS2ρTM8 | QC | pcDNA4/HisC PS2 | pcDNA4/HisC PS1 | 1085, 1086, 1087, 1088 | |
| $H_6$X-PS2ρTM9 | GA | pcDNA4/HisC PS2 | pcDNA4/HisC PS1 | 1034, 1036 | 1033, 1037 |
| $H_6$X-PS2ρTM1-2 | GA | pcDNA4/HisC PS2 | pcDNA4/HisC PS1 | 1024, 1025 | 1022, 1023 |
| $H_6$X-PS2ρTM3-4 | GA | pcDNA4/HisC PS2 | pcDNA4/HisC PS1 | 934, 935 | 936, 937 |
| $H_6$X-PS2ρTM4-5 | QC | pcDNA4/HisC PS2ρTM4 | | 1069, 1070 | |
| $H_6$X-PS2ρTM5-6 | QC | pcDNA4/HisC PS2ρTM6 | | 1069, 1070 | |
| $H_6$X-PS2ρTM6-7 | GA | pcDNA4/HisC PS2 | pcDNA4/HisC PS1 | 1029, 1068 | 1028, 1067 |
| $H_6$X-PS2ρTM1-4 | GA | pcDNA4/HisC PS2 | pcDNA4/HisC PS1 | 934, 1025 | 937, 1022 |
| $H_6$X-PS2ρTM3-6 | GA | pcDNA4/HisC PS2 | pcDNA4/HisC PS1 | 935, 1054 | 936, 1053 |
| $H_6$X-PS2ρTM2/6 | GA | pcDNA4/HisC PS2ρTM6 | pcDNA4/HisC PS1 | 1026, 1024 | 1023, 1027 |
| $H_6$X-PS2ρTM6/9 | GA | pcDNA4/HisC PS2ρTM6 | pcDNA4/HisC PS1 | 1034, 1036 | 1033, 1037 |
| $H_6$X-PS2ρTM2/6/9 | GA | pcDNA4/HisC PS2ρTM2/6 | pcDNA4/HisC PS1 | 1034, 1036 | 1033, 1037 |
| $H_6$X-PS1/2 | GA | pcDNA4/HisC PS1 | pcDNA4/HisC PS2 | 1020, 1039 | 1019, 1038 |
| $H_6$X-PS2/1 | GA | pcDNA4/HisC PS2 | pcDNA4/HisC PS1 | 1034, 1042 | 1033, 1040 |
| $H_6$X-PS2-NTF-PS1TMDs | RBC | pcDNA4/HisC PS2_delHindIII | pTwistAmp_PS2_NTFPS1TMDs | | |
| $H_6$X-PS2-CTF-PS1TMDs | RBC | pcDNA4/HisC PS2_delHindIII | pTwistAmp_PS2_CTFPS1TMDs | | |
| $H_6$X-PS2-All-PS1TMDs | RBC | pcDNA4/HisC PS2-NTF-PS1TMDs | pTwistAmp_PS2_CTFPS1TMDs | | |

The respective PS variants were cloned into the pcDNA4/HisC expression vector (QC = QuikChange mutagenesis, GA = Gibson assembly; RBC = restriction-based cloning).

### 3.1.5 DNA fragment separation and isolation from agarose gels

DNA products of PCR or plasmid DNA restriction digestions were separated in Tris-acetate/EDTA (TAE)-based agarose gels containing 0.25 µg/mL ethidium bromide. Fragment sizes of up to 8000 bp were separated on 1% (w/v) agarose in TAE buffer. For smaller fragments up to 2000 bp, 2% (w/v) agarose in TAE buffer was used. Once the gel was solidified, spacers and comb were removed, and the gel was covered with TAE buffer. DNA samples were mixed with an adequate amount of 6x Loading Dye (Thermo Fisher Scientific) and loaded in the pockets. In parallel, 6 µL Gene Ruler 1 kb DNA Ladder (Thermo Fisher Scientific) or Gene Ruler Low Range DNA Ladder (Thermo Fisher Scientific) were loaded, depending on the expected band size. Electrophoresis was conducted at 80 V for 45 min.

For DNA extraction from agarose gels, the expected PCR products were visualized under UV light at $\lambda = 365$ nm and cut from the gel. The "NucleoSpin Gel and PCR Clean-up" kit (Macherey-Nagel, Düren, Germany) was used for gel digestion and DNA purification according to the provided protocol with a final elution of the DNA in 30 µL of sterile $dH_2O$. DNA concentration was determined by measuring the optical density at $\lambda = 260$ nm ($OD_{260}$) of a 1:40 dilution in a spectrophotometer (Ultrospec 3100 pro, Amersham Bioscience, Amersham, UK). The ratio of $OD_{260}/OD_{280}$ served as a measure for the quality of the DNA solution. Solutions with a ratio ranging from 1.7-2.0 were considered as pure.

TAE buffer (pH 8.0)

| | |
|---|---|
| Tris-HCl | 40 mM |
| Acetic acid | 20 mM |
| EDTA | 1 mM |

### 3.1.6 Gibson Assembly cloning

Gibson Assembly cloning [234] was used to efficiently join two or more large DNA fragments in one reaction. As overlapping sequences of the DNA fragments are required for this technique, primers targeting the desired insert DNA sequence also contained segments of the target sequence and vice versa. For

amplification of the target and insert sequence, PCR was conducted as described above. PCR products were separated on and isolated from agarose gels followed by *Dpn*I restriction digestion (5 U *Dpn*I, 37°C, 60 min) of parental plasmid DNA to ensure high cloning efficiencies. Gibson assembly was performed with the Gibson Assembly Master Mix (New England Biolabs) according to the manufacturer's protocol using a 3-fold excess of insert DNA. After the assembly reaction, 10 µL of the reaction volume were transformed into *Escherichia coli* (*E. coli*) XL1 blue (see 3.1.10).

### 3.1.7 QuikChange mutagenesis

For site-directed mutagenesis of one or two amino acids, QuikChange mutagenesis was conducted [235]. This method utilizes a DNA primer pair containing the desired mutation that is flanked by downstream and upstream binding sites of the target region. Via PCR, plasmid DNA is amplified that contains the mutation of interest. *Dpn*I restriction digestion (5 U *Dpn*I, 37°C, 60 min) of parental plasmid DNA prior to transformation increased cloning efficiencies.

### 3.1.8 Restriction-based cloning

Restriction-based cloning is suitable for transferring large DNA fragments from a DNA donor to a target vector. To this end, target vector and insert DNA are linearized with compatible DNA restriction enzymes with a subsequent ligation step. In order to generate the PS2-NTF-PS1TMDs, PS2-CTF-PS1TMDs, and PS2-All-PS1TMDs vectors, two donor vectors were purchased from Twist Bioscience (Table 3). The fragment pTwistAmp_PS2_NTF_PS1TMDs_part coded for a chimeric PS NTF containing the hydrophobic regions of PS1 in combination with hydrophilic loop regions of PS2. For subsequent cloning, the gene fragment was flanked by a 5' *Not*I and a 3' *Hind*III restriction site. The C-terminal PS1 TMDs in combination with PS2 hydrophilic regions was flanked by a *Hind*III and *Xho*I (5' and 3', respectively) encoded in the pTwistAmp_PS2_CTFPS1TMDs fragment. The original target vector

pcDNA4/HisC PS2 harbors a second, hence interfering *Hind*III restriction site 5' of the gene of interest. Thus, prior to restriction digestion, this second restriction site was removed by site-directed mutagenesis (QuikChange) generating the $H_6$X-PS2_dHindIII construct (Table 5).

For restriction-based cloning, 1 µg of the donor and target vector were digested with 10 U of the respective restriction enzymes at 37°C for 1 h in the appropriate buffers (Thermo Fisher Scientific). The linearized fragments of interest were isolated via agarose gel purification. Ligation was conducted with 50 ng vector DNA and a threefold excess of insert using the T4 DNA ligase (Thermo Fisher Scientific).

| **DNA ligation reaction** | |
|---|---|
| Vector DNA | 50 ng |
| Insert DNA | 50 ng · 3 · length(insert) / length(vector) |
| T4 DNA Ligase buffer (10x) | 2 µL |
| T4 DNA Ligase (10 U) | 1 µL |
| $dH_2O$ | Add to 20 µL |

| **Ligation program** | |
|---|---|
| 37°C | 30 min |
| 20°C | 20 min |
| 65°C | 10 min |
| 4°C | Hold |

### 3.1.9 Preparation of chemically competent *E. coli* XL1

Chemically competent *E. coli* XL1 blue cells were prepared as described by Chung *et al.* [236]. Transformation and storage solution (TSS) buffer was prepared freshly each time and sterile filtered before usage. 250 mL of prewarmed lysogeny broth (LB) medium containing 12.5 µg/mL tetracycline were inoculated with 2.5 mL of a fresh overnight culture of *E. coli* XL1 cells. Cells were incubated at 37°C under constant shaking at 140 rpm (Incubator CH-4103, INFORS, Bottmingen, Switzerland) until the cell density reached $OD_{600}$ of 0.3 (Spectrophotometer Ultrospec 3100 pro, Amersham Bioscience). Afterwards, cells were cooled on ice for 15 min with subsequent centrifugation for 10 min at 4°C and 1000 xg (Avanti J-25 with rotor JLA-16.250, Beckman Coulter, Brea, CA, USA). After discarding the supernatant, the cells were resuspended in 25 mL of precooled TSS buffer. The cell suspension was divided in aliquots of 100 µL in 1.5 mL reaction tubes, frozen in liquid nitrogen, and stored at -80°C.

| LB medium (pH 7.0) | |
|---|---|
| Yeast extract | 0.5% (w/v) |
| Tryptone | 1% (w/v) |
| NaCl | 1% (w/v) |

| TSS buffer | |
|---|---|
| DMSO | 5% (v/v) |
| PEG 3000 | 10% (v/v) |
| $MgCl_2$ | 50 mM |
| In LB medium | |

### 3.1.10 Transformation of chemically competent *E. coli* XL1

For transformation, aliquots of competent cells were thawed on ice for 10 min. 0.5 µL of purified plasmid DNA were added to the cells, mixed carefully, and incubated on ice for 15 min. Heat shock was performed by incubating the cells for 1 min at 42°C with a subsequent cooling on ice for 2 min. After the addition of 900 µL LB medium, the cells were incubated at 37°C (Incucell incubator, MMM Group, Planegg, Germany) for 1 h in a culture wheel. 100 µL of the transformed cells were plated on LB agar plates (LB medium with 1.5% (w/v) agar) containing the appropriate antibiotics (Table 6) and incubated over night at 37°C. Plates containing colonies were sealed with Parafilm (Amcor, Zurich, Switzerland) and stored at 4°C.

**Table 6: Antibiotics for bacterial selection.**

| Antibiotic | Solvent | Stock solution | Working solution |
|---|---|---|---|
| Ampicillin | $dH_2O$ | 100 mg/mL | 100 µg/mL |
| Tetracycline | 70% Ethanol | 10 mg/mL | 12.5 µg/mL |

Stock solutions were sterile filtered (0.22 µM syringe filter). 1 mL aliquots were prepared in reaction tubes and stored at -20°C.

### 3.1.11 Plasmid DNA amplification and preparation

For small scale amplification of plasmid DNA, competent *E. coli* XL1 cells were transformed. The next day, one colony was used to inoculate an overnight culture of 4 mL LB media containing antibiotic selection pressure. After 16 h of incubation at 37°C in the culture wheel, plasmid DNA was isolated using the "NucleoSpin mini Kit for Plasmid DNA Purification" (Macherey-Nagel) according to the provided protocol. For the last step, DNA was eluted in 50 µL of autoclaved $dH_2O$.

If larger amounts of plasmid DNA were required, medium scale plasmid DNA amplification and preparation was performed. 5 mL LB media containing the appropriate antibiotics were inoculated with one colony of the transformed *E. coli* XL1 cells and incubated at 37°C for 16 h in the culture wheel. Subsequently, 250 mL of selection medium were inoculated with 2.5 mL of the overnight culture. The cells were incubated in 1 L Erlenmeyer flasks with baffles at 37°C and 140 rpm overnight. Medium scale preparation of plasmid DNA was performed using the "NucleoSpin Midi Kit for Plasmid DNA Purification" (Macherey-Nagel) following the provided protocol. Plasmid DNA was resuspended in 200 µL sterile $dH_2O$ and stored at -20°C.

## 3.2 Cell culture and cell lines

### 3.2.1 Cell lines and culture media

Cell culture media

Dulbecco's modified Eagle medium (DMEM GlutaMAX, Gibco Thermo Fisher Scientific) supplemented with 10% (v/v) fetal calf serum (FCS, PAN-Biotech, Aidenbach, Germany; LotNo.: P170504) and Penicillin/Streptomycin mix (Pen/Strep) (Sigma-Aldrich) served as the basis for all media. Additional antibiotics were added for selection and maintenance of stable transfections. The maintenance of APPsw expression was achieved by the addition of Geneticin (G418) (Gibco Thermo Fisher Scientific). For selection and preservation of stable transfected PS constructs the media was further supplemented with Zeocin (Zeo) (InvivoGen, San Diego, Ca, USA).

**Table 7: Antibiotics used in cell culture media.**

| Antibiotic | Stock solution | V / 500 mL DMEM | Working solution |
|---|---|---|---|
| G418 | 50 mg/mL | 2 mL | 200 µg/mL |
| Zeo | 100 mg/mL | 1 mL | 200 µg/mL |
| Pen/Strep | Penicillin: 10000 U<br>Streptomycin: 10 mg/mL | 5 mL | Penicillin: 100 U<br>Streptomycin: 0.1 mg/mL |

Cell lines

Human embryonic kidney 293 (HEK293) cells stably overexpressing the AD-causing Swedish mutant of APP (APPsw with K670N/M671L) (HEK293/Sw) were used for control experiments. For analysis of the respective PS variants, transfection of cells harboring knock-outs of endogenous PS1 and PS2 (HEK293/sw PS1/2 $^{-/-}$ dKO) [237] enabled the analysis of PS activity without endogenous protein levels. Both cell lines were kindly provided by Prof. Dr. Harald Steiner (DZNE, Munich, Germany). A list of the generated cell lines is summarized in Table 8.

**Table 8: Cell lines analyzed in this study.**

| Cell line | Antibiotics for selection |
|---|---|
| HEK293/sw | Pen/Strep/G418 |
| HEK293/sw PS1/2 $^{-/-}$ dKO | Pen/Strep/G418 |
| HEK293/sw PS1/2 $^{-/-}$ dKO/$H_6$X-PS1 | Pen/Strep/G418/Zeo |
| HEK293/sw PS1/2 $^{-/-}$ dKO/$H_6$X-PS2 | Pen/Strep/G418/Zeo |
| HEK293/sw PS1/2 $^{-/-}$ dKO/$H_6$X-PS2ρTM2 | Pen/Strep/G418/Zeo |
| HEK293/sw PS1/2 $^{-/-}$ dKO/$H_6$X-PS2ρTM3 | Pen/Strep/G418/Zeo |
| HEK293/sw PS1/2 $^{-/-}$ dKO/$H_6$X-PS2ρTM4 | Pen/Strep/G418/Zeo |
| HEK293/sw PS1/2 $^{-/-}$ dKO/$H_6$X-PS2ρTM5 | Pen/Strep/G418/Zeo |
| HEK293/sw PS1/2 $^{-/-}$ dKO/$H_6$X-PS2ρTM6 | Pen/Strep/G418/Zeo |
| HEK293/sw PS1/2 $^{-/-}$ dKO/$H_6$X-PS2ρTM8 | Pen/Strep/G418/Zeo |
| HEK293/sw PS1/2 $^{-/-}$ dKO/$H_6$X-PS2ρTM9 | Pen/Strep/G418/Zeo |
| HEK293/sw PS1/2 $^{-/-}$ dKO/$H_6$X-PS2ρTM1-2 | Pen/Strep/G418/Zeo |
| HEK293/sw PS1/2 $^{-/-}$ dKO/$H_6$X-PS2ρTM3-4 | Pen/Strep/G418/Zeo |
| HEK293/sw PS1/2 $^{-/-}$ dKO/$H_6$X-PS2ρTM4-5 | Pen/Strep/G418/Zeo |
| HEK293/sw PS1/2 $^{-/-}$ dKO/$H_6$X-PS2ρTM5-6 | Pen/Strep/G418/Zeo |
| HEK293/sw PS1/2 $^{-/-}$ dKO/$H_6$X-PS2ρTM6-7 | Pen/Strep/G418/Zeo |
| HEK293/sw PS1/2 $^{-/-}$ dKO/$H_6$X-PS2ρTM1-4 | Pen/Strep/G418/Zeo |
| HEK293/sw PS1/2 $^{-/-}$ dKO/$H_6$X-PS2ρTM3-6 | Pen/Strep/G418/Zeo |
| HEK293/sw PS1/2 $^{-/-}$ dKO/$H_6$X-PS2ρTM2/6 | Pen/Strep/G418/Zeo |
| HEK293/sw PS1/2 $^{-/-}$ dKO/$H_6$X-PS2ρTM6/9 | Pen/Strep/G418/Zeo |
| HEK293/sw PS1/2 $^{-/-}$ dKO/$H_6$X-PS2ρTM2/6/9 | Pen/Strep/G418/Zeo |
| HEK293/sw PS1/2 $^{-/-}$ dKO/$H_6$X-PS1/2 | Pen/Strep/G418/Zeo |
| HEK293/sw PS1/2 $^{-/-}$ dKO/$H_6$X-PS2/1 | Pen/Strep/G418/Zeo |
| HEK293/sw PS1/2 $^{-/-}$ dKO/$H_6$X-PS2-All-PS1TMDs | Pen/Strep/G418/Zeo |
| HEK293/sw PS1/2 $^{-/-}$ dKO/$H_6$X-PS2-NTF-PS1TMDs | Pen/Strep/G418/Zeo |
| HEK293/sw PS1/2 $^{-/-}$ dKO/$H_6$X-PS2-CTF-PS1TMDs | Pen/Strep/G418/Zeo |

### 3.2.2 Cultivation of HEK293/sw cells

All measures for passaging and manipulation of the cells were performed under sterile condition (Safety cabinet BioWizard, Kojair Tech Oy, Mänttä-Vilppula Finland). Cultivation of all cell lines was conducted at 37°C and 5% $CO_2$ ($CO_2$ incubator HERAcell 150i, Thermo Fisher Scientific) in DMEM containing appropriate antibiotic selection. 8 mL or 4 mL medium were used for 10 cm or 6 cm cell culture dishes (Nunc, Thermo Fisher Scientific), respectively. Confluence of the cells was examined in a transmitted light microscope (Zeiss, Oberkochen, Germany).

Passaging of the cells was performed by removing old media and washing with 3 mL sterile phosphate-buffered saline (PBS). To detach adherently grown cells, 1.5 mL trypsin (Sigma-Aldrich) were added and incubated for 5 min at room temperature. Using 1.5 mL of the respective medium, the cells were transferred to a 15 mL centrifugation tube. After centrifugation for 5 min at 1000 xg and room temperature (Varifuge K, Heraeus, Hanau, Germany), the supernatant was discarded. The pellet was resuspended in fresh media and applied to fresh culture dishes in the desired dilution.

| 10x PBS (pH 7.4) | |
|---|---|
| $Na_2HPO_4 \bullet 2H_2O$ | 100 mM |
| $KH_2PO_4$ | 17.7 mM |
| KCl | 27 mM |
| NaCl | 1.4 M |

### 3.2.3 Cryoconservation of cell stocks

Cryoconservation of cell stocks was performed with cells at a confluence of 70%. Washing and trypsinization was conducted as described above. After centrifugation and removing the supernatant, the cells were resuspended in 1 mL FCS containing 10% (v/v) DMSO and frozen at -80°C.

For reactivation of cells after cryoconservation, stocks were thawed quickly at 37°C in a water bath. Subsequently, the stock solution was transferred to 5 mL

of DMEM without selection pressure and centrifuged for 1000 xg at room temperature for 5 min (Varifuge K, Heraeus). In the next step, the supernatant was discarded, the pellet resuspended in fresh media, and transferred to a fresh culture dish with DMEM without selectin pressure. After overnight incubation at 37°C and 5% $CO_2$, the medium was changed to DMEM containing the appropriate antibiotics.

### 3.2.4 Stable transfection of HEK293/sw cells

For this study, the average effect of a respective PS variant on substrate processing should be assessed by analysis of multiple cells expressing this PS variant. Hence, pooled clones instead of single cell clones were prepared and analyzed. HEK293/sw PS1/2 $^{-/-}$ dKO [237] were grown in a 10 cm culture dish to a confluence of 80% for transfection with expression vectors encoding the individual PS variants. Prior to transfection, the medium was changed to DMEM without selection pressure. 20 µg DNA and 40 µL Lipofectamine 2000 (Invitrogen Thermo Fisher Scientific) were mixed with 1 mL OptiMEM (Gibco Thermo Fisher Scientific) each. The two solutions were mixed, incubated at room temperature for 5 min, and carefully applied to the cells. After overnight incubation in the incubator, the medium was changed to fresh media without selection pressure, followed by incubation for 24 h. Then, medium was changed to DMEM containing Zeo in 1.5-fold of the normal concentration (350 µg/mL) and G418. After passaging and reaching a cell confluence of 100% for the third time, the transfection was considered to be stable and Zeo selection pressure was reduced to the standard concentration. As pooled clones might change average protein expression properties of the PS variants over time, a sufficient amount of stocks was prepared as soon as the selection was stable. Transfected cell lines were cultivated for approximately 6-8 weeks. After this period, fresh stocks were thawed to restore the starting conditions.

## 3.3 Protein biochemical methods

### 3.3.1 Cell harvesting and total cell lysates

For the characterization of protein expression levels and complex maturation of the transfected constructs, total cell lysates were prepared. All steps were conducted on ice to avoid protein degradation. Confluent cells were washed with 3 mL cold PBS and subsequently covered with 1 mL of cold PBS. The adherent cells were scraped with a cell lifter, transferred to 2 mL reaction tubes, and pelleted by centrifugation for 5 min at 3500 xg and 4°C in a tabletop centrifuge (Biofuge Fresco, Thermo Fisher Scientific). Pellets were either stored at -20°C or used directly for protein analysis.

Cell pellets were resuspended in 500 µL STEN-lysis buffer supplemented with a protease inhibitor cocktail (Sigma-Aldrich) by vortexing and lysed on ice for 10 min. The lysates were centrifuged for 10 min at 16000 xg and 4°C to pellet cellular debris (Biofuge Fresco, Thermo Fisher Scientific). After the supernatant fraction was transferred to a fresh 1.5 mL reaction tube, the protein concentration was quantified using the Bradford assay. Proteins were separated on Tris-tricine gradient gels and subjected to immunoblotting.

| STEN-Lysis buffer | |
|---|---|
| Tris-HCl | 50 mM, pH 7.6 |
| NaCl | 150 mM |
| EDTA | 2 mM |
| NP-40 (100%) | 1% (w/v) |

### 3.3.2 Bradford assay for protein quantification

Quantification of protein concentration was determined using the Bradford reagent [238]. Upon non-covalent binding to a protein, the absorption maximum of the coloring agent Coomassie Brilliant Blue G-250 shifts from λ = 465 nm to λ = 595 nm, which can be measured using a spectrophotometer.

For the analysis, 2 µL of total cell lysates were mixed with 1 mL Bradford reagent in a polystyrene cuvette and incubated for 5 min at room temperature. In parallel,

measurement of 10 µg of a BSA standard was included in each measurement for subsequent concentration calculation. Protein concentrations were calculated with equation *(1)* after measuring the absorbance at λ = 595 nm in duplicates.

$$\frac{10\ \mu g\ \mathrm{BSA}}{OD_{595}\ BSA} = \frac{Protein\ amount\ sample}{OD_{595}\ sample} \qquad (1)$$

| Bradford reagent | |
|---|---|
| Coomassie Brilliant Blue G-250 | 0.01% (w/v) |
| Ethanol | 4.7% (w/v) |
| Ortho-phosphoric acid | 8.5% (w/v) |

### 3.3.3 SDS polyacrylamide gel electrophoresis

Tris-tricine gradient gels

Gel electrophoretic separation of the γ-secretase components and cleavage products by their molecular weight was conducted via denaturating polyacrylamide gel electrophoresis (PAGE). Sodium dodecyl sulfate (SDS) was used as denaturating reagent for protein samples. To allow the simultaneous analysis of larger (e.g. NCT) and smaller proteins (AICD), Tris-tricine gradient gels, also referred to as Schägger gradient gels [239], were used. Casting and running of the gels were performed with the PerfectBlue Dual Gel System line of Peqlab (Peqlab Avantor, Radnor, PA, USA) using the “Twin ExW S” setup for large gels (20 cm x 10 cm x 0.8 mm) and the “Twin S” setup for small gels (10 cm x 10 cm x 1 mm). The ingredients listed below were adjusted for one large gel, or two small gels, respectively. Furthermore, the volumes per gel are listed that are required to pour the individual gel layers.

| | Separation gel (16.5%) | Spacer gel (10%) | Stacking gel (4%) |
|---|---|---|---|
| $dH_2O$ | - | 3.5 mL | 4.2 mL |
| Tris-tricine gel buffer | 3 mL | 2.5 mL | 1.55 mL |
| Acrylamide/Bisacrylamide (32:1, 49.5%) | 3 mL | 1.5 mL | 0.5 mL |
| Glycerol 32% (v/v) | 3 mL | - | - |
| APS 10% (w/v) | 54 µL | 70 µL | 60 µL |
| TEMED | 6 µL | 8 µL | 8 µL |
| Volume for one small gel | 3.3 mL | 1.6 mL | |
| Volume for one large gel | 6 mL | 2.8 mL | |

APS and TEMED were added last to the mixture shortly before pouring the individual gel layers. A gradient-like character of the gels was achieved by consecutive pouring of the separation and spacer gel without intermediate waiting steps. The stacking gel was poured after polymerization of the other gel layers.

Samples to be analyzed were mixed with 3x Laemmli sample buffer and heated at 65°C for 5 min prior to loading. For mass identification of protein bands after immunoblotting, 5 µL of the SeeBlue Plus2 pre-stained protein standard (Invitrogen Thermo Fisher Scientific) were included on each gel. SDS-PAGE was conducted with 1x Tris-tricine cathode buffer and 1x Tris-tricine anode buffer for 15 min at 80 V followed by 2.5 h at 120 V.

| 3x Laemmli sample buffer | |
|---|---|
| Tris-HCl | 0.1875 M, pH 6.8 |
| SDS | 6% (w/v) |
| Glycerol | 30% (v/v) |
| β-Mercaptoethanol | 7.5% (v/v) |
| Urea | 6 M |
| Bromophenol blue | 0.01% (w/v) |

| Tris-tricine gel buffer | |
|---|---|
| Tris-HCl | 3 M, pH 8.45 |
| SDS 20% | 0.3% |

| 5x Tris-tricine anode buffer | |
|---|---|
| Tris-HCl | 1 M, pH 8.9 |

| 10x Tris-tricine cathode buffer | |
|---|---|
| Tris-HCl | 1 M |
| Tricine | 1 M |
| SDS | 1% |

Separation of Aβ species on Tris-bicine-urea gels

Individual Aβ species from conditioned media or *in vitro* assays were separated on Tris-bicine gels containing 8 M urea [240]. Casting and running of the gels were performed with the PerfectBlue Dual Gel System "Twin S" setup for small gels (10 cm x 10 cm x 1 mm) (Peqlab Avantor). The following ingredients were calculated for casting two gels.

| | Separation gel (8%) | Spacer gel (12%) | Stacking gel (9%) |
|---|---|---|---|
| Urea | 4.8 g | - | - |
| $dH_2O$ | 1.75 mL | 0.78 mL | 0.81 mL |
| Acrylamide/Bisacrylamide (19:1, 40%) | 2 mL | 1.2 mL | 0.68 mL |
| SDS 20% (w/v) | 50 µL | 20 µL | 15 µL |
| Separation gel buffer | 2.5 mL | - | - |
| Spacer gel buffer | - | 2 mL | - |
| Stacking gel buffer | - | - | 1.5 mL |
| APS 10% (w/v) | 40 µL | 16 µL | 9 µL |
| TEMED | 10 µL | 4 µL | 9 µL |
| Height | 6.65 cm | 1.65 cm | 0.65 cm |

After assembly of the glass plates in the gel system, the indicated heights of the gel layers were marked. APS and TEMED were added to the mixture just before pouring of the gel layers, to prevent early polymerization. Prior to loading, samples were mixed with 3x Wiltfang (WF) sample buffer and heated at 95°C for 10 min. The SeeBlue Plus2 pre-stained protein standard (Invitrogen, Thermo Fisher Scientific) was included on each gel for subsequent mass identification of

protein bands. Gel electrophoresis was conducted for 15 min at 80 V followed by 120 V for 1.5 h with the respective cathode and anode buffer. For an optimized resolution of the analyzed Aβ species, acrylamide concentration in the separation gel could be increased to up to 11.5%.

| Separation gel buffer | |
|---|---|
| Tris-HCl | 1.6 M |
| $H_2SO_4$ | 0.4 M |

| Spacer gel buffer | |
|---|---|
| Bis-Tris | 0.8 M |
| $H_2SO_4$ | 0.2 M |

| Stacking gel buffer | |
|---|---|
| Bis-Tris | 0.72 M |
| Bicine | 0.32 M |

| Tris-bicine anode buffer | |
|---|---|
| Tris-HCl | 0.2 M |
| $H_2SO_4$ | 0.05 M |

| 3x WF sample buffer | |
|---|---|
| Bis-Tris | 1.08 M |
| Bicine | 0.48 M |
| SDS | 3% (w/v) |
| β-Mercaptoethanol | 7.5% (v/v) |
| Sucrose | 45% (w/v) |
| Bromophenol blue | 0.01% (w/v) |

| Tris-bicine cathode buffer | |
|---|---|
| Bicine | 0.2 M |
| NaOH | 0.1 M |
| SDS | 0.25% |

### 3.3.4 Immunoblotting

For the detection of specific protein bands, semi-dry Western blotting was conducted after SDS-PAGE. Depending on the protein of interest and the corresponding antibody, two different types of blotting membranes were used in this thesis. Polyvinylidene difluoride (PVDF) (Immobilon P, 0.45 µm, Merck KGaA, Darmstadt, Germany) and nitrocellulose (Amersham Protran NC, 0.45 µm, Amersham Thermo Fisher Scientific) membranes were used depending on the best performance of each antibody. In addition to this, the choice of the blocking reagent was optimized for all antibodies (Section 3.3.5, Table 9).

Protein transfer

To efficiently transfer proteins from polyacrylamide gels onto blotting membranes, all layers were soaked in Towbin transfer buffer [241] prior to immunoblotting. PVDF membranes were activated by incubation in 2-propanol for 1 min, rinsed once with water, and placed in the transfer buffer. For activation of nitrocellulose membranes, incubation in transfer buffer for 1 min was sufficient. The blotting membrane was placed on four layers of blotting paper sheets (Ahlstrom Munksjö, Bärenstein, Germany) on the anode of the blotting device (Modell SD 1, cti, Idstein, Germany). After removal of the stacking gel, the gel was placed on the blotting membrane and covered by four additional layers of filter paper and the cathode-containing lid. In relation to the membrane size, electro transfer of the proteins was performed with 1.5 mA/cm$^2$ for Tris-bicine-urea gels and 4 mA/cm$^2$ for Tris-tricine gels for 90 min.

Membrane blocking and antibody incubation

Prior to detection of Aβ peptides, the membranes were submerged in boiling PBS for 5 min, directly after protein transfer from the gel. After this, the membranes were incubated in blocking buffer for 1 h at room temperature under constant shaking to saturate unspecific binding sites. For all other proteins, membranes were directly incubated in the respective blocking reagent. After discarding residual blocking solution, the membranes were incubated with the primary antibodies (Section 3.3.5, Table 9) overnight at 4°C while constantly shaking. The next day, the membranes were washed thrice for 5 min with Tris-buffered saline containing 0.1% Tween 20 (TBS-T). Subsequently, the membranes were incubated with the secondary antibodies (Section 3.3.5, Table 10) for 1 h at room temperature with continuous agitation. After three additional washing steps with TBS-T for 5 min, protein detection was performed.

Protein detection using chemiluminescence

Chemiluminescence detection for protein analysis was chosen as it yields a high sensitivity with a large linear response range. By allowing multiple exposures per immunoblot, the detection and quantification of a large range of protein concentrations is possible. Visualization of the proteins was realized using horseradish peroxidase (HRP)-conjugated secondary antibodies in combination with an enhanced chemiluminescence (ECL) reagent. In case of subsequent quantification of band intensities, membranes were developed with Clarity Western ECL Substrate (Bio-Rad, Hercules, CA, USA) for 5 min according to the manufacturer's protocol. Protein bands of immunoblots were quantified using a Western Blot imager (Fusion FX, Vilber Lourmat, Collégien, France) and the Image Studio Lite Ver. 5.2 software (LI-COR Biosciences, Lincoln, NE, USA).

Documentation of complex formation and protein expression levels was conducted with Pierce ECL Western blotting substrate (Thermo Fisher Scientific) according to the provided protocol. The membranes were exposed to X-ray films (Super RX-N, Fujifilm, Tokyo, Japan) for an appropriate time and developed with a film developer (CP100, Agfa, Mortsel, Belgium).

| 10 x TBS-T | |
|---|---|
| Tris-HCl | 100 mM, pH 7.4 |
| NaCl | 1.5 M |
| Tween 20 | 1% (v/v) |

| Towbin transfer buffer | |
|---|---|
| Tris-HCl | 20 mM |
| Glycine | 192 mM |
| Methanol | 20% (v/v) |
| SDS | 0.1% (w/v) |

| I-Block buffer | |
|---|---|
| I-Block | 0.2% (w/v) |
| Tween 20 | 0.05% (v/v) |
| In 1x PBS | |

| BSA blocking buffer | |
|---|---|
| BSA | 2% (w/v) |
| Tween 20 | 0.05% (v/v) |
| In 1x PBS | |

### 3.3.5 Antibodies

For protein analysis, specific antibodies were used for protein detection on immunoblots (Table 9, Table 10) or immunoprecipitation (IP) (Table 11). If no other supplier is stated, primary antibodies were a kind gift by Prof. Dr. Harald Steiner (DZNE, Munich, Germany). Prior to application on immunoblots, antibodies were diluted in either I-Block buffer or BSA blocking buffer. Addition of 0.05% (w/v) sodium azide enhanced the stability of the antibody solutions. Secondary antibodies were purchased from Promega (Madison, WI, USA) or Merck (Darmstadt, Germany) and diluted in the same buffer as the corresponding primary antibodies. HRP-conjugated secondary antibodies were used for subsequent detection via chemiluminescence.

Antibodies for immunoblots

**Table 9: Primary antibodies used for immunoblots.**

| Antibody | Epitope | Dilution | Host | Supplier/Reference |
|---|---|---|---|---|
| N1660 | NCT aa 693-709 | 1:2500 – 1:5000 (I-Block) | Rabbit | Sigma-Aldrich |
| 2G7 | PS1 NTF aa 39-52 | 1 µg/mL (I-Block) | Mouse | [242] |
| 5E12 | PS1 CTF aa 313-333 | 2 µg/mL (I-Block) | Rat | [243] |
| 2972 | PS2 NTF aa 2-87 | 1:500 (I-Block) | Rabbit | [244] |
| HF5C | PS2 CTF aa 297–356 | 1:2000 (I-Block) | Rat | [83] |
| 8557 | PEN-2 N-terminus aa 4-15 | 1 µg/mL (I-Block) | Rabbit | unpublished |
| ADI-SPA-860-D | CTF of Calnexin | 1:7000 (I-Block) | Rabbit | Enzo Life Science (New York, NY, USA) |
| Penta-His | $His_5$ or $His_6$ epitope | 1:5000 (I-Block) | Mouse | Qiagen (Hilden, Germany) |
| 2D8 | Aβ 1-16 | 1:25 (I-Block) | Rat | [227] |

aa = amino acid

**Table 10: Secondary antibodies conjugated to HRP.**

| Antibody | Dilution | Supplier |
|---|---|---|
| anti-rabbit-HRP | 1:5000 – 1:10000 | Promega |
| anti-mouse-HRP | 1:2500 – 1:5000 | Promega |
| anti-rat-HRP | 1:3333 | Merck |

Antibodies for IP

**Table 11: Antibodies used for IP.**

| Antibody | Epitope | Dilution | Host | Supplier/Reference |
|---|---|---|---|---|
| 4G8 | Aβ17-24 | 2.5 - 4 µg/mL | Mouse | Biolegend (San Diego, CA, USA) |
| 3552 | Aβ1-40 | 1:500 – 1:2000 | Rabbit | [178] |
| Y188 | APP C-terminus | 1:2500 | Rabbit | Abcam (Cambridge, UK) |

### 3.3.6 Cell-free γ-secretase assay

In this study the influence of the individual PS variants on cleavage activity and generation of individual cleavage products should be analyzed independent of the localization of the complexes. For this, the *in vitro* activity was assessed in a well-established 3-([3-Cholamidopropyl]dimethylammonio)-2-hydroxy-1-propanesulfonate (CHAPSO)-solubilized γ-secretase system [80].

Preparation of membrane fractions

Harvested cells (Section 3.3.1) were either prepared freshly or thawed on ice. For the preparation of membrane fractions, cells were resuspended in 1 mL hypotonic buffer. After adjusting the $OD_{600}$ to 2 in a total volume of 1 mL, cells were incubated on ice for 10 min. Homogenization was achieved by freezing samples in liquid nitrogen, thawing on ice, and subsequent passing through a needle (0.6 mm x 30 mm) with 10 strokes. To remove cell debris, the homogenized suspension was centrifuged for 15 min at 1000 xg and 4°C. Subsequently, the supernatant was transferred to a fresh 1.5 mL reaction tube

and centrifuged at 16000 xg and 4°C for 45 min (Biofuge Fresco, Thermo Fisher Scientific). The resulting membrane pellets were either frozen in liquid nitrogen and stored at -80°C or used directly for membrane lysis.

CHAPSO membrane lysis

Membrane lysis was conducted in 100 µL of CHAPSO-Lysis buffer (CHAPSO purchased from Avanti Polar Lipids, Birmingham, AL, USA) and incubated on ice for 20 min. Afterwards, the suspension was cleared by ultracentrifugation for 30 min at 100000 xg (rotor: TLA55, Optima TLX Ultracentrifuge, Beckman Coulter) and 4°C. Aliquots of 20 µL of the supernatant containing the lysate were either frozen in liquid nitrogen and stored at -80°C or used directly for the *in vitro* γ-secretase assay.

Measuring the γ-secretase activity in CHAPSO-solubilized membrane fractions

In order to test the γ-secretase activity of the PS chimeras *in vitro*, 5 µL of the membrane lysates were mixed with 5 µL of citrate buffer, 10 µL of 2x C100 assay buffer and 1 µL of 10.5 µM C100-$His_6$ [80]. Purified C100-$His_6$ substrate was a kind gift by Prof. Dr. Harald Steiner (DZNE, Munich, Germany). For the identification of γ-secretase-unrelated cleavage products, an inhibitor control reaction (1.22 µM LY-411575 γ-secretase inhibitor, Sigma-Aldrich) was conducted in parallel for each sample. Reactions without the inhibitor were mixed with an equivalent amount of DMSO. A second control reaction was stored at -20°C. Thus, for each construct, three different reactions were prepared: a) incubation at -20°C, b) incubation at 37°C, and c) incubation at 37°C with γ-secretase inhibitor. Reactions were incubated for 16 h, separated on Tris-tricine gels and analyzed via immunoblotting. Protein bands of immunoblots were quantified using a Western Blot imager (Fusion FX, Vilber Lourmat) and the Image Studio Lite Ver. 5.2 software (LI-COR Biosciences).

To assess γ-secretase activity of the individual PS variants, the generation of cleavage products per active enzyme complex was analyzed. Wildtype PS1 and

PS2 controls were included in each experiment. As full glycosylation of NCT to its mature form $NCT_m$ occurs last during complex formation [131], $NCT_m$ intensities were chosen as a measure for the active enzyme complex. Thus, signal intensities of generated cleavage products (Aβ or AICD) were normalized to the ones of $NCT_m$ and set in relation to levels of PS1. Detection of AICD was conducted with a penta-His antibody targeting the C-terminal $His_6$-tag of C100. Aβ detection was performed using antibody 2D8. For all signal quantifications, a cutoff value for intensity was set to 2500. Samples with signal intensities below this value did not sufficiently stand out from their background and were excluded from analysis.

| Hypotonic buffer | |
|---|---|
| Na-citrate | 15 mM, pH 6.4 |
| KCl | 10 mM |

| Citrate buffer | |
|---|---|
| Na-citrate | 150 mM, pH 6.4 |
| cOmplete protease inhibitor cocktail (Pi) | 1x |

| CHAPSO-Lysis buffer | |
|---|---|
| Na-citrate | 150 mM, pH 6.4 |
| CHAPSO | 1% |
| cOmplete Pi | 1x |

| 2x C100 assay buffer | |
|---|---|
| Na-citrate | 150 mM, pH 6.4 |
| Phosphatidylcholine | 1 mg/mL |
| BSA | 0.2 mg/mL |
| Dithiothreitol | 20 mM |
| cOmplete Pi | 1x |

### 3.3.7 Immunoblot analysis of Aβ peptides from conditioned media

For detecting shifts in the Aβ processing mediated by the PS variants, secreted Aβ was analyzed from conditioned media. Prior to the collection of conditioned media, cells were seeded in DMEM containing the appropriate antibiotics on 10 cm cell culture dishes. Cells stably transfected with PS1 and PS2 constructs were included as controls for each experiment. At a cell confluence of 80%, the medium was changed to 4 mL DMEM containing no selection pressure besides Pen/Strep. After incubation for 16 h, the media was collected and cleared by centrifugation for 5 min at 1000 xg and 4°C in 15 mL reaction tubes (centrifuge Z513K with rotor 220.70 V06, Hermle, Wehingen, Germany). The supernatant

was transferred to fresh 1.5 mL reaction tubes and centrifuged at 16000 xg and 4°C for 45 min in a benchtop centrifuge (Biofuge Fresco, Thermo Fisher Scientific) to remove residual cell debris. Aliquots of the cleared media were mixed with 3x WF sample buffer. To detect differences in Aβ processing, the samples were analyzed on Tris-bicine-urea gels with subsequent immunoblotting.

### 3.3.8 Immunoblot analysis of immunoprecipitated Aβ

To facilitate the analysis of individual Aβ peptides in conditioned media from PS variants with low overall activity, IP was performed prior to immunoblotting. For this, conditioned media were centrifuged at 6000 xg for 10 min and 4°C (centrifuge Z513K, Hermle), to remove cell debris. In case of PS variants with low γ-secretase activity, IP was performed with 4 mL media, 18 µL Protein A Sepharose (PAS)-beads, and 3 µL antibody 3552 overnight at 4°C. Volumes for the more active PS1 control were adjusted to 1 mL media and 2 µL antibody for better comparison of Aβ amounts. The next day, beads were collected by centrifugation at 1500 xg for 5 min and 4°C. Afterwards, samples were subjected to three subsequent wash steps using STEN-NaCl, STEN-SDS, or STEN buffer with 1 mL each, followed by centrifugation at 2000 rpm, 4°C for 5 min in a benchtop centrifuge (Biofuge Fresco, Thermo Fisher Scientific). After discarding the supernatant, 18 µL 1.7x WF sample buffer (Section 3.3.3) were added to the beads and incubated at 95°C for 5 min. The volume on the beads was measured using a Hamilton syringe (Hamilton, Reno, NV, USA) for each sample. Subsequently, half the volume was loaded on Tris-bicine-urea gels for separation of Aβ peptides followed by immunoblotting.

| STEN buffer | |
|---|---|
| Tris-HCl | 50 mM, pH 7.6 |
| NaCl | 150 mM |
| EDTA | 2 mM |
| NP-40 (100%) | 0.2% (w/v) |

| STEN-SDS buffer | |
|---|---|
| Tris-HCl | 50 mM, pH 7.6 |
| NaCl | 150 mM |
| EDTA | 2 mM |
| NP-40 (100%) | 0.2% (w/v) |
| SDS | 0.1% |

| STEN-NaCl buffer | |
|---|---|
| Tris-HCl | 50 mM, pH 7.6 |
| NaCl | 150 mM |
| EDTA | 2 mM |
| NP-40 (100%) | 0.2% (w/v) |
| NaCl | 0.5 M |

### 3.3.9 IP-MS analysis of Aβ peptides from conditioned media

For detailed analysis of the generated cleavage products, Aβ peptides were further analyzed by combined IP and mass spectrometry (MS). Conditioned media was collected as described above (Section 3.3.7) with the exception of using 6 mL medium per 10 cm culture dish. To gain sufficient amounts of secretory Aβ peptides for analysis, media of three 10 cm cell culture dishes were collected and pooled for each cell line, followed by centrifugation for 10 min at 6000 xg and 4°C (centrifuge Z513K, Hermle) to remove cellular debris. After discarding the pellet, 1/25 volume of Tris-EDTA was added to the cleared conditioned medium. For immunoprecipitation, 30 µL Protein G Sepharose (PGS) beads (50% solution in PBS) together with 10 µL antibody 4G8 (final concentration: 2.5 µg/mL) were added to the medium. Samples were incubated overnight at 4°C with constant agitation. The next day, beads were collected by centrifugation in 50 mL centrifugation tubes at 1500 xg and 4°C for 5 min and the supernatant discarded carefully. Beads were resuspended in 1 mL IP-MS buffer and transferred to 1.5 mL reaction tubes. Following centrifugation at 2500 xg at 4°C for 1 min (Biofuge Fresco, Thermo Fisher Scientific), the beads were washed twice with 1 mL IP-MS buffer and three times with 1 mL $dH_2O$. Afterwards, residual water was removed completely, and samples were stored at -20°C.

For mass spectrometric analysis, a matrix solution consisting of a 50% acetonitrile solution, 0.3% Trifluoroacetic acid (TFA), and a large spatula tip of α-Cyano-4-hydroxycinnamic acid (CHCA) was prepared freshly. The mixture was incubated for 10 min at 37°C under constant agitation followed by centrifugation for 15 s at 16000 xg and room temperature. Immunoprecipitated

samples were thawed on ice with subsequent addition of 10 µL matrix solution. Samples were vortexed briefly and centrifuged for 15 s at 16000 xg and room temperature. 0.4 µL of the supernatant were spotted on a stainless steel sample plate. After evaporation of the solvent, the spotting step was repeated twice. The samples were analyzed with a MALDI-TOF (for "Matrix-assisted laser desorption/ionization - time of flight") MS instrument (4800 MALDI TOF/TOF Analyzer, Applied Biosystems) in linear mode with an appropriate laser intensity. MS data were analyzed with the DataExplorer V4.9 Software (Applied Biosystems) and OriginPro 2021 (OriginLab Corporation).

| 20x IP-MS buffer | |
|---|---|
| Tris-HCl | 200 mM, pH 8.0 |
| NaCl | 2.8 M |
| EDTA | 100 mM, pH 8.0 |
| *N*-octylglycopyranoside | 2% |

| Tris-EDTA | |
|---|---|
| Tris-HCl | 750 mM, pH 8.0 |
| EDTA | 125 mM, pH 8.0 |

### 3.3.10 IP-MS analysis of *in vitro* generated Aβ peptides

For IP-MS analysis of *in vitro* generated Aβ peptides, cell-free γ-secretase assays were performed as described before (Section 3.3.6) with a threefold of the indicated volumes. Briefly, 60 µL CHAPSO lysate were mixed with 60 µL sodium citrate buffer, 120 µL 2x C100 assay buffer and 12 µL C100-$His_6$ substrate (10.5 µM). 100 µL of the reaction mixture were incubated with 2.5 µL DMSO at 37°C for 16 h in 1.5 mL reaction tubes. In order to distinguish between specific and unspecific peaks in the mass spectra, control reactions with the γ-secretase inhibitor LY-411575 (1.22 µM, Sigma-Aldrich) instead of DMSO, were conducted in parallel.

After incubation, 20 µL of the reaction volumes were withdrawn for immunoblot analysis. IP of Aβ peptides was performed with the residual volume together with 1 mL IP-MS buffer, 4 µL antibody 4G8, and 12 µL PGS beads over night at 4°C with constant agitation. Afterwards, beads were collected at 2500 xg and 4°C for 1 min and washed three times each with 1 mL IP-MS buffer and 1 mL $dH_2O$. Beads were dried by removing residual water completely and stored at -20°C

until analysis. Mass spectrometric analysis of the Aβ peptides was performed as described before (Section 3.3.9).

### 3.3.11 IP-MS analysis of *in vitro* generated AICD

While the analysis of immunoprecipitated Aβ peptides helped to analyze differences in the stepwise substrate processing, generated AICDs reflect the initial cleavage of the C100 substrate. For this, cell-free γ-secretase assays were conducted in accordance to IP-MS of *in vitro* generated Aβ peptides (Section 3.3.10). Immunoprecipitation of AICDs was performed with 80 µL of the *in vitro* assay sample, 15 µL PAS-bead solution, 0.8 µL antibody Y188, and 1 mL IP-MS buffer overnight at 4°C. Subsequent bead collection and washing steps were performed as described above. For MS analysis, samples were thawed on ice with subsequent addition of 13 µL CHCA matrix solution. The samples were vortexed briefly and centrifuged for 15 s at 16000 xg and room temperature. 0.8 µL of the supernatant were spotted on a stainless steel MALDI sample plate. After evaporation of the solvent, the samples were analyzed with a MALDI-TOF spectrometer (rapifleX Tissuetyper, Bruker Optic GmbH, Ettlingen, Germany) with the associated flexControl software. Data evaluation was performed with the flexAnalysis software and OriginPro2021 (OriginLab Corporation).

## 3.4 Statistics and software

Data are presented as the mean value ± SEM. For statistical analysis of two samples, a two-tailed, unpaired T-test was calculated using Microsoft Excel. In case of multiple comparisons, data were analyzed using one-way analysis of variance (ANOVA) and post hoc Dunnett's test using GraphPad Prism 9 (GraphPad Software). Significance levels were set to $p \leq 0.05$ (*), $p \leq 0.01$ (**), and $p \leq 0.001$ (***). Bar graphs without asterisks showed no statistical significance.

Analyses of DNA-Sequences were conducted with CLC Workbench 6 (Qiagen). Signals intensities from immunoblots were evaluated with Image Studio Lite Ver. 5.2 (Li-COR Biosciences). Programs for evaluation of the mass spectrometric data were either DataExplorer V4.9 Software (Applied Biosystems) or the

combination of flexControl and flexAnalysis Software (Bruker Optic GmbH). For bar graphs and presentation of mass spectra, OriginPro 2021 (OriginLab Corporation) was used. Representations of structural γ-secretase models were prepared with PyMOL (Schrödinger, New York, NY, USA) or VMD (University of Illinois, Champaign, IL, USA). Figures were assembled using Adobe Illustrator CS6 (Adobe, San José, CA, USA).

# 4 Results

## 4.1 The cleavage efficiency of PS1 and PS2

One major aspect of this study was the investigation of the enzyme activity of γ-secretase harboring either one of the naturally occurring PS homologs PS1 and PS2, or chimeric constructs of both. Several previous studies have analyzed the cleavage activity of the homologs *in vitro* and *in cellulo*. While some studies found PS1 to show a higher APP substrate cleavage efficiency compared to PS2 [209, 224, 226, 227], some others showed comparable or even higher activity levels of PS2 [206, 208, 216]. To shed further light on the differences between PS1 and PS2, their activity was tested here in a well-established *in vitro* assay [80]. For this, HEK293/sw PS1/2 $^{-/-}$ dKO cells [237] were used as parental cell line. These cells express human APP carrying the Swedish mutation (APPsw), which is preferentially cleaved by BACE-1 [245]. This facilitates the analysis of Aβ peptides from conditioned media due to higher amounts of the γ-secretase substrate C99. Furthermore, transfection of cells harboring knock-outs of endogenous PS1 and PS2 enabled the analysis of PS activity without endogenous protein levels that might have obscured previous analyzes cited above. In general, this study focused on the analysis of pooled transfectants. By this, possible artefacts mediated by individual cell clone expression levels were circumvented.

The first objective of this thesis was to compare the cleavage efficiency of PS1- and PS2-containing γ-secretase complexes in the double knock-out background to resolve the question of whether the activity of γ-secretase is higher with PS1 or PS2. To this end, CHAPSO-solubilized membrane fractions of pooled clones of the transfected cells were subjected to analysis of *in vitro* activities. CHAPSO was chosen as the detergent since CHAPSO-solubilized γ-secretase components were previously shown to remain associated and in an active conformation [80] and display robust activity with physiological cleavage specificity [75]. The proteolytic activity was measured by analysis of cleavage products from C100, the recombinant variant of C99. We reasoned that if differences in the proteolytic overall activity of the two homologs could be

confirmed, non-homologous domains in the catalytic subunit could be identified as PS domains specifying cleavage efficiency.

### 4.1.1 The NTF largely accounts for the higher *in vitro* activity of PS1

The initial experiments aimed at the activity of the two wildtype homologs. For this, HEK293/sw PS1/2 $^{-/-}$ dKO cells [237] were stably transfected with either PS1 or PS2. The analysis of *in vitro* C100 cleavage was chosen as *in cellulo* analysis of γ-secretase activity has different limitations. First, PS1 and PS2 are known to reside in different cellular compartments, with PS2 being prominently distributed in LE and LYS compared to the localization of PS1 at the plasma membrane [209, 210]. Thus, the differential localization could influence cleavage activity *in cellulo*. Second, the AICD rather than the Aβ production was of particular interest as it directly reflects the initial cleavage activity of the complexes. However, intracellular AICD is rapidly removed by proteolysis [64] which complicates its analysis from whole cell lysates. For this reason, the *in vitro* analysis helped to avoid effects of differential localization or product instability.

Thus, for measuring the enzyme activity, a well-established *in vitro* assay using CHAPSO-solubilized membrane fractions and a recombinant C100-$His_6$ substrate was performed [80]. The samples were analyzed on Tris-tricine gradient gels [239] to allow the simultaneous analysis of larger (e.g. NCT) and smaller proteins (AICD) after immunoblotting. AICD generation was assessed by measuring the chemiluminescence intensity of the respective protein bands with a Western Blot imager. Difficulties with different expression levels of complex partners by the individual cell lines were circumvented by normalizing signals of generated cleavage products to the ones of the active enzyme complex. As full glycosylation of NCT to its mature form $NCT_m$ occurs last during complex formation [131], $NCT_m$ intensities were chosen as a measure for the active enzyme complex. After normalizing the quantified signal of AICD bands to the signal obtained for $NCT_m$, the respective activity levels were set in relation to PS1 activity (100%) (Figure 8A-B). In direct comparison to PS1, PS2 showed a significantly lower cleavage activity, reaching only a level of 22% of PS1 activity.

These findings support previous results reporting a higher PS1 activity *in vitro* [224, 227].

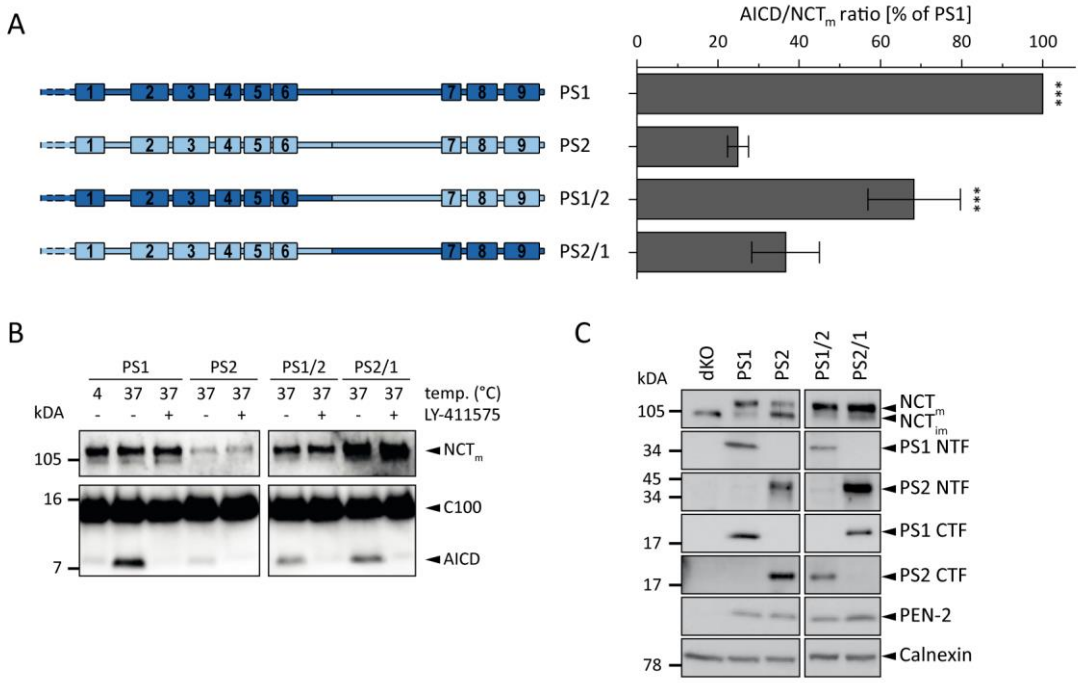


**Figure 8: *In vitro* activity of PS1, PS2, and PS NTF/CTF chimeras. A)** Schematic representation of the transfected constructs (left). PS1 and PS2 are depicted in dark blue or light blue, respectively. The *in vitro* activity was analyzed in CHAPSO-solubilized membrane fractions containing the different γ-secretase complexes using recombinant C100-$His_6$ as substrate (right). Newly generated AICD was quantified by measuring the respective ECL signal intensities on immunoblots using a Western Blot imaging system. The obtained signal intensities of AICDs are normalized to those of $NCT_m$. Normalized AICD levels are shown relative to the level generated by PS1. **B)** Representative immunoblots used for AICD and $NCT_m$ quantification from *in vitro* assays. AICD production was analyzed in the absence or presence of the γ-secretase inhibitor LY-411575. **C)** Analysis of whole cell lysates confirmed that all individual γ-secretase complexes underwent normal complex maturation (as represented by the presence of PEN-2, $NCT_m$, and the endoproteolytically cleaved PS NTF and CTF). Calnexin amounts were analyzed to compare total protein concentrations of the cell lysates. Data in **A)** represent means ± SEM, n = 3-4. Asterisks indicate the significance (one-way ANOVA with Dunnett's post test) of the differences between each presenilin variant and PS2 (***$p < 0.001$).

To exclude the possibility that differences in activity were caused by an impaired biogenesis of the γ-secretase subunits, cell lysates were checked for correct expression, assembly, and maturation of the γ-secretase complexes (Figure 8C). In contrast to the untransfected control, both PS1 and PS2 transfected cells showed fully glycosylated NCT, however, the levels of immature NCT were higher for PS2- compared to PS1-containing γ-secretase. Besides this, presence of PEN-2 and efficient PS endoproteolysis that resulted in the respective NTF and CTF of the catalytic subunit revealed appropriate complex maturation of γ-secretase containing either of the wildtype homologs.

After confirming that PS1 shows a higher proteolytic activity *in vitro*, chimeric PS variants were created, containing either the PS1 NTF and the PS2 CTF (PS1/2), or vice versa (PS2/1), to shed further light on the functional role of both fragments. The endoproteolytic cleavage site served as the natural border between the NTF and the CTF sequence. Detailed information for the individual constructs are listed in (3.1.2, Table 4). CHAPSO-solubilized membrane fractions were prepared from pools of HEK293/sw PS1/2 $^{-/-}$ dKO cells stably expressing the PS NTF/CTF constructs (Figure 8A left). The following *in vitro* measurements revealed the higher importance of the PS NTF for the proteolytic activity (Figure 8A-B). In line with previous studies [210, 226, 231], both chimeric complexes showed normal complex maturation and underwent endoproteolytic cleavage forming the desired PS NTF and CTF combinations (Figure 8C). When analyzed *in vitro*, PS1/2 was sufficient to raise the activity of PS2 to 68% of the PS1 level. Interestingly, also PS2/1 enhanced the activity of PS2; however, only to a smaller extent (37% of PS1 activity) (Figure 8A-B). These observations support results by Strömberg *et al.* [226] showing the bigger importance of the PS NTF for cleavage activity and marked it as highly interesting for further experiments.

### 4.1.2 Subdomains in the PS NTF are important for the activity

In the experimental design of this study a gain of function was considered more meaningful compared to a loss or reduction of function, as the latter can have multiple causes. Hence, this thesis aimed to specify regions within the homologs that can transfer the higher activity from PS1 to PS2. For this reason, all following constructs were based on the PS2 template while substituting different regions by the corresponding ones of PS1. For the following experiments, the Greek letter “ρ” marks the sections that were transferred from PS1 to the PS2 backbone.

The promising results obtained with the PS1/2 construct led to the question which subdomains within the PS NTF show the highest impact on the proteolytic activity. To answer this, the PS NTF was further partitioned into smaller regions for analysis.

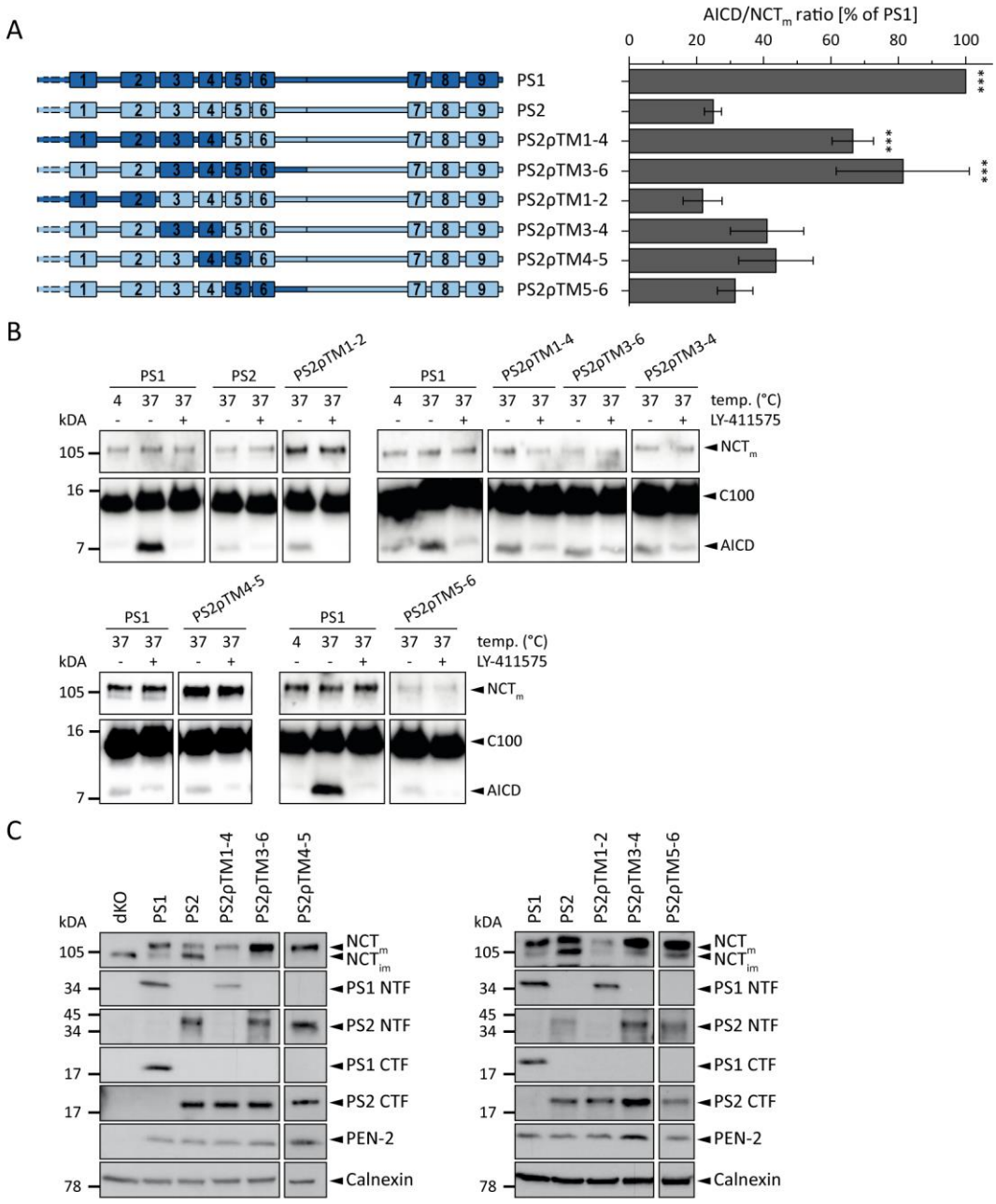


**Figure 9: Substitution of PS2 NTF subdomains can raise the *in vitro* activity. A)** Schematic representation of the transfected constructs (left). PS1 and PS2 are depicted in dark blue or light blue, respectively. The *in vitro* activity was analyzed in CHAPSO-solubilized membrane fractions containing the different γ-secretase complexes using recombinant C100-$His_6$ as a substrate (right). Newly generated AICD was quantified by measuring the respective ECL signal intensities on immunoblots using a Western Blot imaging system. The obtained signal intensities of AICDs were normalized to signals of $NCT_m$. Normalized AICD levels are expressed relative to the level generated by PS1. **B)** Representative immunoblots used for AICD and $NCT_m$ quantification from *in vitro* assays. AICD/$NCT_m$ generation was normalized to PS1 activity for each experiment. Repeated freeze-thaw cycles affected the inhibitor stability resulting in incomplete inhibition of γ-secretase activity in some experiments. **C)** Complex maturation was verified by immunoblot analysis of the complex partners PEN-2, $NCT_m$, and the endoproteolytic PS cleavage products from cell lysates. The parental cell line (dKO) served as control. PS1 and PS2 controls are included for each test. Due to experimental setup the controls of the left blot are reproduced from Figure 8. Calnexin signals were analyzed to compare total protein concentrations of the cell lysates. Data in **A)** represent means ± SEM, n = 2-8 (PS2ρTM1-4: 4, PS2ρTM3-6: 3, PS2ρTM1-2: 6, PS2ρTM3-4: 8, PS2ρTM4-5: 5, PS2ρTM5-6: 2). Asterisks indicate the significance (one-way ANOVA with Dunnett's post test) of the differences between each presenilin variant and PS2 (***$p < 0.001$).

In the first step, PS2 constructs with the PS1 TMDs one to four (PS2ρTM1-4) or three to six (PS2ρTM3-6) were analyzed *in vitro* (Figure 9A left). Both variants were able to raise the activity of PS2 to a comparable extent as the complete NTF replacement (PS1/2), reaching 67% and 81% of the PS1 activity, for PS2ρTM1-4 and PS2ρTM3-6, respectively (Figure 9A). As both substitutions overlapped at the TMDs 3 and 4, it was interesting to know, how the exchange of this TMD combination (PS2ρTM3-4) affects the PS2 activity. In order to scan the complete PS NTF for important neighboring TMD combinations, the pairs TMD1-2 and TMD5-6 were also swapped and analyzed (PS2ρTM1-2 and PS2ρTM5-6, respectively). As the γ-secretase complex containing PS2ρTM3-6 showed a higher proteolytic activity than PS2ρTM1-4, the substitution of TMD4-5 (PS2ρTM4-5) was also added to the set of experiments.

While PS2ρTM1-2 and PS2ρTM5-6 showed no increase in activity, the exchange of the TMD pairs in PS2ρTM3-4 and PS2ρTM4-5 enhanced the proteolytic activity to around 40% of PS1 (Figure 9A-B), however without statistical significance. Despite this remarkable increase, the high proteolytic activity caused by the more extended domain swaps could not be reached. The presence of mature complex partners confirmed that effects on γ-secretase activity originated from the chimeric subunits and were not majorly influenced by impaired complex formation (Figure 9C). It should be noted, however, that $NTC_m$ levels were lower for γ-secretase containing PS2ρTM1-2 compared to the other PS variants, despite comparable PS NTF and CTF levels.

### 4.1.3 The influence of promising NTF and CTF TMD combinations on C100 processing

There is still little knowledge of the mechanisms underlying the higher activity of PS1 compared to PS2. One possibility is that PS1 provides a stronger substrate recruitment or more efficient entry of C100, leading to a quicker substrate turnover. Another one is the optimized positioning of the substrate at the active site. This chapter therefore exploits previous results on the role of different TMDs on PS-substrate interaction. For this, combinations of TMDs in the NTF and CTF

were substituted in the PS2 template. The two catalytic aspartic residues, D257 and D385 of PS1 (residues D263 and D366 of PS2), are located on TMD6 and TMD7, respectively [32, 83]. Surprisingly, the substitutions containing the catalytic site in PS2ρTM6-7 did not improve the proteolytic *in vitro* activity compared to the PS2-containing γ-secretase (Figure 10A-B).

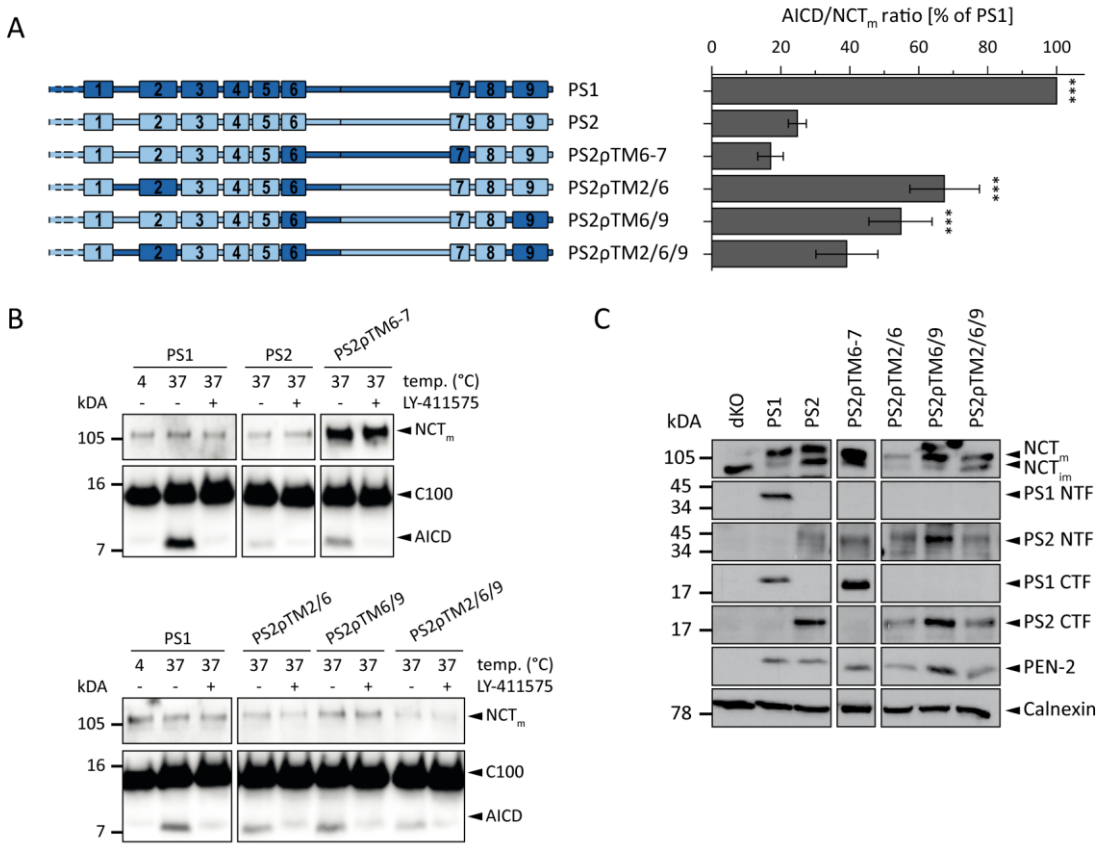


**Figure 10: *In vitro* activity of PS2 variants containing NTF and CTF TMD combinations. A)** Schematic representation of the transfected constructs (left). PS1 and PS2 are depicted in dark blue or light blue, respectively. The *in vitro* activity was analyzed in CHAPSO-solubilized membrane fractions containing the different γ-secretase complexes using recombinant C100-$His_6$ as a substrate (right). Newly generated AICD was quantified by measuring the respective ECL signal intensities on immunoblots using a Western Blot imaging system. The obtained signal intensities of AICDs were normalized to signals of $NCT_m$. Normalized AICD levels are expressed relative to the level generated by PS1. **B)** Representative immunoblots used for AICD and $NCT_m$ quantification from *in vitro* assays. AICD/$NCT_m$ generation was normalized to PS1 activity for each experiment. In consequence of experimental design, wild type controls of PS2ρTM6-7 are identical with Figure 9. Repeated freeze-thaw cycles affected the inhibitor stability resulting in incomplete inhibition of γ-secretase activity in some experiments. **C)** Appropriate complex maturation was verified by immunoblot analysis of the complex partners PEN-2, $NCT_m$, and the endoproteolytic PS cleavage products from cell lysates. PS1 and PS2 controls are included for each test and are identical to Figure 9 due to experimental setup. Calnexin signals were analyzed to compare total protein concentrations of the cell lysates. Data in **A)** represent means ± SEM, n = 6-11 (PS2ρTM6-7: 6, PS2ρTM2/6: 11, PS2ρTM6/9: 11, PS2ρTM2/6/9: 10). Asterisks indicate the significance (one-way ANOVA with Dunnett's post test) of the differences between each presenilin variant and PS2 (***$p < 0.001$).

Also, putative initial substrate binding and entry sites were tested for their effect on PS activity. The TMDs 2, 6, and 9 are located on the same side of the horseshoe-shaped complex and their potential involvement in initial substrate

encounter or entry of C99 have been proposed before [163, 165, 168, 171]. PS2 variants with pairwise substitution of these TMDs (PS2ρTM2/6 and PS2ρTM6/9) as well as the combination of all three (PS2ρTM2/6/9), were created to test their effect on the activity difference between PS1 and PS2 (Figure 10A left). Exchanging these TMDs resulted in a significant increase of substrate cleavage. The biggest effect was seen for PS2ρTM2/6 reaching 68% of the PS1 activity level, which was comparable to that of PS2ρTM1-4 and PS2ρTM3-6 (Figure 10A). Surprisingly, while PS2ρTM6/9 activity reached 55% of PS1, the substitution of all three TMDs resulted in a smaller increase to the level of 39%.

In construct design, non-conserved residues within the neighboring loops of the respective TMDs were included in the substitution (Table 4). In case of TMD6 exchanges without TMD7, substitutions included the long intracellular loop up to the endoproteolytic cleavage site after position M298 (PS2 numbering) (Figure 10A left) [246, 247]. All chimeric constructs showed maturation of the γ-secretase components, however, with variations in the expression levels of the different subunits (Figure 10C). Overall, these results suggest the involvement of the region around the TMDs 2, 6, and 9 in intramembrane proteolysis, hence influencing the different activities between PS1 and PS2.

### 4.1.4 The impact of single TMD swaps on substrate turnover

So far, the data demonstrated that exchanges of larger domains or defined combinations of PS1 TMDs could increase the proteolytic activity in the PS2 template. Now, the question arose, whether single TMDs can be identified that determine the different cleavage efficiency of the homologs. For this, chimeric PS variants with single TMD substitutions were created. If the flanking loops of the TMDs contained residues that were not conserved between the two wildtype PS (Figure 7), they were swapped together with the respective TMDs (Figure 11A left, Table 4).

TMDs 1 and 7 were excluded from the set of single TMD exchanges, since neither TMD1 nor TMD7 showed an effect on the activity levels in the context of PS2ρTM1-2 or PS2ρTM6-7, respectively.

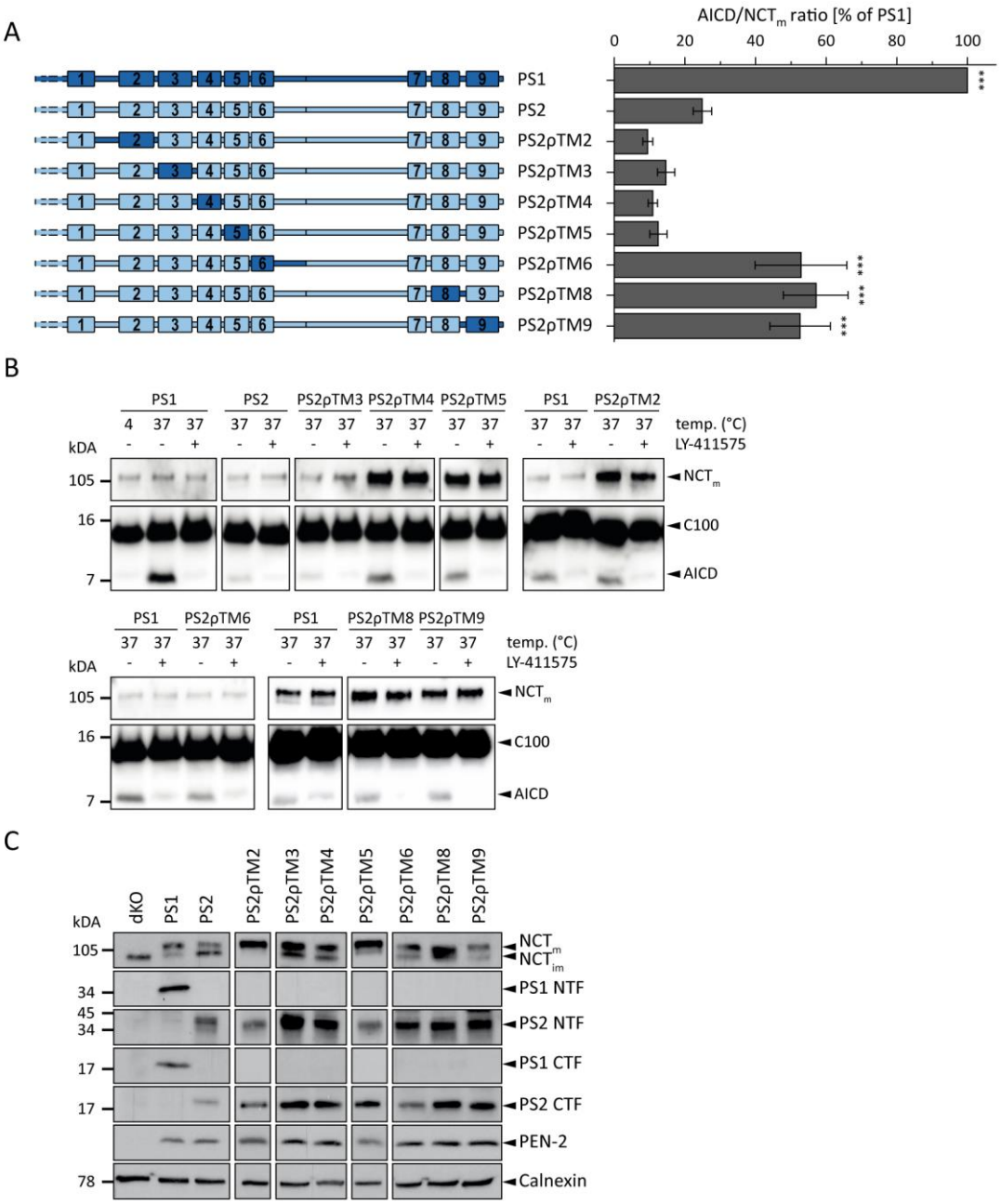


**Figure 11: Impact of single TMD substitutions on the *in vitro* activity of PS2. A)** Schematic representation of the transfected constructs (left). PS1 and PS2 are depicted in dark blue or light blue, respectively. The *in vitro* activity was analyzed in CHAPSO-solubilized membrane fractions containing the different γ-secretase complexes using recombinant C100-$His_6$ as a substrate (right). Newly generated AICD was quantified by measuring the respective ECL signal intensities on immunoblots using a Western Blot imaging system. The obtained signal intensities of AICDs were normalized to signals of $NCT_m$. Normalized AICD levels are expressed relative to the level generated by PS1. **B)** Representative immunoblots used for AICD and $NCT_m$ quantification from *in vitro* assays. For accurate comparison of PS activity, the PS1 control is displayed for the individual experiments. Due to experimental setup, wildtype controls are identical to previous figures for the following PS2 variants: PS2ρTM2 – Figure 9B (PS2ρTM1-4 blot); PS2ρTM3 blot – Figure 9B (PS2ρTM1-2 blot); PS2ρTM6 blot – Figure 10B (PS2ρTM2/6 blot); PS2ρTM8 blot – Figure 9B (PS2ρTM4-5blot). Repeated freeze-thaw cycles affected the inhibitor stability resulting in incomplete inhibition of γ-secretase activity in some experiments. **C)** Appropriate complex maturation was verified by immunoblot analysis of the complex partners PEN-2, $NCT_m$, and the endoproteolytic PS cleavage products from cell lysates. Calnexin signals facilitated the comparison of total protein amounts in the cell lysates. Data in **A)** represent means ± SEM, n = 5-9 (PS2ρTM2: 5, PS2ρTM3: 6, PS2ρTM4: 6, PS2ρTM5: 6, PS2ρTM6: 9, PS2ρTM8: 8, PS2ρTM9: 8). Asterisks indicate the significance (one-way ANOVA with Dunnett's post test) of the differences between each presenilin variant and PS2 (***$p < 0.001$).

All other TMDs showed a functional role in either one or several of the previously tested TMD combinations, and thus were chosen for further analysis.

Among the TMD substitutions within the PS NTF, the single exchange of TMD6 (PS2ρTM6) was able to enhance the activity of PS2 to a level of 52% compared to PS1 (Figure 11A-B). By this, PS2ρTM6 almost reached the same level as the complete NTF substitution in PS1/2 (Figure 8A). Thus, the effects seen for PS2ρTM2/6, PS2ρTM6/9, and PS2ρTM2/6/9 can largely be attributed to the exchanged TMD6. In contrast to this, substitutions of other TMDs in the NTF led to no increase, but rather a minor reduction in C100 cleavage compared to PS2 (Figure 11). Considering the increased activity seen for PS2ρTM3-4 (41%) and PS2ρTM4-5 (44%), these results suggest cooperation of the respective TMDs in defining cleavage activity.

Interestingly, single exchanges of the TMDs 8 and 9 led to a similar increase in activity as PS2ρTM6, with PS2ρTM8 reaching 57% and PS2ρTM9 53% of PS1 activity (Figure 11A-B). By that, they both exceeded the activity mediated by the complete PS1 CTF in the context of PS2/1 (Figure 8A). All transfected PS variants showed the presence of PEN-2, NCT maturation and endoproteolytic PS cleavage indicating appropriate complex formation (Figure 11C). Hence, the observed cleavage activities were not influenced by variations in complex maturation.

### 4.1.5 Importance of hydrophobic domains for the activity of PS

The previous findings showed that the higher activity of PS1 over PS2 could be mapped to a few single TMDs or combinations of them. However, with the exception of PS2ρTM8, flanking loop regions were exchanged together with the TMDs (see 3.1.2, Table 4). To distinguish whether the hydrophobic domains are responsible for the increase in activity or act in combination with the hydrophilic regions, three additional PS variants were tested where only the hydrophobic membrane-spanning TMDs were substituted. In the first construct, all TMDs were exchanged with only the hydrophilic loops of the PS2 template being maintained (PS2-All-PS1TMDs). The other two chimera, PS2-NTF-PS1TMDs

and PS2-CTF-PS1TMDs, contained substitutions of all TMDs in the NTF or CTF, respectively. All individual PS variants retained γ-secretase activity and were able to undergo normal complex formation (Figure 12).

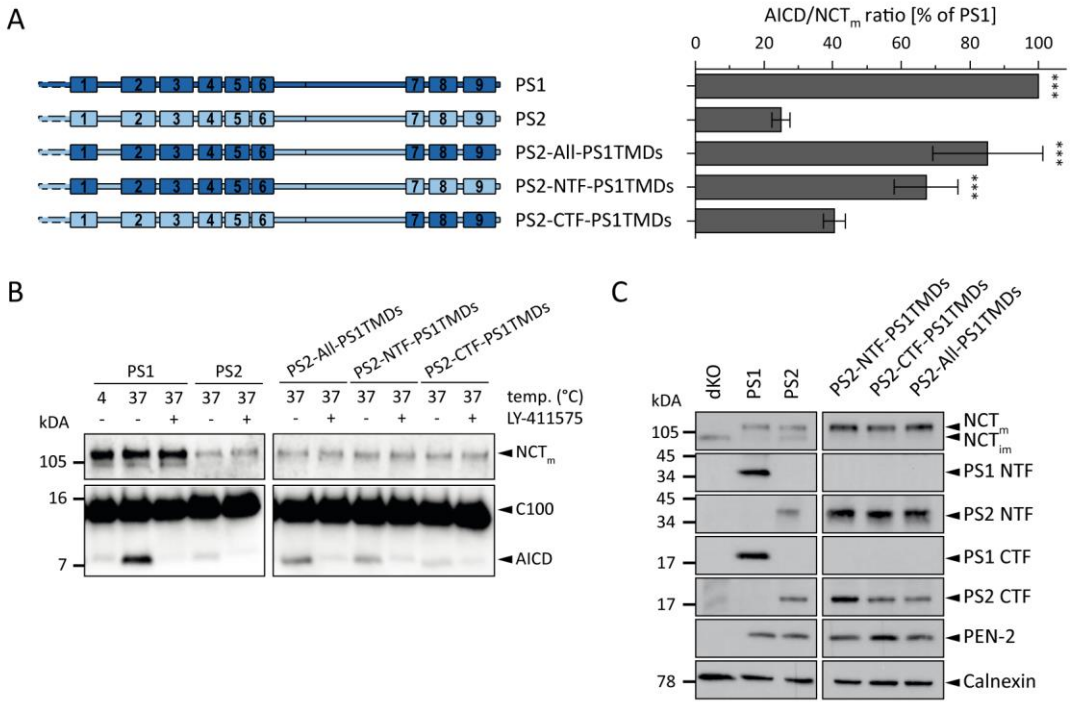


**Figure 12: The hydrophobic domains of PS are the main driver for the differential activity. A)** Schematic representation of the transfected constructs (left). PS1 and PS2 are depicted in dark blue or light blue, respectively. The *in vitro* activity was analyzed in CHAPSO-solubilized membrane fractions containing the different γ-secretase complexes using recombinant C100-$His_6$ as a substrate (right). Newly generated AICD was quantified by measuring the respective ECL signal intensities on immunoblots using a Western Blot imaging system. The obtained signal intensities of AICDs are normalized to signals of $NCT_m$. Normalized AICD levels are expressed relative to the level generated by PS1. **B)** Representative immunoblots used for AICD and $NCT_m$ quantification from *in vitro* assays. In consequence of experimental design, wildtype controls were identical Figure 8B. Repeated freeze-thaw cycles affected the inhibitor stability resulting in incomplete inhibition of γ-secretase activity in some experiments. **C)** Appropriate complex maturation was verified by immunoblot analysis of the complex partners PEN-2, $NCT_m$, and the endoproteolytic PS cleavage products from cell lysates. Calnexin signals facilitated the comparison of total protein amounts in the cell lysates. Data in **A)** are represented as means ± SEM, n = 7-9 (PS2-All-PS1TMDs: 9, PS2-NTF-PS1TMDs: 8, PS2-CTF-PS1TMDs: 7). Asterisks indicate the significance (one-way ANOVA with Dunnett's post test) of the differences between each presenilin variant and PS2 (***$p < 0.001$).

Analysis of the *in vitro* activity showed that the substitution of all PS2 TMDs led to an activity level of 85% of PS1. This indicates that the TMDs alone account for most of the differences between PS1 and PS2. In line with this are the results obtained for PS2-NTF-PS1TMDs (67% PS1) and PS2-CTF-PS1TMDs (40% PS1) (Figure 12A). The latter constructs mimicked almost perfectly the increases in proteolytic activity mediated by the NTF/CTF chimera PS1/2 and PS2/1 (Figure 8). The data indicate that the determinants for the activity difference

between PS1 and PS2 are located within the hydrophobic TMDs that span the lipid bilayer.

### 4.1.6 The PS variants generate comparable amounts of Aβ and AICD

Up to this point, the initial cleavage of C100 assessed by measuring the AICD production was taken as a measure for the cleavage efficiency of the different γ-secretase complexes. Previous studies showed that cleavage of C99 leads to an equimolar production of AICD and Aβ [181, 182]. Nevertheless, to further validate the results gained from the AICD analysis, Aβ production in the *in vitro* assays was measured in parallel. Similar to the AICDs, the generated $Aβ_{total}$, the sum of all individual Aβ peptides, was analyzed via SDS-PAGE with subsequent immunoblotting. Chemiluminescence intensity of the $Aβ_{total}$ bands was further normalized to the signal obtained for $NCT_m$ and set in relation to PS1 activity.

Overall, the results were in line with the AICD measurements for the majority of the PS variants (Figure 13). Both, the PS1 NTF and CTF were able to mediate an enhanced Aβ generation in the respective PS1/2 and PS2/1 constructs, compared to PS2. In particular, the PS1/2 construct almost reached the PS1 activity level. However, this difference should be regarded with care as the variance of PS1/2 Aβ measurements was relatively high. In addition to this, the importance of the TMDs for the higher activity of PS1 could be confirmed as seen for the PS2 variants where only the hydrophobic domains were exchanged (Figure 13).

Surprisingly, while PS2ρTM3-6 showed comparable Aβ and AICD production, PS2ρTM1-4 failed to increase Aβ levels to the same extent as the one of the AICDs. The data revealed only a modest increase to around 33% of PS1 compared to 67% for the AICDs (Figure 13). However, it should be taken in consideration that the sample size of n = 2 for PS2ρTM1-4 Aβ measurement is insufficient for reliable statements. Hence, further replicates are needed to confirm this observation.

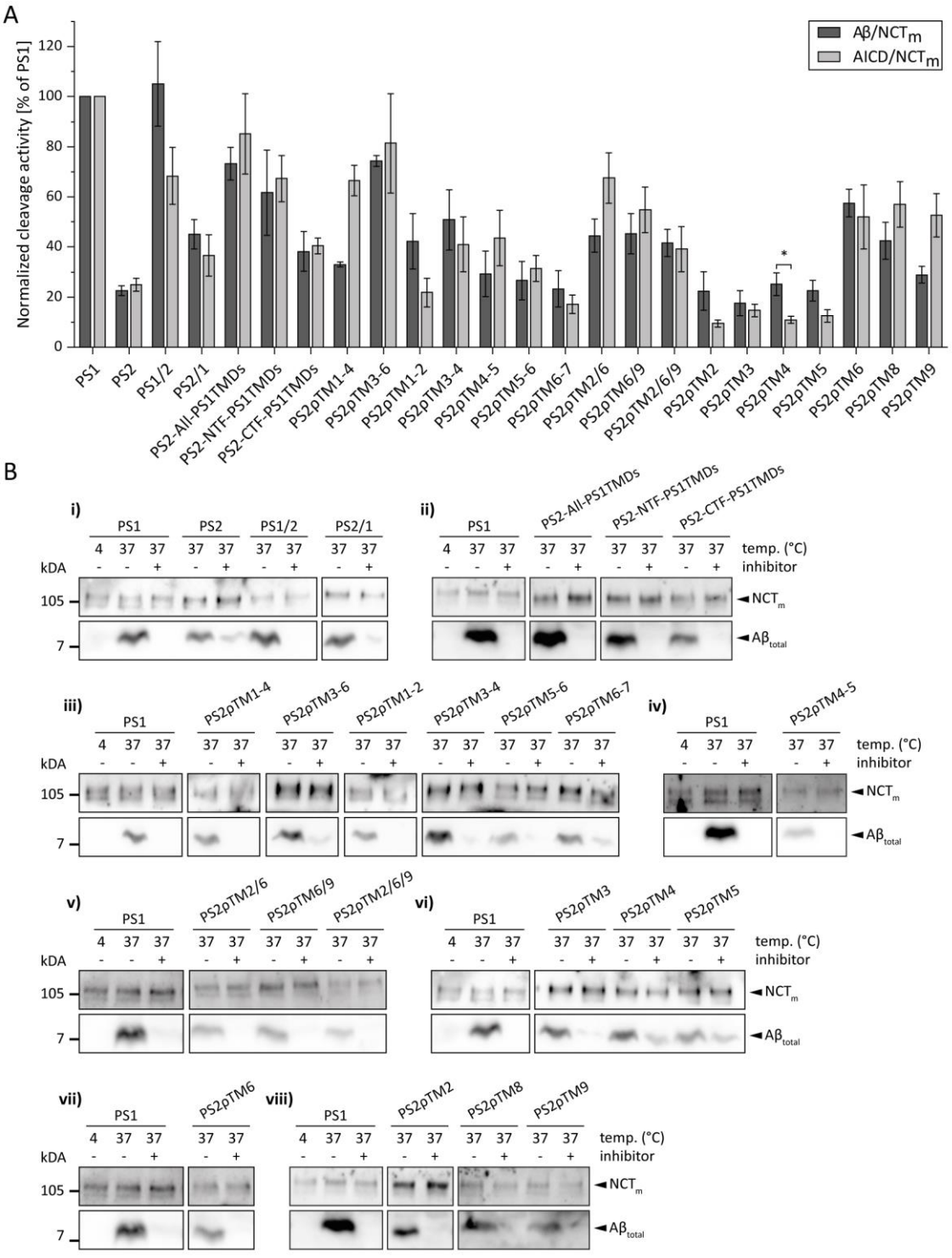


**Figure 13: Comparison of *in vitro* activity measured by AICD and Aβ production. A)** *In vitro* generated AICD or Aβ were quantified by measuring the respective ECL signal intensities on immunoblots. Intensities are normalized to signals of $NCT_m$ and expressed relative to the level of PS1. **B)** Representative immunoblots of Aβ production by the individual γ-secretase complexes from CHAPSO *in vitro* assays. For accurate comparison of Aβ generation, the PS1 control is displayed for the individual experiments. Owing to experimental setup, wildtype controls are identical for the blots i) and vi), ii) and viii, v) and vii). Repeated freeze-thaw cycles affected inhibitor stability resulting in incomplete inhibition of γ-secretase activity in some experiments. Data in **A)** are represented as means ± SEM, AICD: n = 3-11; (Exception: PS2ρTM4-5 n = 2); Aβ: n = 3-11 (Exception: PS2ρTM1-4 n = 2). PS1 and PS2 controls were analyzed in parallel in all experiments. Student's T-tests were performed to evaluate differences between Aβ and AICD levels of each PS variant. Due to their limited sample size, PS2ρTM1-4 and PS2ρTM4-5 were excluded from statistical analysis. Single asterisks denote statistical significance at the 0.05 confidence level.

The opposite effect, although not as dominant, could be seen for PS2ρTM1-2. There, the Aβ production was raised to around 42% of PS1 compared to only 22% for the AICD generation. However, Student's T-tests revealed no statistical significance for this difference. Furthermore, the small reduction of enzyme activity, as seen in the AICD measurements, could not be seen for Aβ in the single substitutions of TMD2, TMD3, TMD4, and TMD5 (Figure 13).

In this context, TMD4 AICD and Aβ production showed a statistically significant difference. Nevertheless, none of them could mediate a positive effect on enzyme activity, similar to the AICD analysis. For single TMD substitutions in the PS CTF, PS2ρTM8 showed comparable results for AICD and Aβ generation. In contrast to this, enzyme activity measured by Aβ generation was reduced for PS2ρTM9 compared to the AICD production, however, without statistical significance.

The predominant role of TMD6 in the NTF for enzyme activity, could be confirmed by measuring Aβ levels. Interestingly, the combination with additional TMD substitutions on the same side of the complex (PS2ρTM2/6, PS2ρTM6/9, and PS2ρTM2/6/9) did not further increase the Aβ production but remained on the same level as the single TMD6 substitution. Consistent with the AICD data, the positive effect mediated by TMD6 was again abolished by the combined substitutions in the variants PS2ρTM5-6 and PS2ρTM6-7 (Figure 13). Enzyme activities of the variants PS2ρTM3-4 and PS2ρTM4-5 were comparable for Aβ and AICD production, with Aβ production being slightly higher or lower for PS2ρTM3-4 and PS2ρTM4-5, respectively. Overall, the results of Aβ production provided comparable results to those of AICD generation.

## 4.2 The cleavage specificity of PS1 and PS2

After the identification of regions that are important for the overall activity of γ-secretase, this study aimed to investigate the relative amounts of the individual Aβ peptides produced by the PS variants. Recent mass spectrometric studies of immunoprecipitated Aβ revealed a different production of smaller Aβ peptides for PS1 and PS2. While cells expressing only PS1 generated higher relative

amounts of Aβ38 compared to the maternal cell line, PS2 showed a remarkable decrease in Aβ38 production [200]. This led to the question if the systematic analysis of the designed chimeric PS constructs can help to identify regions that are involved in the different Aβ processing.

### 4.2.1 IP-MS analyses reveal distinct Aβ production for PS1 and PS2

γ-Secretase cleavage in the endogenous lipid environments was preferred for investigating the identity of Aβ peptides and cleavage specificity to exclude possible detergent artefacts. Therefore, secreted individual Aβ species were analyzed from conditioned media by IP-MS analysis. To clarify whether PS1- and PS2-containing γ-secretase complexes show differences in the production of individual Aβ peptides, HEK293/sw PS1/2 $^{-/-}$ dKO cells were stably transfected with PS1 or PS2. The HEK293/sw cell line that naturally expresses both endogenous homologs served as a reference. Secreted Aβ peptides from conditioned media were subjected to immunoprecipitation with antibody 4G8 and subsequent MALDI-TOF MS analysis.

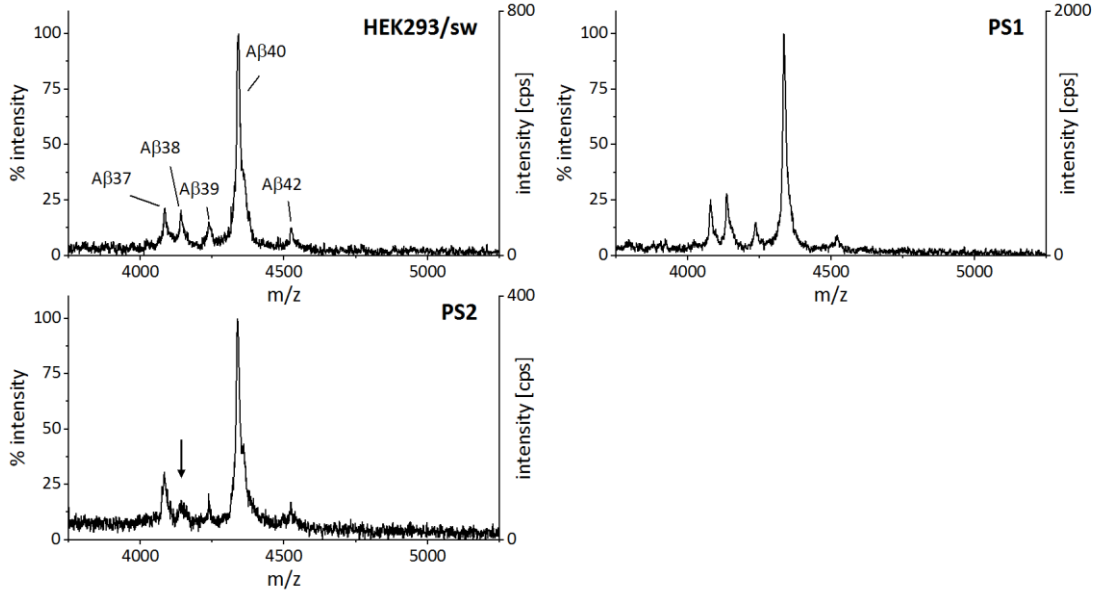


**Figure 14: PS1 and PS2 differ in Aβ37 and Aβ38 production.** Conditioned media of pooled clones of HEK293/sw PS1/2 $^{-/-}$ dKO stably transfected with PS1 or PS2 were collected. Total Aβ was analyzed by MALDI-TOF MS following immunoprecipitation with antibody 4G8 (final concentration 2.5 µg/mL). Aβ production by HEK293/sw cells was used as reference. The intensities of the highest peak were set to 100%. Additionally, the counts per second (cps) are shown on the right y-axis. The black arrow marks the decreased Aβ38 for the PS2 construct.

For all samples, Aβ40 was the most prominent peak with no differences between PS1 and PS2 concerning the production of Aβ42 or Aβ39 relative to Aβ40 (Figure 14). PS1-expressing cells produced similar amounts of Aβ37 and Aβ38 (Aβ37/Aβ40 = 0.28 and Aβ38/Aβ40 = 0.29, respectively) and thereby resembled the HEK293/sw control. For the following experiments this will be denoted the "PS1 phenotype". In contrast to this, for γ-secretase containing PS2 the Aβ38 production was drastically reduced to a Aβ38/Aβ40 ratio of 0.19 with an accompanying small increase of Aβ37/Aβ40 to 0.30 (= "PS2 phenotype") (Figure 14). These results support previous findings by Lessard *et al.* [206] who reported a reduced Aβ38 production by PS2.

### 4.2.2 TMDs in the PS NTF affect Aβ processing

Having shown that PS1 and PS2 did not only show differences in the extent of overall Aβ production but also the stepwise processing after ε-cleavage led to the question of whether this effect can be mapped to certain domains within the catalytic subunit. To answer this, the previously described NTF/CTF chimera, PS1/2 and PS2/1 (Figure 8A), were tested for their production of the distinct Aβ peptides. In parallel, the PS2 variants containing the non-conserved membrane-embedded domains of PS1 (PS2-All-PS1TMDs, PS2-NTF-PS1TMDs, PS2-CTF-PS1TMDs) (Figure 12A) were tested, in order to investigate the impact of the TMDs.

As already seen for the overall AICD and Aβ production, the NTF of PS is the main determinant for the different phenotypes in Aβ production (Figure 15). As the two wildtype PS mainly differed in their production of Aβ37 and Aβ38, the ratio of Aβ38/Aβ37 calculated from the peak intensities served as an additional measure to discriminate between the two phenotypes (Figure 16A). The presence of the PS1 NTF or the respective membrane embedded amino acids was sufficient to increase the Aβ38 production to a close to 1:1 ratio with Aβ37, as seen for the constructs PS1/2, PS2-All-PS1TMDs, and PS2-NTF-PS1TMDs.

Constructs with the PS2 NTF (PS2/1 and PS2-CTF-PS1TMDs), on the other hand, retained the PS2 phenotype. Hence, similar to the results of the overall

AICD and Aβ production (Figure 13), the hydrophobic domains in the PS NTF showed to be the major driver for the phenotype (Figure 15 and Figure 16A). Furthermore, an accumulation of larger Aβ species could not be observed in the measurements. To assess whether the individual PS variants show differences in the overall production of smaller Aβ peptides, the sum of Aβ37 and Aβ38 was set in relation to Aβ40 (Figure 16B).

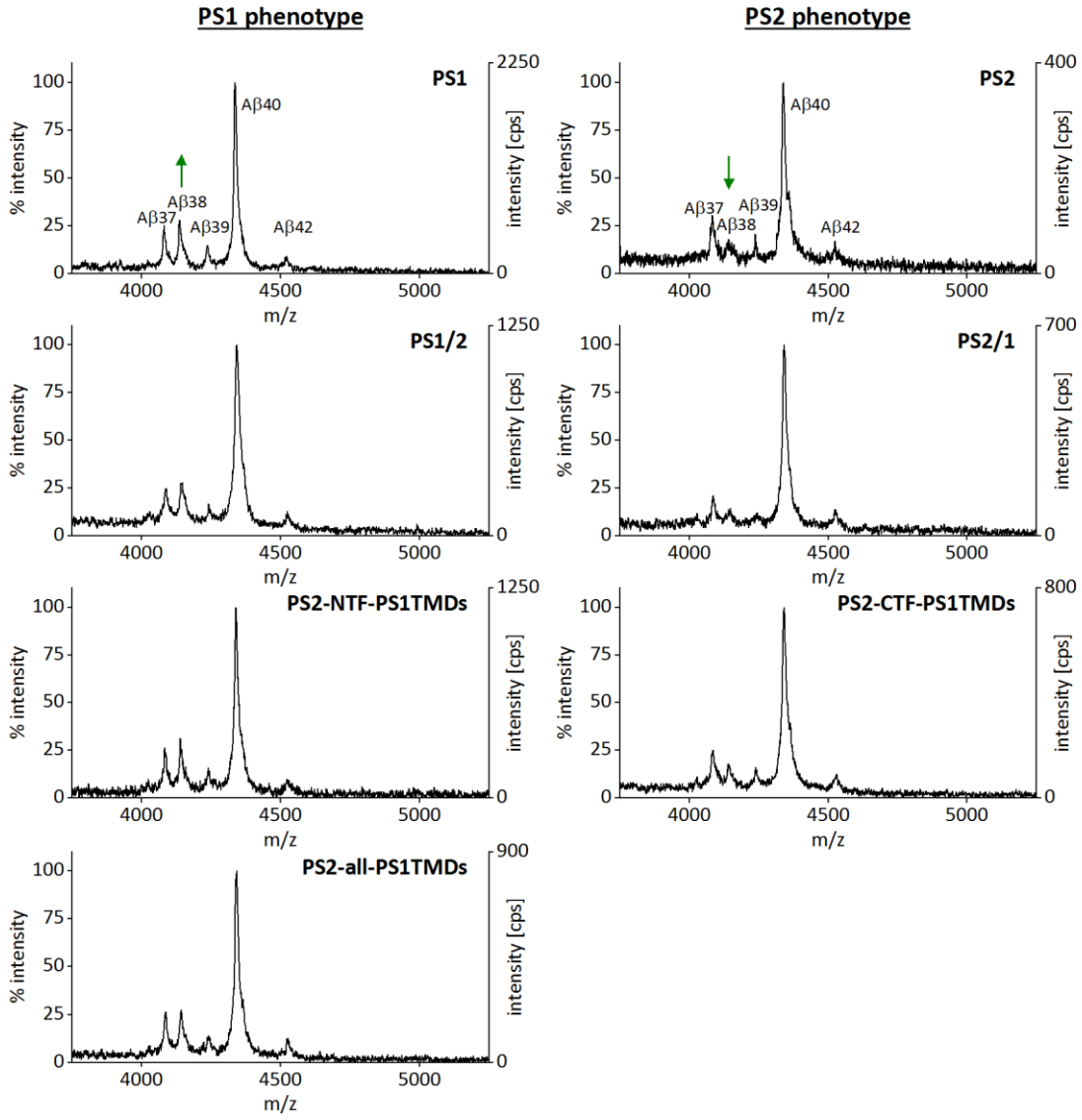


**Figure 15: The hydrophobic domains in the NTF mediate increased Aβ38 production.** Total Aβ from conditioned media was analyzed by MALDI-TOF MS following immunoprecipitation with antibody 4G8 (final concentration 2.5 µg/mL). The intensities of the highest peak were set to 100%. Additionally, the counts per second (cps) are shown on the right y-axis. Green arrows mark Aβ38. Results of the spectra are representatives of more than three independent experiments. Data for PS1 and PS2 are reproduced from Figure 14.

The (Aβ37+Aβ38)/Aβ40 ratio was comparable for most of the constructs, indicating that a reduction of Aβ38 generation is accompanied by a reciprocal

increase in Aβ37 production for the PS2 phenotype. However, PS variants with the PS1 CTF or only the CTF TMDs, revealed an impaired C-terminal trimming activity, although without statistical significance for PS2-CTF-PS1TMDs.

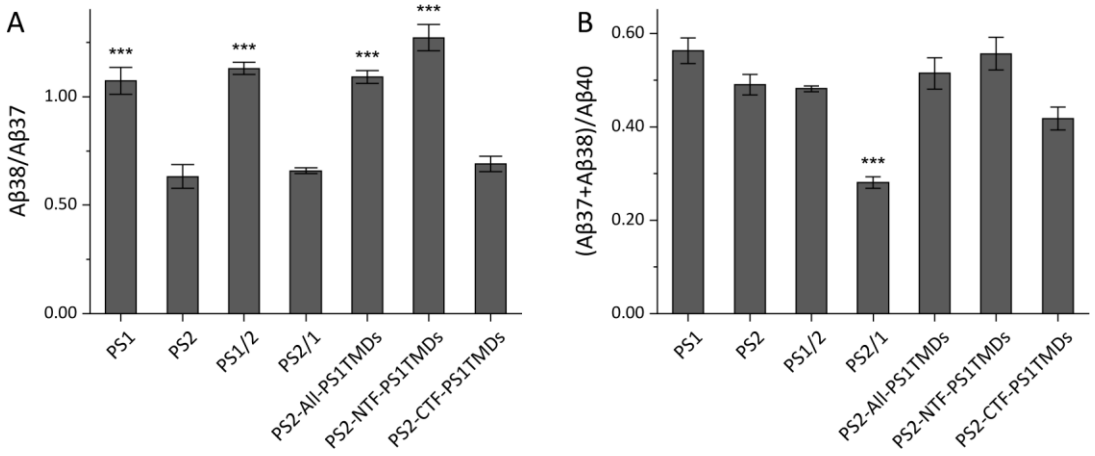


**Figure 16: Aβ38/Aβ37 ratios change upon substitution of hydrophobic domains in the PS NTF.** Aβ ratios were calculated with the respective peak intensities from IP-MS analyses. **A)** The Aβ38/Aβ37 ratio discriminated best between PS1 and PS2 phenotype. **B)** To assess the carboxypeptidase activity, the total amount of small peptides (Aβ37+Aβ38) was set in relation to the main species Aβ40. Means ± SEM, n = 3-4. Asterisks indicate the significance (one-way ANOVA with Dunnett's post test) of the differences between each presenilin variant and PS2 (***$p < 0.001$).

### 4.2.3 PS2ρTM3 reproduces the PS1 phenotype in Aβ production

The next experiments aimed to identify smaller regions within the NTF that are responsible for the phenotype. First, the Aβ production of PS2 variants containing the TMD substitutions PS2ρTM1-2, PS2ρTM1-4, or PS2ρTM3-6 (for graphical representation see Figure 9A) were examined. Interestingly, while PS2ρTM1-2 retained the PS2 phenotype, the other two were able to reproduce the PS1 phenotype (Figure 17, Figure 18A). As both constructs included TMD3 and TMD4, PS2ρTM3-4 and PS2ρTM4-5 were tested for their ability to alter substrate processing. In the IP-MS measurements, PS2ρTM4-5 resembled the PS2 phenotype, but with a small increase in the Aβ38/Aβ37 ratio. However, the exchange of TMD3-4 was enough to increase the Aβ38/Aβ37 ratio to a similar level as PS1, leading to the question if one of the TMDs can mediate the phenotype shift. The analyzed conditioned media of the single TMD3 swap showed that PS2ρTM3 was sufficed to reproduce the PS1 phenotype. Similar to

PS2ρTM4-5, PS2ρTM4 showed a minor increase in the Aβ38/Aβ37 ratio compared to PS2, thus resulting in a mixed phenotype.

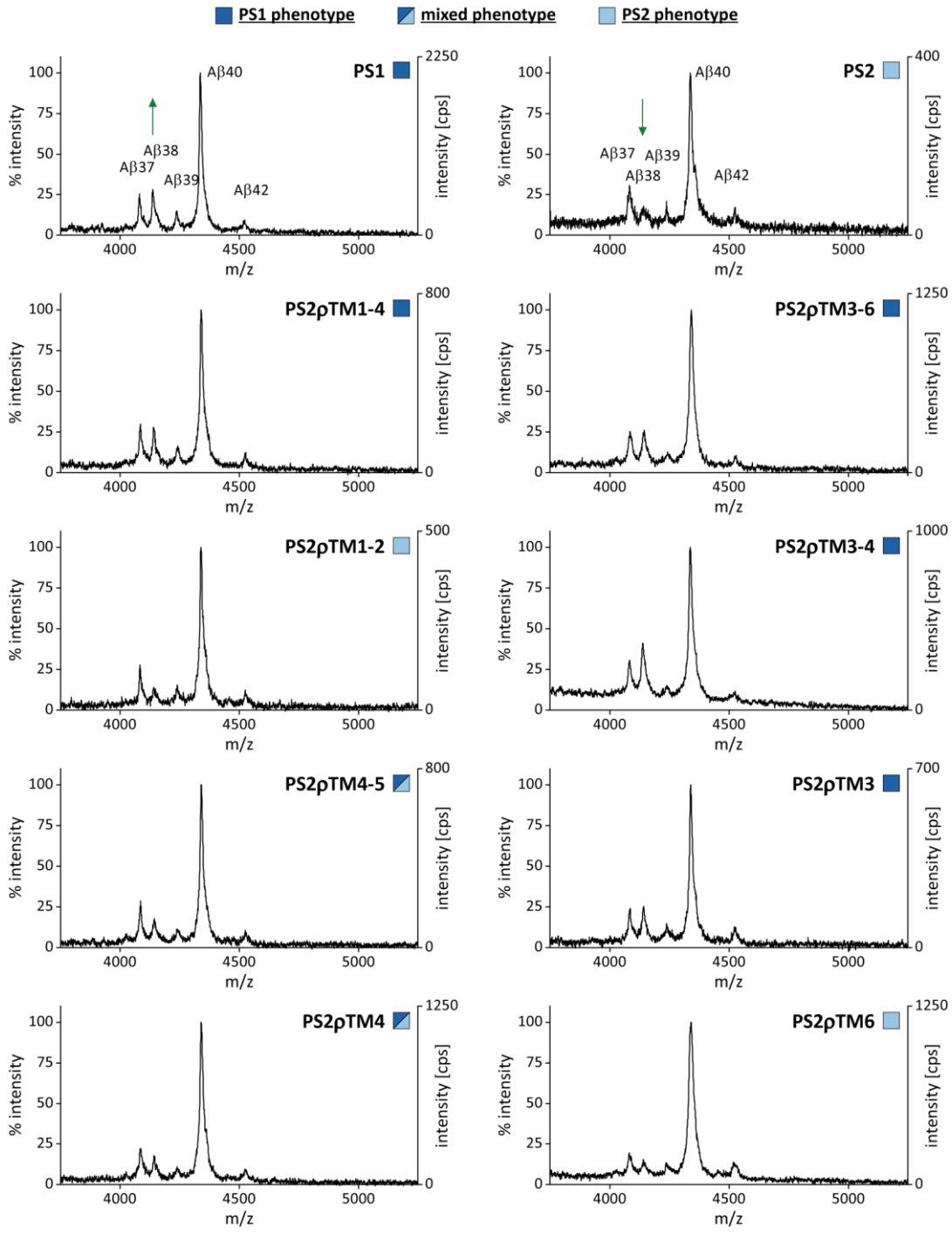


**Figure 17: Aβ generation by PS2ρTM3 resembles the PS1 phenotype.** Pooled clones of HEK293/sw PS1/2 $^{-/-}$ dKO stably transfected with the indicated PS constructs were investigated. Total Aβ was analyzed by MALDI-TOF MS following immunoprecipitation with antibody 4G8 (final concentration 2.5 µg/mL). The intensities of the highest peak were set to 100%. Additionally, the counts per second (cps) are shown on the right y-axis. Green arrows mark Aβ38 production. Results of the spectra are representatives of more than three independent experiments. The spectra were further categorized in PS1 phenotype (dark blue), PS2 phenotype (light blue), or mixed phenotype (mixed). Data for PS1 and PS2 are reproduced from Figure 14.

Since the single substitution of TMD6 showed a high impact on the overall proteolytic activity (Figure 11), the influence of this exchange on the processing phenotype was also tested. However, the IP-MS analysis showed that the substitution in PS2ρTM6 had no discernible effect on the Aβ38/Aβ37 ratio compared to PS2 (Figure 17, Figure 18A).

Surprisingly, the carboxypeptidase activity for the last cleavage steps seemed to be impaired for PS2ρTM6. Thus, the overall production of the smaller Aβ37 and Aβ38 peptides relative to Aβ40 was significantly reduced, compared to PS2 (Figure 18B). Since no increase in signal intensities of >Aβ42 peptides was visible in the spectra, longer precursors were predominantly processed to Aβ40. Unfortunately, due to the low Aβ42 production, no reliable Aβ42/Aβ40 could be calculated since the signals were often hard to discriminate from background noise. Nevertheless, judging from available spectra, no increased Aβ42 production could be observed for any of the tested samples.

In sum, the results nicely demonstrate that the substitution of PS2-TMD3 by the one of PS1 had a remarkable impact on Aβ processing resulting in an apparent phenotype shift from PS2 to PS1.

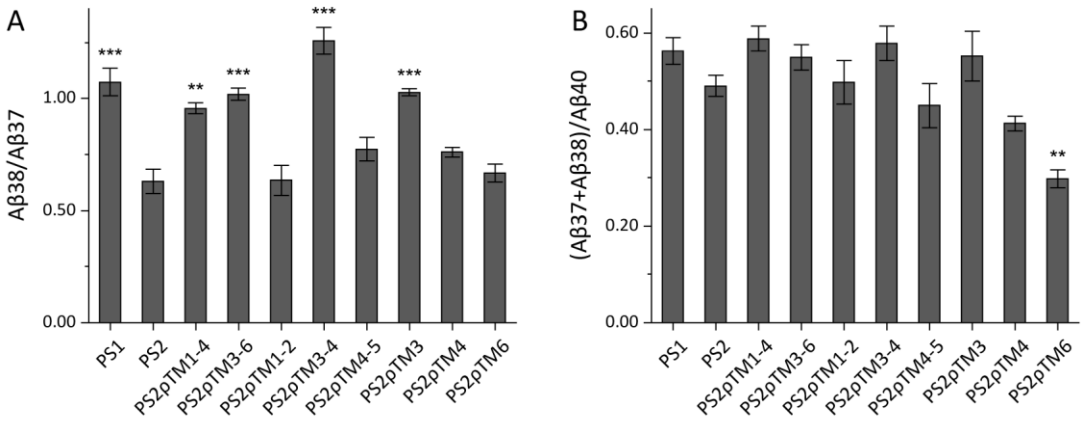


**Figure 18: TMD3 substitution reproduces a PS1-like Aβ38/Aβ37 ratio.** Aβ ratios were calculated with the respective peak intensities from IP-MS analyses. **A)** The Aβ38/Aβ37 ratio marks the difference between PS1 and PS2 phenotype. **B)** To show the carboxypeptidase activity for smaller Aβ species, the total amount of small peptides (Aβ37+Aβ38) was set in relation to the main species Aβ40. Means ± SEM, n = 3-4. Asterisks indicate the significance (one-way ANOVA with Dunnett's post test) of the differences between each presenilin variant and PS2 (**p < 0.01, ***p < 0.001).

### 4.2.4 Tris-bicine-urea gels confirm Aβ processing phenotypes

To confirm the results obtained from the IP-MS measurements, a subset of samples analyzed via MS was further subjected to immunoblot analysis. In the first set of experiments, samples of conditioned media were separated on 8% Tris-bicine SDS gels in the presence of 8 M urea [240]. This gel system has been reported to reliably discriminate between Aβ peptides of different lengths [248]. After immunoblotting with the antibody 2D8, PS1 clearly showed a higher Aβ38 production compared to Aβ37 (Figure 19A-B). This result can also be seen when the variant PS1/2, containing only the NTF of PS1, was present in the complex (Figure 19A). Unfortunately, due to lower amounts of total Aβ in the samples of PS2, Aβ peptides other than Aβ40 could hardly be detected before overexposure of other samples. This also applied to the PS2/1 sample, where the total Aβ concentration (Figure 13) was not sufficient for detailed analysis of smaller Aβ species.

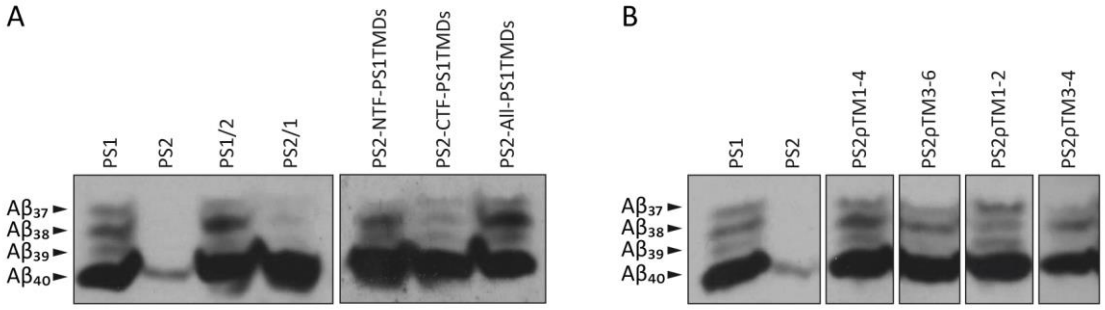


**Figure 19: Detection of individual Aβ species in conditioned media.** Individual Aβ species from conditioned media were separated via 8% Tris-bicine-urea SDS-PAGE and analyzed after immunoblotting using the antibody 2D8. **A)** Substitutions of the PS2 NTF or CTF, or the respective TMDs were analyzed for their impact on Aβ processing. **B)** Analysis of Aβ species from chimeric PS variants with smaller domain swaps in the PS NTF.

On the other hand, PS2 variants where only the TMDs were swapped, showed distinct patterns of Aβ production. PS2-based constructs that contained all TMDs of PS1 or only the ones in the NTF showed the higher Aβ38 production as seen for PS1. In contrast to this, the construct in which only the CTF TMDs were exchanged (PS2-CTF-PS1TMDs), showed a close to 1:1 ratio of Aβ37 and Aβ38. By this, PS2-CTF-PS1TMDs differed in Aβ production compared to PS1, which is in line with its PS2-like phenotype observed in the IP-MS measurement (Figure 15).

The results obtained by IP-MS analysis for smaller domain swaps could also be confirmed (Figure 19B). PS2ρTM1-4 and PS2ρTM3-6 both showed more prominent bands for Aβ38 than Aβ37 on the immunoblots, hence resembled the PS1 phenotype. Also, the substitution in PS2ρTM3-4 was sufficient for this effect, whereas PS2ρTM1-2 rather showed more Aβ37 which is in accordance with the results from the mass spectrometric analysis.

To overcome difficulties when analyzing Aβ species of PS variants with low processing activity, further experiments were performed with an immunoprecipitation of Aβ peptides (antibody 3552) from conditioned media prior to immunoblot analysis. With the aim to compensate differences in the overall Aβ production and thus facilitate detection on immunoblots, immunoprecipitation of Aβ generated by PS2 based variants was performed with four times larger volumes compared to PS1. Finally, while PS1 retained its high Aβ38 generation, PS2 clearly showed a preferential production of Aβ37 in the immunoprecipitated sample (Figure 20).

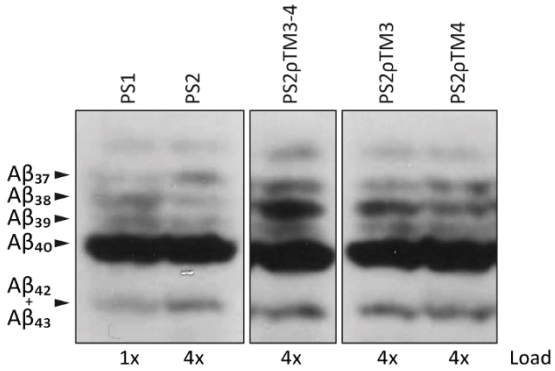


**Figure 20: Combined immunoprecipitation/immunoblotting of Aβ species confirmed differences in Aβ production by PS1 and PS2.** Aβ species from conditioned media were immunoprecipitated with antibody 3552 and separated via 9% Tris-bicine-urea SDS-PAGE. Detection of the individual Aβ species was performed after immunoblotting using antibody 2D8. Note that volumes for immunoprecipitation of cleavage products by PS2, PS2ρTM3-4, PS2ρTM3, and PS2ρTM4 were 4x higher compared to PS1 to compensate differences in the previously tested cleavage activities.

Furthermore, the previously analyzed PS2ρTM3-4 but also PS2ρTM3 showed the PS1 phenotype, while PS2ρTM4 produced equal amounts of Aβ37 and Aβ38. Thus, these results were mainly in line with observations from IP-MS analysis. Even though TMD4 was able to slightly alter Aβ processing, the effects mediated by TMD3 substitution showed the highest impact on Aβ generation. This indicates the importance of TMD3 in substrate processing.

### 4.2.5 Individual Aβ peptides analyzed from *in vitro* assays

After being able to show the capability of TMD3 to reproduce the Aβ cleavage pattern of PS1 in a PS2 template, it was of high interest, whether the initial ε-cleavage by γ-secretase or the subsequent substrate processing lead to the different phenotypes. The ε-cleavage can best be evaluated when analyzing the production of the intracellular domain AICD. However, as mentioned above, analysis of AICD under *in cellulo* conditions is challenging, due to its rapid degradation in the cytoplasm [64]. Thus, *in vitro* γ-secretase assays were analyzed for AICD species to overcome these difficulties. Yet, before analyzing the AICD production, the *in vitro* Aβ production was investigated, to exclude the possibility that the detergent environment abolishes the difference between the PS1 and PS2 phenotype. For this, *in vitro* assays were performed with subsequent IP of Aβ peptides using antibody 4G8.

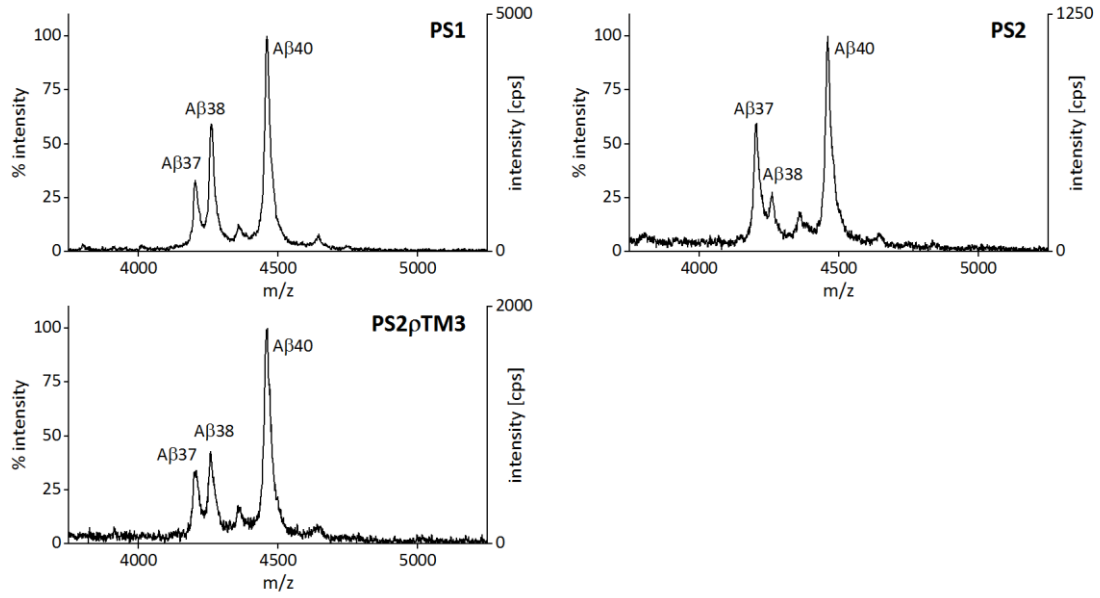


**Figure 21: The single substitution of TMD3 led to an enhanced Aβ38 production *in vitro*.** For *in vitro* generation of Aβ, CHAPSO-solubilized membrane fractions containing the different γ-secretase complexes were prepared. *In vitro* assays using recombinant C100-$His_6$ as a substrate were performed. Subsequent to immunoprecipitation with antibody 4G8 (final concentration 4 µg/mL), total Aβ was analyzed by MALDI-TOF MS. The intensities of the highest peak were set to 100%. Additionally, the counts per second (cps) are shown on the right y-axis. Results of the spectra are representatives of more than three independent experiments.

Results of the mass spectrometric analysis confirmed that PS1- and PS2-containing γ-secretase complexes show distinct patterns of Aβ37 and Aβ38 (Figure 21). However, the carboxypeptidase activity of both homologs was increased compared to the data from conditioned media, leading to higher signal

intensities of smaller Aβ species. Nevertheless, PS1 again showed a higher relative Aβ38 production (Aβ38/Aβ40 ratio of 0.56) than PS2 (0.29) (Figure 22B). Aβ37 production was complementary in that PS2 reached an Aβ37/Aβ40 ratio of 0.56, hence showing a significant difference to PS1 reaching only 0.32 (Figure 22A). In general, the higher carboxypeptidase activity *in vitro* compared to *in cellulo* accentuated differential Aβ37 and Aβ38 production. The Aβ38/Aβ37 ratio of PS2 comprised 0.52 *in vitro* (Figure 22D) compared to around 0.63 obtained from conditioned media (Figure 16A). For PS1 this ratio rose to an Aβ38/Aβ37 ratio of around 1.74 compared to a close to 1:1 ratio in conditioned media. Hence the discrimination between PS1 and PS2 phenotype was facilitated under *in vitro* conditions.

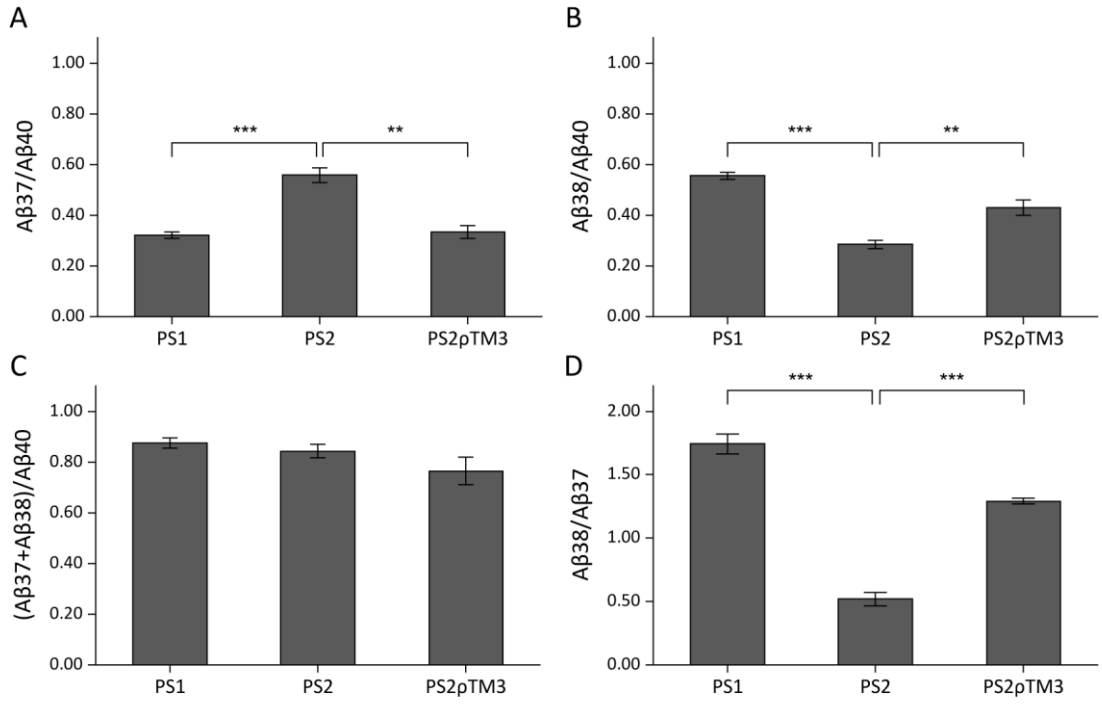


**Figure 22: TMD3 is a main determinant for the Aβ38/Aβ37 ratio *in vitro*.** Aβ ratios were calculated with the respective peak intensities from IP-MS analysis. In relation to signal intensities of Aβ40 the amounts of Aβ37 **(A)** and Aβ38 **(B)** by PS2ρTM3 resembled the ones of PS1. **C)** For the evaluation of the carboxypeptidase activity, the total amount of small peptides (Aβ37+Aβ38) was set in relation to the main species, Aβ40. Despite high differences in production of smaller Aβ peptides, the overall carboxypeptidase activity remained similar. **D)** The decreased Aβ38/Aβ37 ratio of PS2 could be confirmed in the cell-free assay. Means ± SEM, n = 3-4. Asterisks indicate the significance (one-way ANOVA with Dunnett's post test) of the differences between each presenilin variant and PS2 (**$p < 0.01$, ***$p < 0.001$).

In the *in vitro* system, PS2ρTM3 again was able to enhance Aβ38 production accompanied by decreased Aβ37 generation (Figure 21,Figure 22). However, the increase in Aβ38 production compared to PS2 was, despite being clearly visible,

not as pronounced as seen for PS1 (Figure 22B). In spite of the higher effects seen for the different phenotypes, the overall generation of smaller Aβ peptides remained similar in relation to Aβ40 (Figure 22C).

Overall, these results were in accordance with the ones obtained from conditioned media. Even though the differences between both wildtype homologs were more pronounced, this enabled the better discrimination between the homologs and revealed an intermediate behavior of PS2ρTM3 with a strong tendency towards the PS1 phenotype.

### 4.2.6 PS1 and PS2 exhibit differences in ε-cleavage specificity

The observation that the PS1 and PS2 phenotypes of Aβ processing were preserved under *in vitro* conditions confirmed the credibility of analyzing the cleavage specificity using the cell-free assay. Thus, ε-cleavage was then assessed by analysis of individual AICD production using the same conditions.

Analysis of immunoprecipitated samples via MALDI-TOF MS revealed that the two PS homologs also produced distinct AICD patterns after initial cleavage at the individual ε-cleavage sites (Figure 23). For both wildtype PS, the major cleavage site of the substrate was at position ε49, generating the 50 amino acid long AICDε49 and an Aβ49 peptide. However, differences were seen for the second most common cleavage at position ε48 that produces an Aβ48 peptide and intracellular AICDε48. There, cleavage by PS1 was noticeably more frequent than the one by PS2. Comparing the peak heights of these major cleavage products, the ratios of ε48/ε49 were 0.85 for PS1 and 0.74 for PS2 (Figure 24A).

Aβ48 and Aβ49 have previously been described as the predominant starting points of their respective product lines [63, 186]. However, while Aβ49 solely originates from ε49 cleavage, Aβ48 can also be formed from its precursor Aβ51 [63], a product of ε51 cleavage that could also be observed here (Figure 23). For the position ε51, PS2 showed enhanced cleavage preference compared to PS1 with ratios of ε51/ε49 of 0.49 and 0.36, respectively (Figure 24B). As Aβ51 and Aβ48 contribute to the Aβ48 product line that opposes the Aβ49 product line,

the initial preference of the homologs for the two product lines was assessed by combining the AICDε48 and AICDε51 signal intensities. Interestingly, the analysis showed similar ratios for (ε48+ε51)/ε49 with 1.21 and 1.23 for PS1 and PS2, respectively (Figure 24C). This means that even though the preferences for the exact position of initial cleavage differed between PS1 and PS2, the choice of product line was similar. Additionally, the results showed that both homologs exhibit a slight preference for the product line of Aβ48.

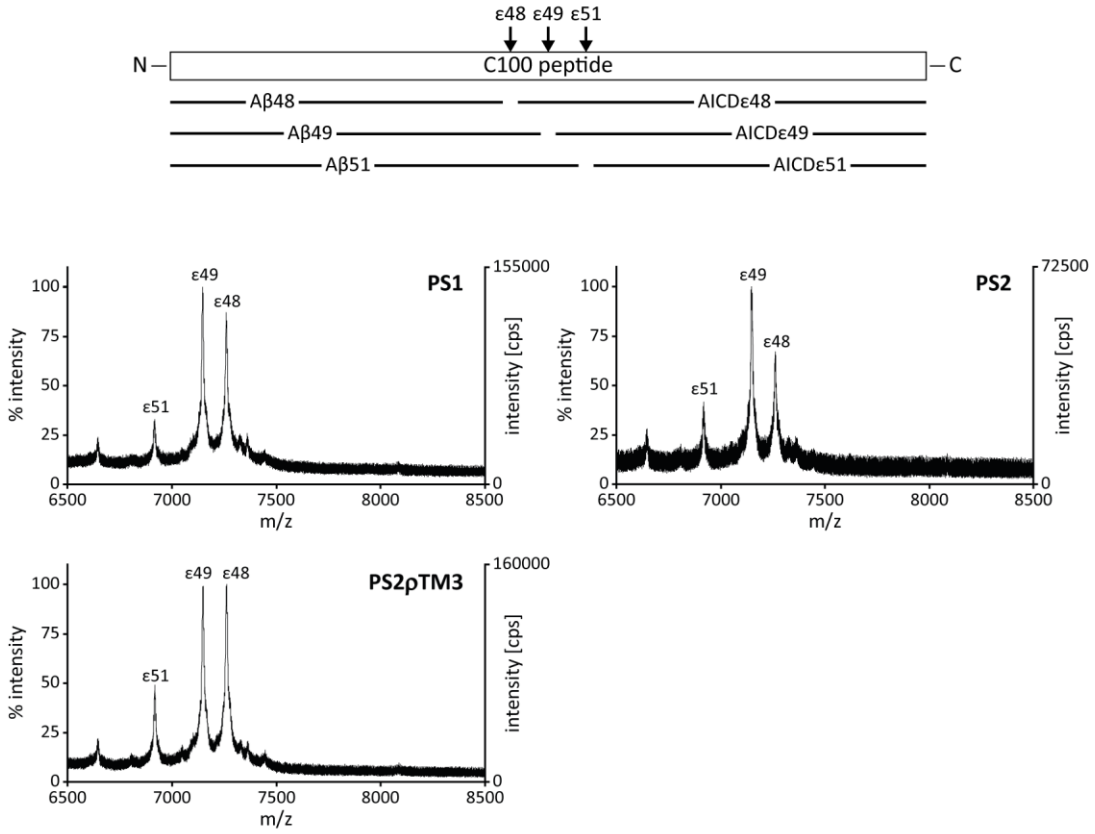


**Figure 23: PS2ρTM3 drastically changes ε-cleavage specificity *in vitro.*** The respective Aβ and AICD products originating from cleavage at ε48, ε49, and ε51 are schematically displayed at the top. For *in vitro* generation of AICD, CHAPSO-solubilized membrane fractions containing the different γ-secretase complexes were prepared. *In vitro* assays using recombinant C100-$His_6$ as a substrate were performed. Total AICD from the reaction volumes was analyzed by MALDI-TOF MS subsequent to immunoprecipitation with antibody Y188. The intensities of the highest peak were set to 100%. Additionally, the counts per second (cps) are shown on the right y-axis. Due to malfunction of the previously used MS device, the spectra were recorded with a different instrument, resulting in higher overall intensities. Results of the spectra are representatives of more than three independent experiments

The single substitution of TMD3 in the PS2 template had a major impact on the Aβ product pattern *in cellulo* and *in vitro*. Now, it was interesting to know whether this observation can be traced back to the initial cleavage of C100 or the subsequent substrate processing within the product lines. To answer this question, the AICD production by PS2ρTM3 was analyzed in parallel to the two

wildtype PS (Figure 23). In contrast to the wildtype variants, PS2ρTM3 did not show a clear preference for one of the two major initial cleavage sites with an ε48/ε49 ratio of 1.07 (Figure 24A). This indicated that the single substitution of TMD3 was able to shift the choice of cleavage site in favor of ε48, exceeding the level of PS1.

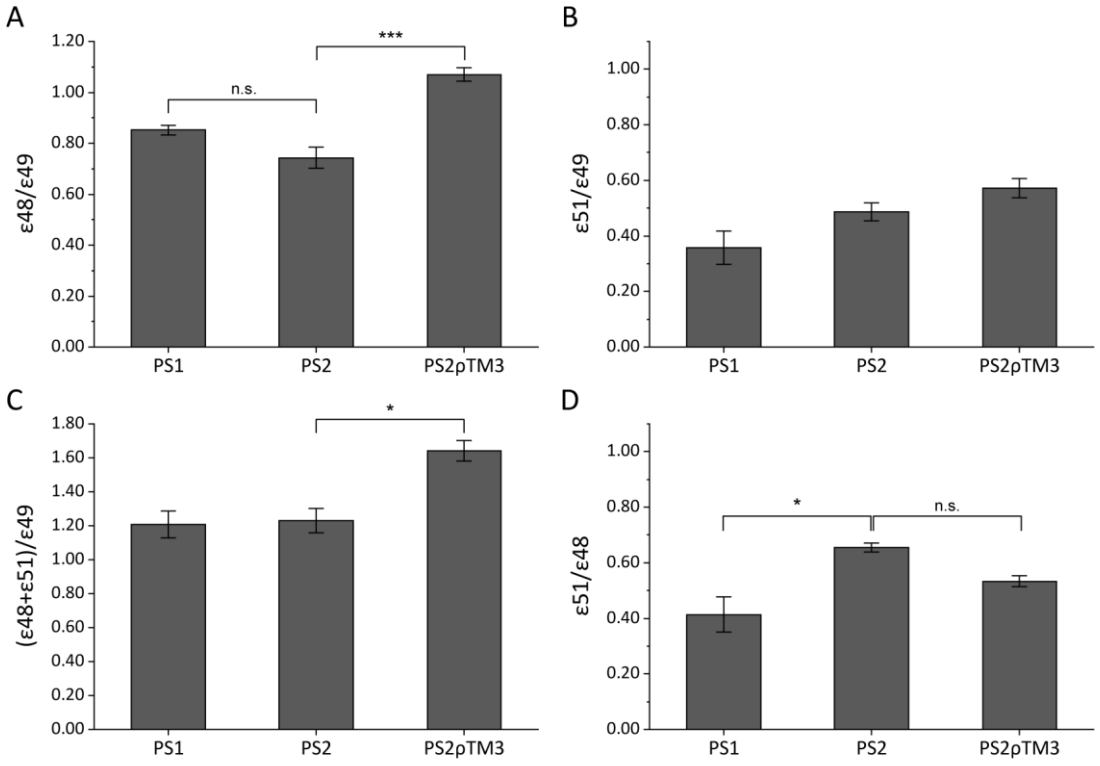


**Figure 24: AICD generation by PS2ρTM3 revealed shifts in initial cleavage site and choice of Aβ product line.** ε-Ratios were calculated with the respective peak intensities from IP-MS analysis. **A)** Preferences for the major cleavage sites ε48 and ε49 are displayed as the ratio of both. **B)** Differences in the production of AICDε51 are displayed in relation to AICDε49. **C)** The starting positions of the respective Aβ product lines were set in relation to each other. Aβ48 and Aβ51 belong to the Aβ48 product line, while the Aβ49 line solely starts with ε49 cleavage. **D)** The shift within the Aβ48 cleavage line is illustrated. Means ± SEM, n = 4. Asterisks indicate the significance (one-way ANOVA with Dunnett's post test) of the differences between each presenilin variant and PS2 (*$p < 0.05$, ***$p < 0.001$, n.s. = not significant).

On the other side, the strong peak for ε51 resembled the one of PS2, but again, the ε51/ε49 ratio (0.57) exceeded the one of PS2 (0.49) (Figure 24B). Remarkably, the (ε48+ε51)/ε49 ratio of PS2ρTM3 (1.64) was significantly higher compared to the two wildtype PS (Figure 24C). Thereby, PS2ρTM3 exhibits a stronger preference for the Aβ48 product line. Also, the shift from ε48 to ε51 that was observed for PS2, was partly reversed in PS2ρTM3, however, without statistical significance (Figure 24D). By this, initial cleavage by PS2ρTM3 showed an ε-cleavage pattern that was distinct from both wildtype PS. Regarding

ε51/ε48, it rather resembled the one of PS1; however, with an additional decrease in ε49 cleavage (Figure 23, Figure 24C). Overall, this indicates that the PS1-like Aβ peptide pattern of PS2ρTM3 was already influenced by the choice of the initial cleavage site. The fact that the single substitution of TMD3 could mediate effects of this extent underlines the unique role of this hydrophobic domain in the cleavage of the C100.

# 5 Discussion

By systematically analyzing the presenilin homologs PS1 and PS2, this thesis aimed to identify functional roles of PS subdomains in the different steps of substrate turnover. Mechanistically, substrate turnover can be divided into substrate recognition, substrate entry, substrate positioning and helical unwinding followed by the different cleavage steps and product release (Figure 25).

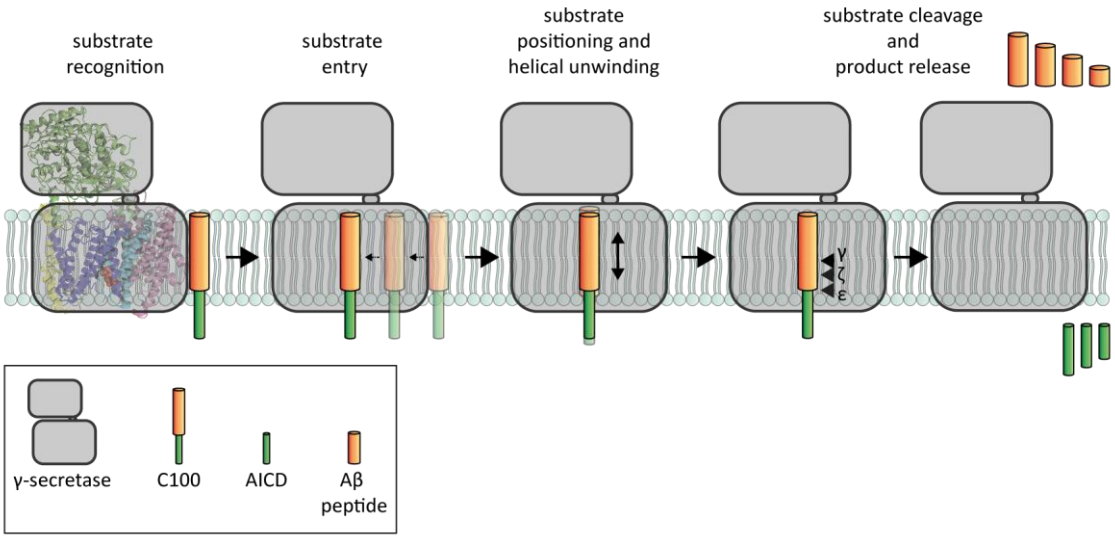


**Figure 25: Schematic view on the different steps of substrate processing**. While the cleavage efficiency is influenced by all steps until substrate cleavage, the ε-cleavage specificity mainly depends on substrate positioning.

In the present work, HEK293/sw PS1/2 $^{-/-}$ dKO cells [237] were stably transfected with the PS homologs or corresponding chimeric variants to monitor the *in vitro* and *in cellulo* production of Aβ and AICD. In general, the observation that chimeric PS variants can be incorporated into the enzyme complex with appropriate complex maturation is in line with previous studies [210, 226, 231]. We note that some of the investigated cell lines (PS2ρTM1-2, PS2ρTM3-4 PS2ρTM1-4, PS2ρTM3-6, PS2ρTM2/6, and PS2ρTM6/9) showed variations in the expression levels of the individual γ-secretase subunits (Figure 9, Figure 10, Figure 11). To counter these differences in γ-secretase levels, the analysis of cleavage efficiency included the normalization of AICD and Aβ production on $NCT_m$ as a measure for the active enzyme complex. Still, it cannot be excluded that alterations in expression levels of the subunits caused minor variations in substrate turnover. Nevertheless, the lack of endogenous PS expression in the

HEK293/sw PS1/2 $^{-/-}$ dKO cells allowed us to attribute the observed differences in ε-cleavage efficiency and specificity to the substituted PS domains.

## 5.1 The cleavage efficiency of PS can be attributed to PS subdomains

The first set of experiments presented here targeted the overall proteolytic activities of the two homologs. AICD production by the individual PS variants was analyzed *in vitro* after expression in the HEK293/sw PS1/2 $^{-/-}$ dKO cell line [237]. The strength of this setup is the localization-independent analysis of the initial cleavage efficiency without background effects of endogenous PS.

### 5.1.1 The PS NTF and PS CTF are involved in substrate recognition and substrate entry

In general, the observation that the cleavage efficiencies measured by Aβ production were mostly in line with the ones of AICD generation (Figure 13) suggests that the rate limiting step accounting for the differences in PS activities lies prior to or during the initial cleavage of the substrates. PS1 showed a 5x higher cleavage activity compared to PS2, with the NTF of PS1 being the main determinant for this difference, as shown by the NTF/CTF chimeras (Figure 8). However, also the CTF of PS1 in combination with the PS2 NTF (PS2/1) enhanced the cleavage activity of the PS2 template. Together, this indicates a cooperative role of NTF and CTF in optimized substrate processing by PS1. These observations support studies by Strömberg *et al.* who analyzed PS activity *in cellulo* using a luciferase-based assay [226]. However, their assay showed only small, non-significant differences between PS1, PS2, and the chimeric variants. This might be explained by their indirect measurement of cleavage activity, as signal detection required the translocation of the released ICD to the nucleus for transcription activation of the luciferase gene. In contrast to this, the direct analysis of generated AICD in the *in vitro* assay used in the current study enabled a considerably better discrimination between the wildtype homologs and their variants.

Besides the contribution of NTF and CTF to the active site, their importance to overall activity may be explained by their functional role in substrate binding. In photoaffinity mapping experiments using C99 variants with the photocrosslinkable amino acid variant Bpa, Fukumori and Steiner identified substrate binding sites of the γ-secretase complex. These were located in particular at the PS1 NTF, but also at PEN-2, NCT, and to some extent at the PS1 CTF [157]. A number of C99-Bpa variants covalently bound to the PS1 NTF could still be processed by γ-secretase, indicating that NTF-bound substrates can acquire proper positioning for cleavage at the active site. Hence, the stronger impact of the PS1 NTF on substrate cleavage might be explained by its greater importance for C100 binding, translocation to the active site and positioning for cleavage. In addition to this, this thesis shows for the first time that the hydrophobic domains mainly account for the differences in activity between PS1 and PS2 (Figure 12). This suggests that enzyme-substrate interactions within the membrane bilayer rather than outside of it mainly determine cleavage efficiency.

### 5.1.2 TMD6 and TMD9 contribute to binding and entry of C99

Further subdivision of the PS NTF and CTF revealed the functional role of smaller domains for the activity of PS. Concerning the PS NTF, PS2ρTM6 is of particular interest, representing the only single TMD substitution that increased C100 turnover (Figure 11). TMD6 and TMD7 of PS1 each harbor one of the two active site aspartate residues D257 and D385 [32] (residues D263 and D366 in PS2 [83]) that are indispensable for PS activity. As both TMDs form a critical part of the catalytic cleft [141], sequence differences in these domains are expected to have an effect on substrate cleavage.

Sequence identity analysis showed that PS1 and PS2 share an overall similarity of 67% at the amino acid level [216] that is increased to 83% in the TMDs (Table 12). While TMD7 shows a conservation level of over 90% between the two homologs, four non-conserved residues in TMD6 reduce its conservation level to 80%. In the substrate-bound cryo-EM structure of PS1, all non-conserved TMD6 residues either face TMD2 (T245) or the surface of the complex (L248,

A251, and V252) [141]. Thus, these residues might play a role in substrate recruitment of γ-secretase. In fact, several studies discussed the involvement of TMD6 in initial substrate binding [163-165]. Furthermore, substrate entry either between TMDs 2 and 6 [26, 168-170] or TMDs 6 and 9 [136, 171] has been discussed. Since these TMDs are located on the same side of the horseshoe-shaped architecture (Figure 4) [138], it was interesting to know, whether combinations of these helices could enhance substrate processing. However, neither the pairwise combination (PS2ρTM2/6 and PS2ρTM6/9), nor the combined exchange of these TMDs (PS2ρTM2/6/9), was able to remarkably increase the activity in the PS2 template compared to PS2ρTM6 (Figure 11, Figure 13). Thus, it is possible that the substitution of TMD6 is sufficient to enhance substrate entry to the level of PS1.

**Table 12: Conservation levels of PS TMDs at amino acid level.**

| TMD | N.h. residues / total number of aa | Conservation level [%] | FAD mutations in PS1 |
|---|---|---|---|
| 1 | 1/ 24 | 95.83 | 14 |
| 2 | 6/31 | 80.65 | 26 |
| 3 | 8/30 | 73.33 | 30 |
| 4 | 8/21 | 61.90 | 15 |
| 5 | 1/22 | 95.45 | 15 |
| 6 | 4/20 | 80.00 | 9 |
| 7 | 1/16 | 93.75 | 11 |
| 8 | 2/25 | 92.00 | 8 |
| 9 | 6/29 | 79.31 | 5 |
| NTF-TMDs | 28/148 | 81.08 | 109 |
| CTF-TMDs | 9/70 | 87.14 | 24 |
| Sum | 37/218 | 83.03 | 133 |

aa = amino acid; n.h. = non-homologous. The numbers of residues per TMDs were calculated according to membrane-embedded residues in the cryo-EM structure of γ-secretase at atomic resolution (PDB 5FN3). FAD mutations per TMD originate from the cumulated “pathogenic” and “likely pathogenic” mutations within the membrane-embedded regions listed on [230].

Within the PS CTF, the single substitution in PS2ρTM9 increased the PS activity to a similar extent as PS2ρTM6 (Figure 11). TMD9 has been discussed to be involved in substrate binding and acquisition of the active state [220]. Overall,

the TMD9 of PS1 and PS2 share a homology of 79% at the amino acid level with the non-homologous residues being distributed across the center and C-terminal third of the TMD (Figure 7 and Table 12). Interestingly, contacts between the APP TMD and the residues 443-451 of PS1 could be observed in MD simulations [167]. In this amino acid stretch, three out of the six non-homologous TMD9 residues are located, indicating that differences mediated by TMD9 might be due to differential interaction with the APP substrate TMD. Substrate binding by TMD9 has been suggested before [171], with D450 of PS1 being of special importance by contributing to a possible initial binding site [166] and forming salt bridges with K28 of C99 [167]. Even though the aspartic residue is conserved between PS1 and PS2 (= D431 in PS2), many of the surrounding residues are not (Figure 7). Instead of Q454 in PS1, PS2 contains a R435 on the corresponding position, which is located four residues C-terminal of D431. Due to the 3.6 residue-periodicity of an ideal α-helix, the two residues show an adjacent location in the PS2 structure [222], close enough to form an intrahelical salt bridge between the side chains. This might reduce the ability of PS2 D431 to interact with the substrate TMD. It should be noted, however, that the interaction between PS1 D450 and K28 of C99 might be only transient since this proximity cannot be observed in the substrate-bound γ-secretase structure [141] and thus needs further investigation.

Furthermore, recent simulations of the PS2 structure by the Kepp group revealed strong TMD9 dynamics in PS2, resulting in a two-state behavior that is not seen in PS1 [222, 223]. The less dynamic movements of TMD9 of PS1 could increase the stability of enzyme conformations that are important for substrate interaction and cleavage. When PS1 TMD9 is grafted onto PS2 this could also mediate the increase in activity observed in the current study. However, the interpretation of different TMD9 dynamics is challenging, as they are highly dependent on surrounding domains in the complex. Hence, it cannot be excluded that TMD9 is stabilized by its TMD environment in PS1 rather than stabilizing the enzyme conformations on its own.

The cumulated effects of PS2ρTM6 and PS2ρTM9 (both around 60% of PS1) (Figure 11) would exceed the activity of PS1. It is, however, possible that both

form binding sites that compete for substrate binding during initial substrate encounter. This is in line with observations that principle substrate binding sites were observed in the PS NTF and the PS CTF [157]. Hence, the absence of one binding site might be compensated by the other to a certain extent.

TMD2 has been reported to be involved in substrate interaction [167], entry [26, 168-170], and positioning within the active site [140, 141]. Furthermore, it shows major dynamics in simulations of PS1 and PS2 [219, 220, 222]. Nevertheless, neither PS2ρTM2 nor PS2ρTM1-2 influenced the amount of newly generated AICD. This indicates that even though TMD2 may play a role in substrate recognition and processing, it is not important for the different activities of PS1 and PS2.

### 5.1.3 The involvement of TMD6 in helical unwinding and cleavage of the substrate

For substrate positioning and helical unwinding the functional role of a sequence C-terminal of TMD6 was previously shown. This region was reported to form a β-strand (named β1, PS1 residues 287-290) that contributes to a three-stranded β-sheet including residues 377-381 neighboring TMD7 (β2), and a β-strand formed by V50-K54 of C99 adjacent to the ε-cleavage region (Figure 5) [141]. Upon substrate binding this β-sheet formation is accompanied by a fully extended conformation of the C99 helix at position T48, L49, and V50, thus facilitating cleavage of the peptide bonds at either the ε48 or ε49 site. In contrast to the conserved β1-strand region, 20% of the TMD6 residues are not conserved between PS1 and PS2. While the substitution of TMD6 had no effect on the different cleavage specificity of the homologs (Figure 17), the putatively better substrate binding by PS1 TMD6 might ease the helical unwinding of the substrate TMD. As the extended conformation at the ε-site facilitates initial cleavage [141], this might contribute to the increased proteolytic activity of PS2ρTM6 (Figure 11) besides improved initial substrate binding and entry (Figure 25). Furthermore, when analyzing six different cryo-EM structures of PS1, TMD6 showed the highest tilt angle variations among the TMDs with direct correlation

to the distance between the catalytic aspartates [249]. As a small distance between these aspartates is required for cleavage, differences in TMD6 dynamics of PS1 and PS2 might further contribute to the enhanced ε-cleavage efficiency of PS2ρTM6.

Unexpectedly, combining the substitution of TMD6 with either of its neighboring TMDs (PS2ρTM5-6 and PS2ρTM6-7) abolished the effect of the single TMD6 exchange (Figure 9, Figure 10). For TMD5, R220 of PS1 is the single non-homologous residue located at the intracellular end of the helix, which is replaced to V226 in PS2. Hence, a polar-ionizable residue is replaced by an apolar one. Even though the charge state of ionizable residues within the membrane is controversially discussed [250-252], polar residues can change the behavior of a TMD in the membrane environment. Since TMD5 is located in the center of the complex (Figure 4) [138], subtle changes of TMD5 position could have abrogated the enhanced substrate interaction of TMD6 by pleiotropic effects within the enzyme.

The impeding effect of PS1 TMD7 on the activity of the PS2ρTM6-7 construct might also be explained by its altered position in the complex. Even though TMD7 only contains one non-conserved residue between PS1 and PS2 (Table 12), the design of the PS2ρTM6-7 variant also included the substitution of the intracellular loop between TMD6 and TMD7 (Table 4, Figure 10). While the β2-strand forming region [141] is conserved between the homologs, seven out of eight upstream PS2 residues form a stretch of negatively charged residues, intracellularly flanking TMD7 (Figure 7). The respective region of PS1 also contains four negatively charged residues. However, it is possible that the higher number of negatively charged amino acids changes the position of TMD7 in the membrane due to increased repulsion with the negatively charged lipid head groups of the phospholipids on the cytoplasmic side of the membrane [253]. Hence, TMD7 of PS1 in the PS2 backbone could affect its proteolytic activity, either by its own positioning or by influencing the dynamics of surrounding TMDs in the complex.

### 5.1.4 PS2ρTM3-4 might improve substrate interaction and entry

The moderate increase in cleavage efficiency by PS2ρTM3-4 might result from an involvement of TMD3 and TMD4 in substrate recognition and entry. Based on the high flexibility of the TMD3 N-terminus and TMD2 observed in MD simulations, Hitzenberger and Zacharias postulated a possible substrate entry site between both helices [165]. This is in agreement with occasional contacts of the APP substrate with TMD3-4, observed in MD simulations [167]. Furthermore, TMD3 forms a part of the catalytic pore [172, 173] and direct contacts between W165 and S169 of TMD3 and the C83 substrate in the structure have been observed [141]. With a considerably large sequence difference of 27% between TMD3 of PS1 and PS2 (Table 12), some non-conserved TMD3 residues might weaken the interaction of PS with C100, hence explaining the lower overall PS2 activity.

For TMD4, the highly conserved glycines G206 and G209 (PS1 numbering) are likely to increase the flexibility of the C-terminus of the helix. The cytoplasmic site of TMD4 was previously crosslinked to the N-terminus of TMD7 after introducing suitable pairs of cysteines. This suggests that the two TMDs can get in close proximity and TMD4 is involved in formation of the catalytic pore structure [173]. The observation that the single exchanges of TMD3 or TMD4 do not enhance PS2 activity suggests a cooperative function of both. By its high flexibility, TMD4 might affect proteolytic activity by influencing the TMD3 position during substrate acquisition and entry [221]. With 62%, TMD4 shows the lowest conservation level among the PS TMDs (Table 12). It is possible that the non-conserved regions alter TMD4 dynamics and position which are further transmitted onto TMD3. However, while experimental and computational studies revealed dynamic conformational changes of TMD3 during the activation of the γ-secretase complex for PS1 [172, 219] and PS2 [222], TMD4 movements have not been observed in the simulations. Hence, other pleiotropic effects of the combined substitution in PS2ρTM3-4 cannot be excluded.

How the substitution in PS2ρTM8 alters the overall substrate turnover remains elusive. One of the two non-conserved residues in TMD8, I427 of PS1 (V408 of PS2), points away from the complex. The second non-homologous residue, I408

of PS1, is exchanged to L389 on PS2 and faces TMD4 of APH-1a. Even though PS1 I408T is a reported FAD mutation, the pathogenicity remains unclear [230, 254]. Also, the artificial mutation I408C did not drastically alter total Aβ production or Aβ42/Aβ40 ratios [174]. Hence, the influence of the exchanged TMD8 must result from pleiotropic effects within the complex that cannot be evaluated with the present results.

## 5.2 The role of individual TMDs in substrate positioning and cleavage

Besides the ε-cleavage efficiency of γ-secretase, the processing of the substrate at the ζ-, and γ-sites are of high interest, as Aβ42 and Aβ43 species are the major contributors to the development of AD [14, 15, 255]. The choice of cleavage site is predominantly dependent on the positioning of the substrate within the complex and the susceptibility of the peptide bond. Hence, the identification of subdomains that modulate substrate positioning and thereby the endo- and exoproteolytic specificity of PS is of central importance to gain further insight in this complex mechanism.

### 5.2.1 PS1 and PS2 show individual patterns of ε-, ζ-, and γ-cleavage

The IP-MS analyses performed in this study demonstrated that PS1- and PS2-containing γ-secretase complexes show remarkable differences in C100 processing. The noticeably reduced production of Aβ38 by PS2 compared to PS1 and HEK293/sw cells was first observed *in cellulo* (Figure 14) and could be confirmed *in vitro* (Figure 21). Interestingly, the decrease in Aβ38 for PS2 is accompanied by an increase in Aβ37. This could especially be observed in the *in vitro* (Figure 16) assays but was also apparent *in cellulo* (Figure 22). Previously, only a few studies observed a reduced production of Aβ38 by PS2 compared to PS1, either by Enzyme-linked Immunosorbent Assay (ELISA) measurements [112] or MS analysis [200]. Also, reduced Aβ38 generation was observed by analysis of electrochemiluminescence signals when comparing PS1 knock out

cells, harboring PS2 as the sole catalytic homolog, with wild type cells [256]. However, the differences in production of Aβ37 have not been described before.

Gel electrophoretic separation of Aβ species from conditioned media confirmed the lower Aβ38 production for PS2 (Figure 20). This is in line with differences in Aβ38 and Aβ37 production by PS1 and PS2 as seen on immunoblots and IP-MS spectra performed by De Strooper and colleagues [225] that however remain unmentioned by the authors.

Due to low signal intensities for Aβ42, a reliable Aβ42/Aβ40 ratio could not be calculated from the IP-MS measurements. However, MS analysis of neither the conditioned media (Figure 14, Figure 15, Figure 17) nor the *in vitro* assays (Figure 21) showed differences in the relative production of Aβ42. These results support studies suggesting a comparable Aβ42/Aβ40 ratio produced by the homologs [209, 210] and

Even though PS1 and PS2 also showed differences in the choice of initial cleavage sites, differential ε-cleavage specificity did not account for the differences in Aβ38/Aβ37 ratio between PS1 and PS2. For both homologs, ε49 was shown to be the major cleavage site, followed by ε48 which is in line with previous reports (Figure 23, Figure 24) [182, 200, 257]. However, while PS1 rarely cleaved at ε51, PS2 used this cleavage site frequently at the expense of ε48. Aβ51, the N-terminal product of ε51-cleavage is processed to Aβ48, which can also originate from ε48-cleavage [63, 186, 189]. The results demonstrated that PS1 and PS2 initiate the Aβ48 product line to the same extent (Figure 24C), suggesting that downstream processing of the Aβ peptides must vary between the two.

At the time of writing, the differences between PS1 and PS2 in ε-cleavage have not been reported before. It should be noted, that contradictory results have been observed by others [112, 200]. However, while Lessard *et al.* did not report a significant difference between ε49 and ε48 site specificity of PS1 and PS2, closer examination of their IP-MS spectra showed a trend of reduced ε48 for PS2, similar to the one observed here (see Figure 3 in [200]). Unfortunately, ε51 cleavage is not reported by the authors and the spectra did not include the

expected size of AICDε51. In case of the results by Acx *et al.*, AICD generation was analyzed via immunoblot analysis, which is less sensitive than MS data [112]. Furthermore, their study did not include the analysis of the ε51 cleavage site.

Our results are fully consistent with one study where AICDs generated by different membrane fractions indicated the higher preference of PS2 for ε51 cleavage. Mass spectrometric analysis revealed that plasma membrane-rich fractions derived from HeLa cells generated almost exclusively AICDε49. In contrast, production in endosome-rich fractions resulted in mostly AICDε51 generation [214]. Since PS2-containing γ-secretase complexes reside in LE and LYS [209, 210], the enhanced AICDε51 production most likely originated from this homolog.

### 5.2.2 PS1 and PS2 use unique Aβ processing pathways

As reported before, γ-secretase generates different cleavage products using distinct processing pathways (see 1.4.3, Figure 6) [63, 186, 189]. In the current study, ε-cleavage analyses showed that both homologs start the Aβ48 product line 1.2x more frequently than the Aβ49 product line (Figure 24). Since for both wildtype PS Aβ40 comprised the main species of total Aβ production, both seem to have frequently switched from the Aβ48 product line to the Aβ49 line. So far, the only known crossing point that could enhance Aβ40 production from the Aβ48 product line is the generation of its precursor Aβ43 from Aβ48 (Figure 6) [63, 186]. For the enhanced generation of Aβ37 by PS2, this homolog may use the Aβ48 →Aβ43 switch more frequently than PS1. Alternatively, generation of small amounts of Aβ37 from the precursor Aβ42 has been reported [63] or PS2 might use additional crossing points that have not been identified so far.

Previously*, in vitro* and *in cellulo* assays using re-transfected PS double knock-out MEF cells had indicated that the carboxypeptidase activity of PS2 is less efficient than the one of PS1, especially along the Aβ48 product line [112]. Although the authors did not consider product line switches, their results give hints on putatively used crossing points. In their experiments, the production of

Aβ43, Aβ42, Aβ40, and Aβ38 as well as AICD production were analyzed. Their results indicated for PS2 that besides a reduced conversion Aβ42 →Aβ38 also the Aβ42 production was reduced to ~40% compared to the PS1 control. The authors argue that a reduced second and third turnover, from the Aβ48 and Aβ45 precursors, respectively, led to the reduced Aβ42 production. However, an alternative interpretation of the data is that Aβ48 was converted to Aβ43 in a product line crossing by PS2 to a greater extent as in the case of PS1, thus explaining Aβ42 reduction [63]. Furthermore, Aβ38 production by PS2 was abolished almost completely, which is in line with the results of the current study. The reduction of the fourth cleavage step (Aβ42 →Aβ38) proposed by the authors could alternatively indicate the predominant generation of Aβ37 or Aβ39 from the Aβ42 precursor. Unfortunately, neither of these two peptides had been analyzed [112].

### 5.2.3 TMD3 alters substrate positioning and ε-cleavage specificity

The different Aβ profiles are mainly determined by the hydrophobic domains in the PS NTF (Figure 15, Figure 16). In particular, the single TMD exchange in PS2ρTM3 was able to phenocopy PS1 with an apparent increase in Aβ38 production observed in MS analyses (Figure 17) and Tris-bicine-urea gels of secreted Aβ (Figure 20). *In vitro* experiments confirmed the prominent shift seen for Aβ37 and Aβ38; however, not to the same extent as in PS1 (Figure 21), indicating an intermediate phenotype of PS2ρTM3 between PS1 and PS2. These differences in Aβ generation originate from the unique ε-cleavage pattern of PS2ρTM3. In contrast to both wildtype presenilins, PS2ρTM3 showed an increased preference for the Aβ48 product line, with enhanced production of AICDε48 and AICDε51 at the expense of AICDε49 (Figure 23, Figure 24). As most of Aβ38 originates from the Aβ48 product line [63], this resulted in elevated Aβ38 levels of PS2ρTM3 compared to PS2.

Besides this, the subsequent ζ- and γ-cleavage steps within and across the product lines seem not to be affected by the TMD3 substitution. In a scenario where PS2ρTM3 would mimic the product line switching of PS1, its Aβ38 levels

would be expected to exceed the ones of PS1, due to the prevalent start in the Aβ48 pathway. However, even though the increase in Aβ38 generation of PS2ρTM3 was remarkable compared to PS2, Aβ38 production by PS2ρTM3 was still lower than that by PS1. Hence, it is most likely, that PS2ρTM3 mainly influences the choice of initial cleavage sites by altering substrate positioning but utilizes the Aβ processing pathway of PS2 (Figure 26). This means that TMD3 is not the main determinant for the different phenotypes of the PS homologs. Instead, the PS1-like phenotype in Aβ generation by PS2ρTM3 mainly results from its increased preference for the Aβ48 product line.

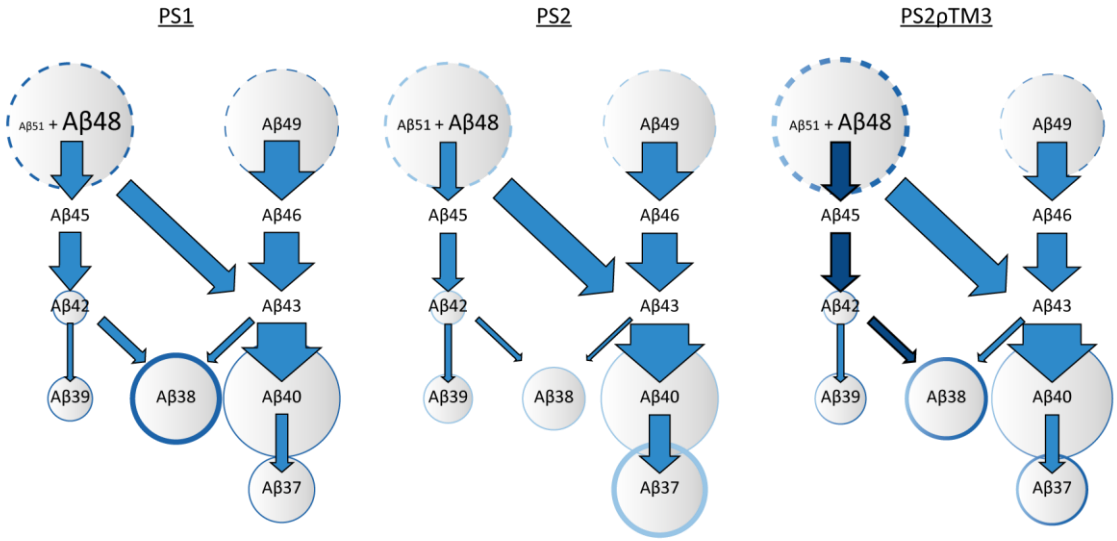


**Figure 26: Schematic product line usage of PS1, PS2, and PS2ρTM3**. The circle diameter reflects the relative amounts of the peptides at the start (dashed lines) or end (solid lines) of the respective Aβ product processing. Font size of Aβ48 and Aβ51 represent their contribution to the Aβ48 product line. Arrow sizes indicate the usage of the respective cleavage steps that could lead to the respective Aβ patterns. Arrows in dark blue indicate a possible explanation for the increased Aβ38 production by PS2ρTM3 compared to PS2, due to the prevalent start in the Aβ48 product line.

The functional role of TMD3 in γ-secretase conformational dynamics and substrate positioning has been indicated before. Experimental, computational, and cryo-EM studies have elucidated the participation of TMD3 in the formation of the catalytic pore and the acquisition of the active site conformation in PS1 [138, 141, 172, 219] and PS2 [222]. In studies using a substituted cysteine accessibility method, binding of the GSM E2012 led to a conformational change of TMD3. This caused an expansion of the catalytic cavity that was reported by the authors to be crucial for the reduction of Aβ42 production [258]. Furthermore, the importance of TMD3 for the Aβ production by PS1 is underlined by the fact

that over 20% of all FAD mutations are located in TMD3 (Table 12) which comprises less than 7% of all amino acids of PS1. Among these is the very aggressive L166P mutation, which is associated with an early onset of AD and has been shown to cause a dramatic increase in longer Aβ species [259].

Interestingly, photoaffinity mapping showed L166P to alter the crosslinking efficiency of PS1 with the ε-site of C99 [157]. This indicates that TMD3 influences the interaction of PS with the initial cleavage region. Furthermore, V44 of C99 was identified as one of the major interaction points involved in γ-secretase binding [157]. In the substrate-bound structure, the substrate is located between TMD2 and TMD3 with a direct contact between C99-V44 and W165 of PS1 TMD3 [26, 141]. While W165 is conserved between the two PS homologs, the neighboring A164 of PS1 is replaced by a G170 in PS2 (Figure 7). As mentioned above, glycines are likely to increase conformational flexibility and change the collective dynamics of transmembrane helices [260, 261]. Hence, different conformational dynamics of PS1 and PS2 around the W165 interaction site could lead to its altered interaction with V44 of C99. By grafting TMD3 of PS1 onto PS2, the PS1-like interaction might have been restored. However, in the context of the PS2 template, altered dynamics of PS1 TMD3 possibly lead to a different positioning of C100 at the active site. Thus, TMD3 might influence substrate positioning within the active site prior to cleavage, which would directly affect the choice of initial cleavage site. Considering the relatively low conservation level of only 73% of TMD3 (Table 12), other differences between the TMD3 sequences of PS1 and PS2 may further influence substrate positioning.

The substitution of TMD4 had a minor impact on cleavage specificity producing an Aβ processing phenotype in between those of PS1 and PS2 (Figure 17, Figure 20). This indicates its involvement in substrate positioning. However, even though the luminal part of TMD4 has been suggested to be involved in the formation of the catalytic pore [173], no close contacts with the substrate have been observed before, nor are they visible in the substrate-bound structure [141]. It has been speculated by others that G206 and G209 (PS1 numbering) increase the flexibility of the C-terminal half of TMD4 that can help to stabilize

TMD3 positioning during cleavage [221]. However, as both glycines are conserved between the two homologs, they might only be involved indirectly by conferring conformational changes of TMD4 on TMD3. With TMD4 showing the lowest conservation levels of all TMDs (Table 12), alterations in TMD4 conformation might affect TMD3 and thereby substrate positioning differently in PS1 and PS2. However, other pleiotropic effects cannot be excluded.

### 5.2.4 The ε-cleavage efficiency and specificity of PS are uncoupled

The results of this study suggest that the ε-cleavage efficiency of PS is uncoupled from the ε-cleavage specificity. On the one hand, the single substitution in PS2ρTM3 determined the choice of ε-site (Figure 23, Figure 24), but did not influence the overall activity (Figure 9, Figure 13). On the other hand, TMD6 substitution was able to drastically change the cleavage efficiency of PS2 (Figure 9, Figure 13), but had no impact on the Aβ38/Aβ37 ratio (Figure 17, Figure 18). While differences in ε-cleavage by PS2ρTM6 cannot be excluded, its PS2-like Aβ38/Aβ37 ratio may suggest an unchanged ε-cleavage specificity.

Interestingly, even though PS2ρTM6 might not alter substrate positioning during initial cleavage, substrate interaction with TMD6 during the successive stepwise cleavage process could be important. The relatively low (Aβ37+Aβ38)/Aβ40 ratio of PS2ρTM6 (Figure 18B) indicates a higher relative production of the Aβ40 peptide. It is possible that an altered substrate positioning within PS2ρTM6 during the stepwise Aβ processing impede cleavage at G37 or G38 of the substrate. However, the mechanisms by which PS2ρTM6 confers the higher Aβ40 production remain elusive.

## 5.3 The biological significance of PS1 and PS2 cleavage

In order to understand the individual roles of the PS homologs, putative functions of the generated Aβ peptides are of particular interest. Among other aspects, Aβ peptides are thought to be important for memory formation, neuroprotection, antimicrobial activity, and blocking leaks at the blood-brain-barrier under

physiological conditions [11, 262]. These extracellular tasks require a quick response with tight regulation and most are distorted in AD. Given the localization of PS1 at the plasma membrane [72, 209, 210], the higher activity of PS1-containing γ-secretase complexes might be important to answer this requirement by a faster production of Aβ than PS2-containing complexes.

PS2 on the other hand is thought to be important for intracellular Aβ homeostasis. Even though Aβ peptides can be taken up from the surrounding environment in human neuronal cells [263, 264], the PS2-containing γ-secretase complexes have been shown to be the main source of intracellular Aβ pools due to its more limited localization in LE and LYS [210]. Furthermore, the compartmentalization in the cell influences the Aβ concentration and the pH, which in turn affects the conformation and aggregation behavior of Aβ peptides [263, 264]. Intraneuronal accumulation of Aβ42 was reported to be an early event in AD which precedes extracellular accumulations [217, 218]. Therefore, the lower cleavage activity of PS2 could be a prerequisite for the physiological intracellular Aβ homeostasis.

The differences in Aβ processing of PS1 and PS2, resulting in different Aβ37 and Aβ38 amounts, might reflect alternative strategies of the cell to avoid accumulation of toxic Aβ species like Aβ42. While PS1 shows a quite robust production of Aβ38 from both product lines [63, 188], Aβ38 generation by PS2 from the Aβ42 precursor seems to be hampered [112]. Hence, to circumvent Aβ42 accumulation, PS2 may have evolved with an enhanced product line switching to the Aβ49 product line by the described Aβ48 →Aβ43 transition (Figure 26) [63] which finally results in increased Aβ37 production.

## 5.4 Conclusion and outlook

We can conclude that the mechanisms that lead to the higher activity of PS1 crucially depend on membrane-embedded residues, predominantly in the NTF, but also the CTF of PS1. Without doubt, the interplay of several TMDs is important for the substrate cleavage efficiency and specificity of PS1. Nevertheless, this study showed that TMD6, TMD8, and TMD9 are principal

players in controlling the cleavage efficiency of γ-secretase (Figure 27). While the role of TMD8 in determining cleavage activity may result from pleiotropic effects, the PS1 TMD6 and TMD9 might enhance substrate turnover by improved substrate binding and providing better access through differently arranged entry sites. The combination of TMD3 and TMD4 also enhances cleavage activity to a moderate extent probably by improved substrate interaction. Additionally, TMD3 majorly influences substrate positioning prior to cleavage, directly affecting the specificity of AICD and Aβ generation.

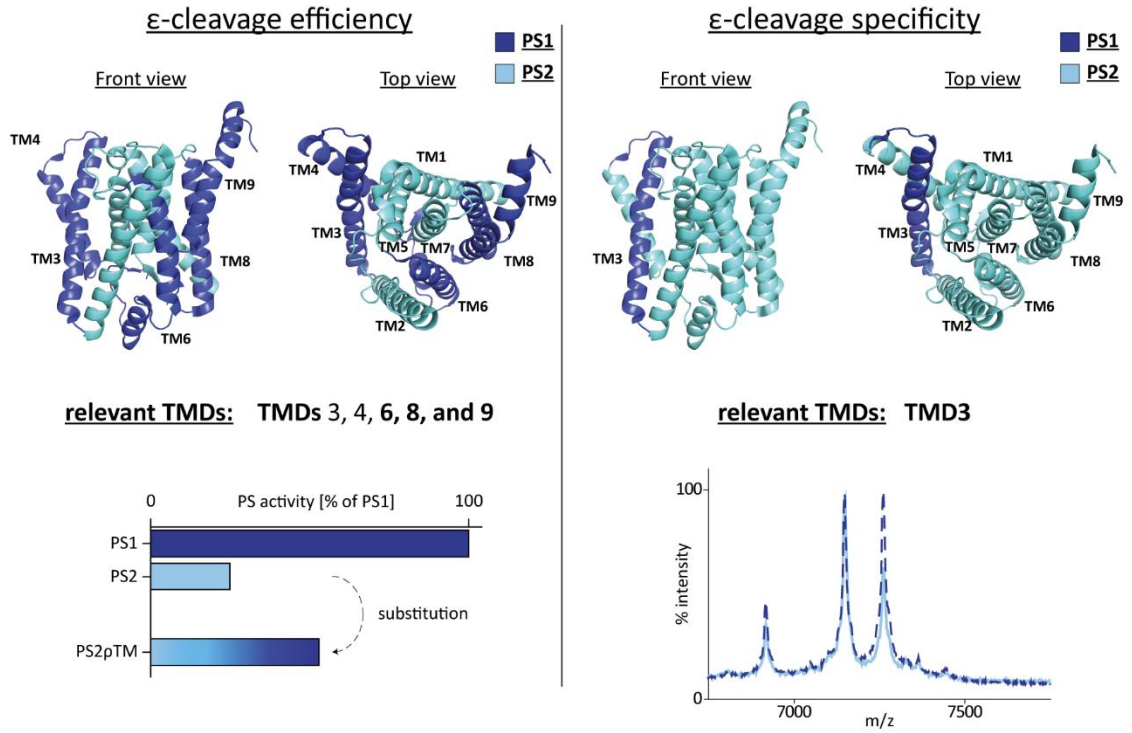


**Figure 27: PS TMDs involved in ε-cleavage efficiency and specificity.** The PS2 template is displayed in light blue. PS1 TMDs that influence either efficiency or specificity upon substitution are represented in dark blue. Multiple TMDs and combinations of such can raise the ε-cleavage efficiency *in vitro* (left). In contrast to this, the substitution of TMD3 alone can alter ε-cleavage specificity (right - dashed line) compared to PS2 (solid line).

How exactly the two homologs shape their subsequent Aβ processing pathways needs further investigation. So far, mass spectrometric studies focused on generated Aβ by total membrane lysates, therefore from a mixture of PS1 and PS2 [63, 186]. In future experiments, LC-MS studies of the free byproducts of the stepwise Aβ processing by either sole PS1 or PS2 could help to identify their individual crossing points between the major Aβ product lines and thereby help to further understand the complex mechanism of Aβ processing and its modulation.

Furthermore, it remains to be analyzed whether the substrate binding (defined by the Michaelis constant, $K_M$), substrate entry, or the catalytic turnover ($k_{cat}$) is different between PS1 and PS2. So far, enzyme kinetics have only been studied for PS1-containing γ-secretase complexes [182, 265, 266]. Repetition of these experiments with PS2 would expand our knowledge on how the different γ-secretase complexes interact with their substrate. This could help the development of PS1- or PS2-specific GSM in novel AD therapies. The contribution of TMD3 in ε-site specificity could be of high relevance for the optimization of these GSM. Even though GSM are thought not to alter the initial cleavage [113, 198, 199], recent AICD IP-MS analyses could detect their impact on PS1 and PS2 mediated ε-cleavage [200]. Also, the involvement of TMD3 in the function of GSM has only recently been shown [258].

In summary, the findings of this study have deepened our understanding of the differences between the catalytic homologs PS1 and PS2. It provides additional puzzle pieces to understand the mechanisms that regulate intramembrane proteolysis in the context of AD. For AD therapy, the development of potent GSM is of high importance. Here, the results underline that TMD3 is a promising target that should be focused on in future experiments.

# 6 References

[1] Reitz C, Brayne C, Mayeux R. Epidemiology of Alzheimer disease. Nature Reviews Neurology. 2011; 7:137-52.

[2] Lane C, Hardy J, Schott J. Alzheimer's disease. European journal of neurology. 2018; 25:59-70.

[3] Organization WH. Global status report on the public health response to dementia. 2021.

[4] Guerchet M, Prince M, Prina M. Numbers of people with dementia worldwide: An update to the estimates in the World Alzheimer Report 2015. 2020.

[5] Perl DP. Neuropathology of Alzheimer's disease. Mount Sinai Journal of Medicine. 2010; 77:32-42.

[6] Alzheimer A. Über eine eigenartige Erkrankung der Hirnrinde. Allgemeine Zeitschrift fur Psychiatrie und Psychisch-gerichtliche Medizin. 1907; 64:146-8.

[7] Lee G, Neve RL, Kosik KS. The microtubule binding domain of tau protein. Neuron. 1989; 2:1615-24.

[8] Amos LA. Microtubule structure and its stabilisation. Organic & biomolecular chemistry. 2004; 2:2153-60.

[9] Grundke-Iqbal I, Iqbal K, Tung Y-C, Quinlan M, Wisniewski HM, Binder LI. Abnormal phosphorylation of the microtubule-associated protein tau (tau) in Alzheimer cytoskeletal pathology. Proceedings of the National Academy of Sciences. 1986; 83:4913-7.

[10] Köpke E, Tung Y-C, Shaikh S, Alonso AdC, Iqbal K, Grundke-Iqbal I. Microtubule-associated protein tau. Abnormal phosphorylation of a non-paired helical filament pool in Alzheimer disease. Journal of Biological Chemistry. 1993; 268:24374-84.

[11] Kent SA, Spires-Jones TL, Durrant CS. The physiological roles of tau and Aβ: implications for Alzheimer's disease pathology and therapeutics. Acta Neuropathologica. 2020; 140:417-47.

[12] Ballatore C, Lee VM-Y, Trojanowski JQ. Tau-mediated neurodegeneration in Alzheimer's disease and related disorders. Nature reviews neuroscience. 2007; 8:663-72.

[13] Selkoe DJ. Resolving controversies on the path to Alzheimer's therapeutics. Nature medicine. 2011; 17:1060-5.

[14] Iwatsubo T, Odaka A, Suzuki N, Mizusawa H, Nukina N, Ihara Y. Visualization of Aβ42 (43) and Aβ40 in senile plaques with end-specific Aβ monoclonals: evidence that an initially deposited species is Aβ42 (43). Neuron. 1994; 13:45-53.

[15] Saito T, Suemoto T, Brouwers N, Sleegers K, Funamoto S, Mihira N, et al. Potent amyloidogenicity and pathogenicity of Aβ43. Nature neuroscience. 2011; 14:1023-32.

[16] Shoji M, Golde TE, Ghiso J, Cheung TT, Estus S, Shaffer LM, et al. Production of the Alzheimer amyloid β protein by normal proteolytic processing. Science. 1992; 258:126-9.

[17] Estus S, Golde TE, Kunishita T, Blades D, Lowery D, Eisen M, et al. Potentially amyloidogenic, carboxyl-terminal derivatives of the amyloid protein precursor. Science. 1992; 255:726-8.

[18] Haass C, Kaether C, Thinakaran G, Sisodia S. Trafficking and Proteolytic Processing of APP. Cold Spring Harbor Perspectives in Medicine. 2012:1-26.

[19] Hardy J, Allsop D. Amyloid deposition as the central event in the aetiology of Alzheimer's disease. Trends in pharmacological sciences. 1991; 12:383-8.

[20] Hardy JA, Higgins GA. Alzheimer's disease: the amyloid cascade hypothesis. Science. 1992; 256:184-6.

[21] Selkoe DJ, Hardy J. The amyloid hypothesis of Alzheimer's disease at 25 years. EMBO molecular medicine. 2016; 8:595-608.

[22] Tanzi RE, Gusella JF, Watkins PC, Bruns G, St George-Hyslop P, Van Keuren ML, et al. Amyloid β protein gene: cDNA, mRNA distribution, and genetic linkage near the Alzheimer locus. Science. 1987; 235:880-4.

[23] Olson MI, Shaw C-M. Presenile dementia and Alzheimer's disease in mongolism. Brain. 1969; 92:147-56.

[24] Lemere C, Blusztajn J, Yamaguchi H, Wisniewski T, Saido T, Selkoe D. Sequence of deposition of heterogeneous amyloid β-peptides and APO E in Down syndrome: implications for initial events in amyloid plaque formation. Neurobiology of disease. 1996; 3:16-32.

[25] Rovelet-Lecrux A, Hannequin D, Raux G, Le Meur N, Laquerriere A, Vital A, et al. APP locus duplication causes autosomal dominant early-onset Alzheimer disease with cerebral amyloid angiopathy. Nat Genet. 2006; 38:24-6.

[26] Fukumori A, Feilen LP, Steiner H. Substrate recruitment by γ-secretase. Seminars in Cell and Developmental Biology. 2020:1-10.

[27] Mutations | Alzforum. (n.d.) Retrieved March 21, 2022, from https://www.alzforum.org/mutations

[28] Sherrington R, Rogaev E, Liang Ya, Rogaeva E, Levesque G, Ikeda M, et al. Cloning of a gene bearing missense mutations in early-onset familial Alzheimer's disease. Nature. 1995; 375:754-60.

[29] Levy-Lahad E, Wasco W, Poorkaj P, Romano DM, Oshima J, Pettingell WH, et al. Candidate gene for the chromosome 1 familial Alzheimer's disease locus. Science. 1995; 269:973-7.

[30] Rogaev E, Sherrington R, Rogaeva E, Levesque G, Ikeda M, Liang Y, et al. Familial Alzheimer's disease in kindreds with missense mutations in a gene on chromosome 1 related to the Alzheimer's disease type 3 gene. Nature. 1995; 376:775-8.

[31] De Strooper B, Saftig P, Craessaerts K, Vanderstichele H, Guhde G, Annaert W, et al. Deficiency of presenilin-1 inhibits the normal cleavage of amyloid precursor protein. Nature. 1998; 391:387-90.

[32] Wolfe MS, Xia W, Ostaszewski BL, Diehl TS, Kimberly WT, Selkoe DJ. Two transmembrane aspartates in presenilin-1 required for presenilin endoproteolysis and γ-secretase activity. Nature. 1999; 398:513-7.

[33] Kimberly WT, Xia W, Rahmati T, Wolfe MS, Selkoe DJ. The transmembrane aspartates in presenilin 1 and 2 are obligatory for γ-secretase activity and amyloid β-protein generation. Journal of Biological Chemistry. 2000; 275:3173-8.

[34] Li YM, Xu M, Lai MT, Huang Q, Castro JL, DiMuzio-Mower J, et al. Photoactivated γ-secretase inhibitors directed to the active site covalently label presenilin 1. Nature. 2000; 405:689-94.

[35] Esler WP, Kimberly WT, Ostaszewski BL, Diehl TS, Moore CL, Tsai JY, et al. Transition-state analogue inhibitors of gamma-secretase bind directly to presenilin-1. Nat Cell Biol. 2000; 2:428-34.

[36] Steiner H, Kostka M, Romig H, Basset G, Pesold B, Hardy J, et al. Glycine 384 is required for presenilin-1 function and is conserved in bacterial polytopic aspartyl proteases. Nat Cell Biol. 2000; 2:848-51.

[37] Liu CC, Liu CC, Kanekiyo T, Xu H, Bu G. Apolipoprotein E and Alzheimer disease: risk, mechanisms and therapy. Nat Rev Neurol. 2013; 9:106-18.

[38] Corder EH, Saunders AM, Strittmatter WJ, Schmechel DE, Gaskell PC, Small GW, et al. Gene dose of apolipoprotein E type 4 allele and the risk of Alzheimer's disease in late onset families. Science. 1993; 261:921-3.

[39] Castellano JM, Kim J, Stewart FR, Jiang H, DeMattos RB, Patterson BW, et al. Human apoE isoforms differentially regulate brain amyloid-β peptide clearance. Science translational medicine. 2011; 3:89ra57-89ra57.

[40] Rebeck GW, Reiter JS, Strickland DK, Hyman BT. Apolipoprotein E in sporadic Alzheimer's disease: allelic variation and receptor interactions. Neuron. 1993; 11:575-80.

[41] Bateman RJ, Xiong C, Benzinger TL, Fagan AM, Goate A, Fox NC, et al. Clinical and biomarker changes in dominantly inherited Alzheimer's disease. N Engl J Med. 2012; 367:795-804.

[42] Hutton M, Lendon CL, Rizzu P, Baker M, Froelich S, Houlden H, et al. Association of missense and 5′-splice-site mutations in tau with the inherited dementia FTDP-17. Nature. 1998; 393:702-5.

[43] Poorkaj P, Bird TD, Wijsman E, Nemens E, Garruto RM, Anderson L, et al. Tau is a candidate gene for chromosome 17 frontotemporal dementia. Annals of neurology. 1998; 43:815-25.

[44] Hardy J, Selkoe DJ. The amyloid hypothesis of Alzheimer's disease: progress and problems on the road to therapeutics. science. 2002; 297:353-6.

[45] Long JM, Holtzman DM. Alzheimer disease: an update on pathobiology and treatment strategies. Cell. 2019; 179:312-39.

[46] Shen J, Kelleher RJ. The presenilin hypothesis of Alzheimer's disease: evidence for a loss-of-function pathogenic mechanism. Proceedings of the National Academy of Sciences. 2007; 104:403-9.

[47] Karran E, De Strooper B. The amyloid cascade hypothesis: are we poised for success or failure? Journal of neurochemistry. 2016; 139:237-52.

[48] Muresan V, Muresan ZL. Amyloid-β precursor protein: multiple fragments, numerous transport routes and mechanisms. Experimental cell research. 2015; 334:45-53.

[49] Greenfield JP, Tsai J, Gouras GK, Hai B, Thinakaran G, Checler F, et al. Endoplasmic reticulum and trans-Golgi network generate distinct populations of Alzheimer β-amyloid peptides. Proceedings of the National Academy of Sciences. 1999; 96:742-7.

[50] Agostinho P, Pliassova A, Oliveira CR, Cunha RA. Localization and trafficking of amyloid-β protein precursor and secretases: Impact on Alzheimer's disease. Journal of Alzheimer's Disease. 2015; 45:329-47.

[51] Haass C, Koo EH, Mellon A, Hung AY, Selkoe DJ. Targeting of cell-surface β-amyloid precursor protein to lysosomes: alternative processing into amyloid-bearing fragments. Nature. 1992; 357:500-3.

[52] Sandbrink R, Masters CL, Beyreuther K. Beta A4-amyloid protein precursor mRNA isoforms without exon 15 are ubiquitously expressed in rat tissues including brain, but not in neurons. Journal of Biological Chemistry. 1994; 269:1510-7.

[53] Golde TE, Estus S, Usiak M, Younkin LH, Younkin SG. Expression of β amyloid protein precursor mRNAs: recognition of a novel alternatively spliced form and quantitation in Alzheimer's disease using PCR. Neuron. 1990; 4:253-67.

[54] Esch FS, Keim PS, Beattie EC, Blacher RW, Culwell AR, Oltersdorf T, et al. Cleavage of amyloid β peptide during constitutive processing of its precursor. Science. 1990; 248:1122-4.

[55] Sisodia S, Koo E, Beyreuther K, Unterbeck A, Price D. Evidence that β-amyloid protein in Alzheimer's disease is not derived by normal processing. Science. 1990; 248:492-5.

[56] Kuhn PH, Wang H, Dislich B, Colombo A, Zeitschel U, Ellwart JW, et al. ADAM10 is the physiologically relevant, constitutive α-secretase of the amyloid precursor protein in primary neurons. The EMBO journal. 2010; 29:3020-32.

[57] Haass C, Hung AY, Schlossmacher MG, Teplow DB, Selkoe DJ. beta-Amyloid peptide and a 3-kDa fragment are derived by distinct cellular mechanisms. Journal of Biological Chemistry. 1993; 268:3021-4.

[58] Hong L, Koelsch G, Lin X, Wu S, Terzyan S, Ghosh AK, et al. Structure of the protease domain of memapsin 2 (β-secretase) complexed with inhibitor. Science. 2000; 290:150-3.

[59] Vassar R, Bennett BD, Babu-Khan S, Kahn S, Mendiaz EA, Denis P, et al. β-Secretase cleavage of Alzheimer's amyloid precursor protein by the transmembrane aspartic protease BACE. science. 1999; 286:735-41.

[60] Sinha S, Anderson JP, Barbour R, Basi GS, Caccavello R, Davis D, et al. Purification and cloning of amyloid precursor protein β-secretase from human brain. Nature. 1999; 402:537-40.

[61] Yan R, Bienkowski MJ, Shuck ME, Miao H, Tory MC, Pauley AM, et al. Membrane-anchored aspartyl protease with Alzheimer's disease β-secretase activity. Nature. 1999; 402:533-7.

[62] Haass C, Selkoe DJ. Cellular processing of β-amyloid precursor protein and the genesis of amyloid β-peptide. Cell. 1993; 75:1039-42.

[63] Matsumura N, Takami M, Okochi M, Wada-Kakuda S, Fujiwara H, Tagami S, et al. γ-secretase associated with lipid rafts: Multiple interactive pathways in the stepwise processing of β-carboxylterminal fragment. Journal of Biological Chemistry. 2014; 289:5109-21.

[64] Edbauer D, Willem M, Lammich S, Steiner H, Haass C. Insulin-degrading enzyme rapidly removes the β-amyloid precursor protein intracellular domain (AICD). Journal of Biological Chemistry. 2002; 277:13389-93.

[65] Bukhari H, Glotzbach A, Kolbe K, Leonhardt G, Loosse C, Müller T. Small things matter: Implications of APP intracellular domain AICD nuclear signaling in the progression and pathogenesis of Alzheimer's disease. Progress in neurobiology. 2017; 156:189-213.

[66] Allinson TM, Parkin ET, Turner AJ, Hooper NM. ADAMs family members as amyloid precursor protein α-secretases. Journal of neuroscience research. 2003; 74:342-52.

[67] Cai H, Wang Y, McCarthy D, Wen H, Borchelt DR, Price DL, et al. BACE1 is the major β-secretase for generation of Aβ peptides by neurons. Nature neuroscience. 2001; 4:233-4.

[68] Roberds SL, Anderson J, Basi G, Bienkowski MJ, Branstetter DG, Chen KS, et al. BACE knockout mice are healthy despite lacking the primary β-secretase activity in brain: implications for Alzheimer's disease therapeutics. Human molecular genetics. 2001; 10:1317-24.

[69] Lichtenthaler SF, Haass C, Steiner H. Regulated intramembrane proteolysis–lessons from amyloid precursor protein processing. Journal of neurochemistry. 2011; 117:779-96.

[70] Nitsch RM, Slack BE, Wurtman RJ, Growdon JH. Release of Alzheimer amyloid precursor derivatives stimulated by activation of muscarinic acetylcholine receptors. Science. 1992; 258:304-7.

[71] Postina R, Schroeder A, Dewachter I, Bohl J, Schmitt U, Kojro E, et al. A disintegrin-metalloproteinase prevents amyloid plaque formation and hippocampal defects in an Alzheimer disease mouse model. The Journal of clinical investigation. 2004; 113:1456-64.

[72] Watanabe H, Imaizumi K, Cai T, Zhou Z, Tomita T, Okano H. Flexible and accurate substrate processing with distinct presenilin/γ-secretases in human cortical neurons. eNeuro. 2021; 8:1-20.

[73] Vassar R. Bace 1. Journal of Molecular Neuroscience. 2004; 23:105-13.

[74] Francis R, McGrath G, Zhang J, Ruddy DA, Sym M, Apfeld J, et al. aph-1 and pen-2 are required for Notch pathway signaling, γ-secretase cleavage of βAPP, and presenilin protein accumulation. Developmental cell. 2002; 3:85-97.

[75] Winkler E, Hobson S, Fukumori A, Dümpelfeld B, Luebbers T, Baumann K, et al. Purification, pharmacological modulation, and biochemical characterization of interactors of endogenous human γ-secretase. Biochemistry. 2009; 48:1183-97.

[76] Teranishi Y, Hur JY, Welander H, Frånberg J, Aoki M, Winblad B, et al. Affinity pulldown of γ-secretase and associated proteins from human and rat brain. Journal of cellular and molecular medicine. 2010; 14:2675-86.

[77] Wakabayashi T, Craessaerts K, Bammens L, Bentahir M, Borgions F, Herdewijn P, et al. Analysis of the γ-secretase interactome and validation of its association with tetraspanin-enriched microdomains. Nature cell biology. 2009; 11:1340-6.

[78] Kimberly WT, LaVoie MJ, Ostaszewski BL, Ye W, Wolfe MS, Selkoe DJ. γ-Secretase is a membrane protein complex comprised of presenilin, nicastrin, aph-1, and pen-2. Proceedings of the National Academy of Sciences. 2003; 100:6382-7.

[79] Sato T, Diehl TS, Narayanan S, Funamoto S, Ihara Y, De Strooper B, et al. Active γ-secretase complexes contain only one of each component. Journal of Biological Chemistry. 2007; 282:33985-93.

[80] Edbauer D, Winkler E, Regula JT, Pesold B, Steiner H, Haass C. Reconstitution of γ-secretase activity. Nature Cell Biology. 2003; 5:486-8.

[81] Takasugi N, Tomita T, Hayashi I, Tsuruoka M, Niimura M, Takahashi Y, et al. The role of presenilin cofactors in the γ-secretase complex. Nature. 2003; 422:438-41.

[82] Alzheimer's Disease Collaborative G. The structure of the presenilin 1 (S182) gene and identification of six novel mutations in early onset AD families. Nat Genet. 1995; 11:219-22.

[83] Steiner H, Duff K, Capell A, Romig H, Grim MG, Lincoln S, et al. A loss of function mutation of presenilin-2 interferes with amyloid β- peptide production and Notch signaling. Journal of Biological Chemistry. 1999; 274:28669-73.

[84] Laudon H, Hansson EM, Melén K, Bergman A, Farmery MR, Winblad B, et al. A nine-transmembrane domain topology for presenilin 1. Journal of Biological Chemistry. 2005; 280:35352-60.

[85] Spasic D, Tolia A, Dillen K, Baert V, De Strooper B, Vrijens S, et al. Presenilin-1 maintains a nine-transmembrane topology throughout the secretory pathway. Journal of Biological Chemistry. 2006; 281:26569-77.

[86] Thinakaran G, Borchelt DR, Lee MK, Slunt HH, Spitzer L, Kim G, et al. Endoproteolysis of presenilin 1 and accumulation of processed derivatives in vivo. Neuron. 1996; 17:181-90.

[87] Podlisny MB, Citron M, Amarante P, Sherrington R, Xia W, Zhang J, et al. Presenilin proteins undergo heterogeneous endoproteolysis between Thr291and Ala299and occur as stable N- and C-terminal fragments in normal and Alzheimer brain tissue. Neurobiology of Disease. 1997; 3:325-37.

[88] Seeger M, Nordstedt C, Petanceska S, Kovacs DM, Gouras GK, Hahne S, et al. Evidence for phosphorylation and oligomeric assembly of presenilin 1. Proceedings of the National Academy of Sciences. 1997; 94:5090-4.

[89] Yu G, Nishimura M, Arawaka S, Levitan D, Zhang L, Tandon A, et al. Nicastrin modulates presenilin-mediated notch/glp-1 signal transduction and βAPP processing. Nature. 2000; 407:48-54.

[90] Chung H-M, Struhl G. Nicastrin is required for Presenilin-mediated transmembrane cleavage in Drosophila. Nature cell biology. 2001; 3:1129-32.

[91] Li T, Ma G, Cai H, Price DL, Wong PC. Nicastrin is required for assembly of presenilin/γ-secretase complexes to mediate Notch signaling and for processing and trafficking of β-amyloid precursor protein in mammals. Journal of Neuroscience. 2003; 23:3272-7.

[92] Edbauer D, Winkler E, Haass C, Steiner H. Presenilin and nicastrin regulate each other and determine amyloid β-peptide production via complex formation. Proceedings of the National Academy of Sciences. 2002; 99:8666-71.

[93] Capell A, Beher D, Prokop S, Steiner H, Kaether C, Shearman MS, et al. γ-Secretase complex assembly within the early secretory pathway. J Biol Chem. 2005; 280:6471-8.

[94] Bolduc DM, Montagna DR, Gu Y, Selkoe DJ, Wolfe MS. Nicastrin functions to sterically hinder γ-secretase-substrate interactions driven by substrate transmembrane domain. Proc Natl Acad Sci U S A. 2016; 113:E509-18.

[95] Urban S. Nicastrin guards Alzheimer's gate. Proceedings of the National Academy of Sciences. 2016; 113:1112-4.

[96] Lee JY, Feng Z, Xie X-Q, Bahar I. Allosteric modulation of intact γ-secretase structural dynamics. Biophysical journal. 2017; 113:2634-49.

[97] Chen F, Yu G, Arawaka S, Nishimura M, Kawarai T, Yu H, et al. Nicastrin binds to membrane-tethered Notch. Nature cell biology. 2001; 3:751-4.

[98] Shah S, Lee S-F, Tabuchi K, Hao Y-H, Yu C, LaPlant Q, et al. Nicastrin functions as a γ-secretase-substrate receptor. Cell. 2005; 122:435-47.

[99] Petit D, Hitzenberger M, Lismont S, Zoltowska KM, Ryan NS, Mercken M, et al. Extracellular interface between APP and Nicastrin regulates Aβ length and response to γ-secretase modulators. The EMBO Journal. 2019; 38:1-18.

[100] Zhang X, Chunjiang JY, Sisodia SS. The topology of pen-2, a γ-secretase subunit, revisited: evidence for a reentrant loop and a single pass transmembrane domain. Molecular neurodegeneration. 2015; 10:1-8.

[101] Sun L, Zhao L, Yang G, Yan C, Zhou R, Zhou X, et al. Structural basis of human γ -secretase assembly. Proceedings of the National Academy of Sciences of the United States of America. 2015; 112:6003-8.

[102] Watanabe N, Tomita T, Sato C, Kitamura T, Morohashi Y, Iwatsubo T. Pen-2 is incorporated into the γ-secretase complex through binding to transmembrane domain 4 of presenilin 1. J Biol Chem. 2005; 280:41967-75.

[103] Prokop S, Shirotani K, Edbauer D, Haass C, Steiner H. Requirement of PEN-2 for stabilization of the presenilin N-/C-terminal fragment heterodimer within the γ-secretase complex. Journal of Biological Chemistry. 2004; 279:23255-61.

[104] Isoo N, Sato C, Miyashita H, Shinohara M, Takasugi N, Morohashi Y, et al. Aβ42 overproduction associated with structural changes in the catalytic pore of γ-secretase: common effects of Pen-2 N-terminal elongation and fenofibrate. Journal of Biological Chemistry. 2007; 282:12388-96.

[105] Hitzenberger M, Götz A, Menig S, Brunschweiger B, Zacharias M, Scharnagl C. The dynamics of γ-secretase and its substrates. Seminars in Cell and Developmental Biology. 2020:1-16.

[106] Goutte C, Tsunozaki M, Hale VA, Priess JR. APH-1 is a multipass membrane protein essential for the Notch signaling pathway in Caenorhabditis elegans embryos. Proceedings of the National Academy of Sciences. 2002; 99:775-9.

[107] De Strooper B. Aph-1, Pen-2, and nicastrin with presenilin generate an active γ-secretase complex. Neuron. 2003; 38:9-12.

[108] Shirotani K, Edbauer D, Prokop S, Haass C, Steiner H. Identification of distinct γ-secretase complexes with different APH-1 variants. Journal of Biological Chemistry. 2004; 279:41340-5.

[109] Hébert SS, Serneels L, Dejaegere T, Horré K, Dabrowski M, Baert V, et al. Coordinated and widespread expression of γ-secretase in vivo: evidence for size and molecular heterogeneity. Neurobiology of disease. 2004; 17:260-72.

[110] Serneels L, Van Biervliet J, Craessaerts K, Dejaegere T, Horré K, Van Houtvin T, et al. γ-Secretase heterogeneity in the Aph1 subunit: Relevance for Alzheimer's disease. Science. 2009; 324:639-42.

[111] Yonemura Y, Futai E, Yagishita S, Kaether C, Ishiura S. Specific combinations of presenilins and Aph1s affect the substrate specificity and activity of γ-secretase. Biochemical and Biophysical Research Communications. 2016; 478:1751-7.

[112] Acx H, Chávez-Gutiérrez L, Serneels L, Lismont S, Benurwar M, Elad N, et al. Signature Amyloid β Profiles Are Produced by Different γ-Secretase Complexes. Journal of Biological Chemistry. 2014; 289:4346-55.

[113] Ebke A, Luebbers T, Fukumori A, Shirotani K, Haass C, Baumann K, et al. Novel gamma-secretase enzyme modulators directly target presenilin protein. J Biol Chem. 2011; 286:37181-6.

[114] Siegel G, Gerber H, Koch P, Bruestle O, Fraering PC, Rajendran L. The Alzheimer's Disease gamma-Secretase Generates Higher 42:40 Ratios for beta-Amyloid Than for p3 Peptides. Cell Rep. 2017; 19:1967-76.

[115] Niimura M, Isoo N, Takasugi N, Tsuruoka M, Ui-Tei K, Saigo K, et al. Aph-1 contributes to the stabilization and trafficking of the γ-secretase complex through mechanisms involving intermolecular and intramolecular interactions. Journal of Biological Chemistry. 2005; 280:12967-75.

[116] LaVoie MJ, Fraering PC, Ostaszewski BL, Ye W, Kimberly WT, Wolfe MS, et al. Assembly of the γ-secretase complex involves early formation of an intermediate subcomplex of Aph-1 and nicastrin. Journal of Biological Chemistry. 2003; 278:37213-22.

[117] Pardossi-Piquard R, Yang S-P, Kanemoto S, Gu Y, Chen F, Böhm C, et al. APH1 polar transmembrane residues regulate the assembly and activity of presenilin complexes. Journal of Biological Chemistry. 2009; 284:16298-307.

[118] Capell A, Kaether C, Edbauer D, Shirotani K, Merkl S, Steiner H, et al. Nicastrin interacts with γ-secretase complex components via the N-terminal part of its transmembrane domain. Journal of Biological Chemistry. 2003; 278:52519-23.

[119] Kaether C, Capell A, Edbauer D, Winkler E, Novak B, Steiner H, et al. The presenilin C-terminus is required for ER-retention, nicastrin-binding and γ-secretase activity. The EMBO journal. 2004; 23:4738-48.

[120] Steiner H, Winkler E, Haass C. Chemical cross-linking provides a model of the γ-secretase complex subunit architecture and evidence for close proximity of the C-terminal fragment of presenilin with APH-1. Journal of Biological Chemistry. 2008; 283:34677-86.

[121] Fraering PC, LaVoie MJ, Ye W, Ostaszewski BL, Kimberly WT, Selkoe DJ, et al. Detergent-dependent dissociation of active γ-secretase reveals an interaction between Pen-2 and PS1-NTF and offers a model for subunit organization within the complex. Biochemistry. 2004; 43:323-33.

[122] Kim S-H, Sisodia SS. Evidence that the “NF” motif in transmembrane domain 4 of presenilin 1 is critical for binding with PEN-2. Journal of Biological Chemistry. 2005; 280:41953-66.

[123] Luo W-j, Wang H, Li H, Kim BS, Shah S, Lee H-J, et al. PEN-2 and APH-1 coordinately regulate proteolytic processing of presenilin 1. Journal of Biological Chemistry. 2003; 278:7850-4.

[124] Ratovitski T, Slunt HH, Thinakaran G, Price DL, Sisodia SS, Borchelt DR. Endoproteolytic processing and stabilization of wild-type and mutant presenilin. Journal of Biological Chemistry. 1997; 272:24536-41.

[125] Capell A, Grünberg Jr, Pesold B, Diehlmann A, Citron M, Nixon R, et al. The proteolytic fragments of the Alzheimer's disease-associated presenilin-1 form heterodimers and occur as a 100–150-kDa molecular mass complex. Journal of Biological Chemistry. 1998; 273:3205-11.

[126] Steiner H, Capell A, Pesold B, Citron M, Kloetzel PM, Selkoe DJ, et al. Expression of Alzheimer’s disease-associated presenilin-1 is controlled by proteolytic degradation and complex formation. Journal of Biological Chemistry. 1998; 273:32322-31.

[127] Kimberly WT, LaVoie MJ, Ostaszewski BL, Ye W, Wolfe MS, Selkoe DJ. Complex N-linked glycosylated nicastrin associates with active γ-secretase and undergoes tight cellular regulation. Journal of Biological Chemistry. 2002; 277:35113-7.

[128] Yang D-S, Tandon A, Chen F, Yu G, Yu H, Arawaka S, et al. Mature Glycosylation and Trafficking of Nicastrin Modulate Its Binding to Presenilins. Journal of Biological Chemistry. 2002; 277:28135-42.

[129] Leem JY, Vijayan S, Han P, Cai D, Machura M, Lopes KO, et al. Presenilin 1 is required for maturation and cell surface accumulation of nicastrin. Journal of Biological Chemistry. 2002; 277:19236-40.

[130] Herreman A, Van Gassen G, Bentahir M, Nyabi O, Craessaerts K, Mueller U, et al. γ-Secretase activity requires the presenilin-dependent trafficking of nicastrin through the Golgi apparatus but not its complex glycosylation. Journal of cell science. 2003; 116:1127-36.

[131] Dries DR, Yu G. Assembly, maturation, and trafficking of the γ-secretase complex in Alzheimer's disease. Current Alzheimer research. 2008; 5:132-46.

[132] López AR, Dimitrov M, Gerber H, Braman V, Hacker DL, Wurm FM, et al. Production of active glycosylation-deficient γ-secretase complex for crystallization studies. Biotechnology and bioengineering. 2015; 112:2516-26.

[133] Moniruzzaman M, Ishihara S, Nobuhara M, Higashide H, Funamoto S. Glycosylation status of nicastrin influences catalytic activity and substrate preference of γ-secretase. Biochemical and Biophysical Research Communications. 2018; 502:98-103.

[134] Nogales E, Scheres SH. Cryo-EM: a unique tool for the visualization of macromolecular complexity. Molecular cell. 2015; 58:677-89.

[135] Xie T, Yan C, Zhou R, Zhao Y, Sun L, Yang G, et al. Crystal structure of the γ-secretase component nicastrin. Proceedings of the National Academy of Sciences. 2014; 111:13349-54.

[136] Li X, Dang S, Yan C, Gong X, Wang J, Shi Y. Structure of a presenilin family intramembrane aspartate protease. Nature. 2013; 493:56-61.

[137] Lu P, Bai X-c, Ma D, Xie T, Yan C, Sun L, et al. Three-dimensional structure of human γ-secretase. Nature. 2014; 512:166-70.

[138] Bai X-c, Yan C, Yang G, Lu P, Ma D, Sun L, et al. An atomic structure of human γ-secretase. Nature. 2015; 525:212-7.

[139] Bai X-C, Rajendra E, Yang G, Shi Y, Scheres SH. Sampling the conformational space of the catalytic subunit of human γ-secretase. eLife. 2015; 4:e11182.

[140] Yang G, Zhou R, Zhou Q, Guo X, Yan C, Ke M, et al. Structural basis of Notch recognition by human γ-secretase. Nature. 2019.

[141] Zhou R, Yang G, Guo X, Zhou Q, Lei J, Shi Y. Recognition of the amyloid precursor protein by human γ-secretase. Science. 2019; 0930:1-13.

[142] Wolfe MS. γ-Secretase in biology and medicine. Seminars in cell & developmental biology: Elsevier; 2009. p. 219-24.

[143] Güner G, Lichtenthaler SF. The substrate repertoire of γ-secretase/presenilin. Seminars in Cell and Developmental Biology. 2020:0-1.

[144] Oikawa N, Walter J. Presenilins and γ-Secretase in Membrane Proteostasis. Cells. 2019; 8:209.

[145] Bray SJ. Notch signalling in context. Nature reviews Molecular cell biology. 2016; 17:722-35.

[146] Borggrefe T, Lauth M, Zwijsen A, Huylebroeck D, Oswald F, Giaimo BD. The Notch intracellular domain integrates signals from Wnt, Hedgehog, TGFβ/BMP and hypoxia pathways. Biochimica et Biophysica Acta (BBA)-Molecular Cell Research. 2016; 1863:303-13.

[147] Laurent SA, Hoffmann FS, Kuhn P-H, Cheng Q, Chu Y, Schmidt-Supprian M, et al. γ-Secretase directly sheds the survival receptor BCMA from plasma cells. Nature communications. 2015; 6:1-12.

[148] Struhl G, Adachi A. Requirements for presenilin-dependent cleavage of notch and other transmembrane proteins. Molecular cell. 2000; 6:625-36.

[149] Funamoto S, Sasaki T, Ishihara S, Nobuhara M, Nakano M, Watanabe-Takahashi M, et al. Substrate ectodomain is critical for substrate preference and inhibition of γ-secretase. Nature Communications. 2013; 4.

[150] Kopan R, Ilagan MXG. γ-Secretase: proteasome of the membrane? Nature reviews Molecular cell biology. 2004; 5:499-504.

[151] Hemming ML, Elias JE, Gygi SP, Selkoe DJ. Proteomic profiling of γ-secretase substrates and mapping of substrate requirements. PLoS biology. 2008; 6:e257.

[152] Annaert WG, Esselens C, Baert V, Boeve C, Snellings G, Cupers P, et al. Interaction with telencephalin and the amyloid precursor protein predicts a ring structure for presenilins. Neuron. 2001; 32:579-89.

[153] Pester O, Barrett PJ, Hornburg D, Hornburg P, Pröbstle R, Widmaier S, et al. The backbone dynamics of the amyloid precursor protein transmembrane helix provides a rationale for the sequential cleavage mechanism of γ-secretase. Journal of the American Chemical Society. 2013; 135:1317-29.

[154] Götz A, Mylonas N, Högel P, Silber M, Heinel H, Menig S, et al. Modulating hinge flexibility in the APP transmembrane domain alters γ-secretase cleavage. Biophysical journal. 2019; 116:2103-20.

[155] Kukar TL, Ladd TB, Robertson P, Pintchovski SA, Moore B, Bann MA, et al. Lysine 624 of the amyloid precursor protein (APP) is a critical determinant of amyloid β peptide length: support for a sequential model of γ-secretase intramembrane proteolysis and regulation by the amyloid β precursor protein (APP) juxtamembrane region. Journal of Biological Chemistry. 2011; 286:39804-12.

[156] Zhang J, Ye W, Wang R, Wolfe MS, Greenberg BD, Selkoe DJ. Proteolysis of chimeric β-amyloid precursor proteins containing the Notch transmembrane domain yields amyloid β-like peptides. Journal of Biological Chemistry. 2002; 277:15069-75.

[157] Fukumori A, Steiner H. Substrate recruitment of γ-secretase and mechanism of clinical presenilin mutations revealed by photoaffinity mapping. The EMBO Journal. 2016; 35:1628-43.

[158] Chávez-Gutiérrez L, Tolia A, Maes E, Li T, Wong PC, De Strooper B. Glu332 in the nicastrin ectodomain is essential for γ-secretase complex maturation but not for its activity. Journal of Biological Chemistry. 2008; 283:20096-105.

[159] Dries DR, Shah S, Han Y-H, Yu C, Yu S, Shearman MS, et al. Glu-333 of nicastrin directly participates in γ-secretase activity. Journal of Biological Chemistry. 2009; 284:29714-24.

[160] Beher D, Fricker M, Nadin A, Clarke E. EE, Wrigley JDJ, Li YM, et al. In vitro characterization of the presenilin-dependent γ-secretase complex using a novel affinity ligand. Biochemistry. 2003; 42:8133-42.

[161] Tian G, Sobotka-Briner CD, Zysk J, Liu X, Birr C, Sylvester MA, et al. Linear non-competitive inhibition of solubilized human γ-secretase by pepstatin A methylester, L685458, sulfonamides, and benzodiazepines. Journal of Biological Chemistry. 2002; 277:31499-505.

[162] Kornilova AY, Bihel F, Das C, Wolfe MS. The initial substrate-binding site of γ-secretase is located on presenilin near the active site. Proceedings of the National Academy of Sciences of the United States of America. 2005; 102:3230-5.

[163] Watanabe N, Takagi S, Tominaga A, Tomita T, Iwatsubo T. Functional analysis of the transmembrane domains of presenilin 1: Participation of transmembrane domains 2 and 6 in the formation of initial substrate-binding site of γ-secretase. Journal of Biological Chemistry. 2010; 285:19738-46.

[164] Tomita T, Iwatsubo T. Structural biology of presenilins and signal peptide peptidases. Journal of Biological Chemistry. 2013; 288:14673-80.

[165] Hitzenberger M, Zacharias M. Structural Modeling of γ-Secretase Aβ n Complex Formation and Substrate Processing. ACS Chemical Neuroscience. 2019; 10:1826-40.

[166] Takagi-Niidome S, Sasaki T, Osawa S, Sato T, Morishima K, Cai T, et al. Cooperative roles of hydrophilic loop 1 and the C-terminus of presenilin 1 in the substrate-gating mechanism of γ-secretase. J Neurosci. 2015; 35:2646-56.

[167] Li S, Zhang W, Han W. Initial Substrate Binding of γ-Secretase: The Role of Substrate Flexibility. ACS Chemical Neuroscience. 2017; 8:1279-90.

[168] Kong R, Chang S, Xia W, Wong STC. Molecular dynamics simulation study reveals potential substrate entry path into γ-secretase/presenilin-1. Journal of Structural Biology. 2015; 191:120-9.

[169] Somavarapu AK, Kepp KP. The dynamic mechanism of presenilin-1 function: Sensitive gate dynamics and loop unplugging control protein access. Neurobiology of Disease. 2016; 89:147-56.

[170] Dehury B, Tang N, Kepp KP. Molecular dynamics of C99-bound γ-secretase reveal two binding modes with distinct compactness, stability, and active-site retention: implications for Aβ production. Biochemical Journal. 2019; 476:1173-89.

[171] Tolia A, Horré K, De Strooper B. Transmembrane domain 9 of presenilin determines the dynamic conformation of the catalytic site of γ-secretase. Journal of Biological Chemistry. 2008; 283:19793-803.

[172] Cai T, Morishima K, Takagi-Niidome S, Tominaga A, Tomita T. Conformational Dynamics of Transmembrane Domain 3 of Presenilin 1 Is Associated with the Trimming Activity of γ-Secretase. The Journal of neuroscience : the official journal of the Society for Neuroscience. 2019; 39:8600-10.

[173] Tominaga A, Cai T, Takagi-Niidome S, Iwatsubo T, Tomita T. Conformational Changes in Transmembrane Domain 4 of Presenilin 1 Are Associated with Altered Amyloid-β 42 Production. Journal of Neuroscience. 2016; 36:1362-72.

[174] Sato C, Takagi S, Tomita T, Iwatsubo T. The C-terminal PAL motif and transmembrane domain 9 of presenilin 1 are involved in the formation of the catalytic pore of the γ-secretase. Journal of Neuroscience. 2008; 28:6264-71.

[175] Zhou R, Yang G, Shi Y. Macromolecular complex in recognition and proteolysis of amyloid precursor protein in Alzheimer's disease. Current Opinion in Structural Biology. 2020; 61:1-8.

[176] Wang J, Beher D, Nyborg AC, Shearman MS, Golde TE, Goate A. C-terminal PAL motif of presenilin and presenilin homologues required for normal active site conformation. Journal of neurochemistry. 2006; 96:218-27.

[177] Tomita T, Watabiki T, Takikawa R, Morohashi Y, Takasugi N, Kopan R, et al. The first proline of PALP motif at the C terminus of presenilins is obligatory for stabilization, complex formation, and γ-secretase activities of presenilins. Journal of Biological Chemistry. 2001; 276:33273-81.

[178] Yamasaki A, Eimer S, Okochi M, Smialowska A, Kaether C, Baumeister R, et al. The GxGD motif of presenilin contributes to catalytic function and substrate identification of γ-secretase. Journal of Neuroscience. 2006; 26:3821-8.

[179] Kretner B, Fukumori A, Kuhn PH, Pérez-Revuelta BI, Lichtenthaler SF, Haass C, et al. Important functional role of residue x of the presenilin Gx GD protease active site motif for APP substrate cleavage specificity and substrate selectivity of γ-secretase. Journal of neurochemistry. 2013; 125:144-56.

[180] Sastre M, Steiner H, Fuchs K, Capell A, Multhaup G, Condron MM, et al. Presenilin-dependent γ-secretase processing of β-amyloid precursor protein at a site corresponding to the S3 cleavage of Notch. EMBO reports. 2001; 2:835-41.

[181] Sato T, Dohmae N, Qi Y, Kakuda N, Misonou H, Mitsumori R, et al. Potential Link between Amyloid β-Protein 42 and C-terminal Fragment γ 49-99 of β-Amyloid Precursor Protein. Journal of Biological Chemistry. 2003; 278:24294-0301.

[182] Kakuda N, Funamoto S, Yagishita S, Takami M, Osawa S, Dohmae N, et al. Equimolar Production of Amyloid β-Protein and Amyloid Precursor Protein Intracellular Domain from β-Carboxyl-terminal Fragment by γ-Secretase. Journal of Biological Chemistry. 2006; 281:14776-86.

[183] Weidemann A, Eggert S, Reinhard FB, Vogel M, Paliga K, Baier G, et al. A novel ϵ-cleavage within the transmembrane domain of the Alzheimer amyloid precursor protein demonstrates homology with Notch processing. Biochemistry. 2002; 41:2825-35.

[184] Gu Y, Misonou H, Sato T, Dohmae N, Takio K, Ihara Y. Distinct intramembrane cleavage of the β-amyloid precursor protein family resembling γ-secretase-like cleavage of Notch. Journal of Biological Chemistry. 2001; 276:35235-8.

[185] Yu C, Kim SH, Ikeuchi T, Xu H, Gasparini L, Wang R, et al. Characterization of a presenilin-mediated amyloid precursor protein carboxyl-terminal fragment gamma. Evidence for distinct mechanisms involved in gamma -secretase processing of the APP and Notch1 transmembrane domains. J Biol Chem. 2001; 276:43756-60.

[186] Olsson F, Schmidt S, Althoff V, Munter LM, Jin S, Rosqvist S, et al. Characterization of Intermediate Steps in Amyloid Beta (Aβ) Production under Near-native Conditions. Journal of Biological Chemistry. 2014; 289:1540-50.

[187] Takami M, Nagashima Y, Sano Y, Ishihara S, Morishima-Kawashima M, Funamoto S, et al. γ-Secretase: Successive Tripeptide and Tetrapeptide Release from the Transmembrane Domain of β-Carboxyl Terminal Fragment. Journal of Neuroscience. 2009; 29:13042-52.

[188] Bolduc DM, Montagna DR, Seghers MC, Wolfe MS, Selkoe DJ. The amyloid-beta forming tripeptide cleavage mechanism of γ-secretase. eLife. 2016; 5:1-4.

[189] Morishima-Kawashima M. Molecular mechanism of the intramembrane cleavage of the β-carboxyl terminal fragment of amyloid precursor protein by γ-Secretase. Frontiers in Physiology. 2014; 5:1-7.

[190] Okochi M, Tagami S, Yanagida K, Takami M, Kodama TS, Mori K, et al. γ-Secretase Modulators and Presenilin 1 Mutants Act Differently on Presenilin/γ-Secretase Function to Cleave Aβ42 and Aβ43. Cell Reports. 2013; 3:42-51.

[191] Weggen S, Beher D. Molecular consequences of amyloid precursor protein and presenilin mutations causing autosomal-dominant Alzheimer's disease. Alzheimer's research & therapy. 2012; 4:1-14.

[192] Dovey H, John V, Anderson J, Chen L, de Saint Andrieu P, Fang L, et al. Functional gamma-secretase inhibitors reduce beta-amyloid peptide levels in brain. Journal of neurochemistry. 2001; 76:173-81.

[193] Micchelli CA, Esler WP, Kimberly WT, Jack C, Berezovska O, Kornilova A, et al. γ-Secretase/presenilin inhibitors for Alzheimer's disease phenocopy Notch mutations in Drosophila. The FASEB Journal. 2003; 17:79-81.

[194] Geling A, Steiner H, Willem M, Bally-Cuif L, Haass C. A γ-secretase inhibitor blocks Notch signaling in vivo and causes a severe neurogenic phenotype in zebrafish. EMBO reports. 2002; 3:688-94.

[195] Doody RS, Raman R, Farlow M, Iwatsubo T, Vellas B, Joffe S, et al. A phase 3 trial of semagacestat for treatment of Alzheimer's disease. New England Journal of Medicine. 2013; 369:341-50.

[196] Coric V, Salloway S, van Dyck CH, Dubois B, Andreasen N, Brody M, et al. Targeting prodromal Alzheimer disease with avagacestat: a randomized clinical trial. JAMA neurology. 2015; 72:1324-33.

[197] Bursavich MG, Harrison BA, Blain J-Fo. Gamma secretase modulators: new Alzheimer's drugs on the horizon? Journal of medicinal chemistry. 2016; 59:7389-409.

[198] Dimitrov M, Alattia JR, Lemmin T, Lehal R, Fligier A, Houacine J, et al. Alzheimers disease mutations in APP but not 3-secretase modulators affect epsilon-cleavage-dependent AICD production. Nature Communications. 2013; 4.

[199] Lessard CB, Cottrell BA, Maruyama H, Suresh S, Golde TE, Koo EH. γ-secretase modulators and APH1 isoforms modulate γ-secretase cleavage but not position of ε-cleavage of the amyloid precursor protein (APP). PLoS ONE. 2015; 10:1-19.

[200] Lessard CB, Rodriguez E, Ladd TB, Minter LM, Osborne BA, Miele L, et al. γ-Secretase modulators exhibit selectivity for modulation of APP cleavage but inverse γ-secretase modulators do not. Alzheimer's research & therapy. 2020; 12:61.

[201] Ryman DC, Acosta-Baena N, Aisen PS, Bird T, Danek A, Fox NC, et al. Symptom onset in autosomal dominant Alzheimer disease: a systematic review and meta-analysis. Neurology. 2014; 83:253-60.

[202] Shen J, Bronson RT, Chen DF, Xia W, Selkoe DJ, Tonegawa S. Skeletal and CNS defects in Presenilin-1-deficient mice. Cell. 1997; 89:629-39.

[203] Wong PC, Zheng H, Chen H, Becher MW, Sirinathsinghji DJ, Trumbauer ME, et al. Presenilin 1 is required for Notch 1 and Dll1 expression in the paraxial mesoderm. Nature. 1997; 387:288-92.

[204] Herreman A, Hartmann D, Annaert W, Saftig P, Craessaerts K, Serneels L, et al. Presenilin 2 deficiency causes a mild pulmonary phenotype and no changes in amyloid precursor protein processing but enhances the embryonic lethal phenotype of presenilin 1 deficiency. Proceedings of the National Academy of Sciences. 1999; 96:11872-7.

[205] Serneels L, Dejaegere T, Craessaerts K, Horré K, Jorissen E, Tousseyn T, et al. Differential contribution of the three Aph1 genes to γ-secretase activity in vivo. Proceedings of the National Academy of Sciences. 2005; 102:1719-24.

[206] Lessard CB, Rodriguez E, Ladd TB, Minter LM, Osborne BA, Miele L, et al. Individual and combined presenilin 1 and 2 knockouts reveal that both have highly overlapping functions in HEK293T cells. J Biol Chem. 2019; 294:11276-85.

[207] Stanga S, Vrancx C, Tasiaux B, Marinangeli C, Karlström H, Kienlen-Campard P. Specificity of presenilin-1- and presenilin-2-dependent γ-secretases towards substrate processing. Journal of Cellular and Molecular Medicine. 2018; 22:823-33.

[208] Pimenova AA, Goate AM. Novel presenilin 1 and 2 double knock-out cell line for in vitro validation of PSEN1 and PSEN2 mutations. Neurobiol Dis. 2020; 138:104785.

[209] Meckler X, Checler F. Presenilin 1 and presenilin 2 target ??-secretase complexes to distinct cellular compartments. Journal of Biological Chemistry. 2016; 291:12821-37.

[210] Sannerud R, Esselens C, Ejsmont P, Mattera R, Rochin L, Tharkeshwar AK, et al. Restricted Location of PSEN2/γ-Secretase Determines Substrate Specificity and Generates an Intracellular Aβ Pool. Cell. 2016; 166:193-208.

[211] Holmes O, Paturi S, Ye W, Wolfe MS, Selkoe DJ. Effects of membrane lipids on the activity and processivity of purified γ-secretase. Biochemistry. 2012; 51:3565-75.

[212] Aguayo-Ortiz R, Straub JE, Dominguez L. Influence of membrane lipid composition on the structure and activity of γ-secretase. Physical Chemistry Chemical Physics. 2018; 20:27294-304.

[213] Winkler E, Kamp F, Scheuring J, Ebke A, Fukumori A, Steiner H. Generation of Alzheimer disease-associated amyloid β42/43 peptide by γ-secretase can be inhibited directly by modulation of membrane thickness. Journal of Biological Chemistry. 2012; 287:21326-34.

[214] Fukumori A, Okochi M, Tagami S, Jiang J, Itoh N, Nakayama T, et al. Presenilin-dependent γ-secretase on plasma membrane and endosomes is functionally distinct. Biochemistry. 2006; 45:4907-14.

[215] Fraering PC, Ye W, Strub JM, Dolios G, LaVoie MJ, Ostaszewski BL, et al. Purification and characterization of the human γ-secretase complex. Biochemistry. 2004; 43:9774-89.

[216] Yonemura Y, Futai E, Yagishita S, Suo S, Tomita T, Iwatsubo T, et al. Comparison of presenilin 1 and presenilin 2 γ-secretase activities using a yeast reconstitution system. Journal of Biological Chemistry. 2011; 286:44569-75.

[217] Welikovitch LA, Do Carmo S, Maglóczky Z, Szocsics P, Lőke J, Freund T, et al. Evidence of intraneuronal Aβ accumulation preceding tau pathology in the entorhinal cortex. Acta neuropathologica. 2018; 136:901-17.

[218] Daini E, Secco V, Liao W, Zoli M, Vilella A. A regional and cellular analysis of the early intracellular and extracellular accumulation of Aβ in the brain of 5XFAD mice. Neuroscience Letters. 2021; 754:135869.

[219] Somavarapu AK, Kepp KP. Membrane Dynamics of γ-Secretase Provides a Molecular Basis for β-Amyloid Binding and Processing. ACS Chemical Neuroscience. 2017; 8:2424-36.

[220] Hitzenberger M, Zacharias M. γ-secretase studied by atomistic molecular dynamics simulations: Global dynamics, enzyme activation, water distribution and lipid binding. Frontiers in Chemistry. 2019; 7.

[221] Cai T, Tomita T. Structure-activity relationship of presenilin in γ-secretase-mediated intramembrane cleavage. Seminars in Cell and Developmental Biology. 2020:0-1.

[222] Dehury B, Tang N, Blundell TL, Kepp KP. Structure and dynamics of γ-secretase with presenilin 2 compared to presenilin 1. RSC Advances. 2019; 9:20901-16.

[223] Dehury B, Tang N, Kepp KP. Insights into membrane-bound presenilin 2 from all-atom molecular dynamics simulations. J Biomol Struct Dyn. 2020; 38:3196-210.

[224] Lai MT, Chen E, Crouthamel MC, DiMuzio-Mower J, Xu M, Huang Q, et al. Presenilin-1 and presenilin-2 exhibit distinct yet overlapping γ-secretase activities. Journal of Biological Chemistry. 2003; 278:22475-81.

[225] Bentahir M, Nyabi O, Verhamme J, Tolia A, Horré K, Wiltfang J, et al. Presenilin clinical mutations can affect γ-secretase activity by different mechanisms. Journal of neurochemistry. 2006; 96:732-42.

[226] Strömberg K, Hansson EM, Laudon H, Bergstedt S, Näslund J, Lundkvist J, et al. γ-secretase complexes containing N- and C-terminal fragments of different presenilin origin retain normal γ-secretase activity. Journal of Neurochemistry. 2005; 95:880-90.

[227] Shirotani K, Tomioka M, Kremmer E, Haass C, Steiner H. Pathological activity of familial Alzheimer's disease-associated mutant presenilin can be executed by six different γ-secretase complexes. Neurobiology of disease. 2007; 27:102-7.

[228] Saura CA, Tomita T, Davenport F, Harris CL, Iwatsubo T, Thinakaran G. Evidence that intramolecular associations between presenilin domains are obligatory for endoproteolytic processing. J Biol Chem. 1999; 274:13818-23.

[229] PSN2_Human| UniProt. (n.d.). Retrieved March 21, 2022 from https://www.uniprot.org/uniprot/P49810

[230] PSN1_Human| UniProt. (n.d.). Retrieved March 21, 2022 from https://www.uniprot.org/uniprot/P49768

[231] Zhao B, Yu M, Neitzel M, Marugg J, Jagodzinski J, Lee M, et al. Identification of γ-Secretase Inhibitor Potency Determinants on Presenilin. Journal of Biological Chemistry. 2008; 283:2927-38.

[232] Lee J, Song L, Terracina G, Bara T, Josien H, Asberom T, et al. Identification of presenilin 1-selective γ-secretase inhibitors with reconstituted γ-secretase complexes. Biochemistry. 2011; 50:4973-80.

[233] Steiner H, Winkler E, Edbauer D, Prokop S, Basset G, Yamasaki A, et al. PEN-2 is an integral component of the γ-secretase complex required for coordinated expression of presenilin and nicastrin. Journal of Biological Chemistry. 2002; 277:39062-5.

[234] Gibson DG, Young L, Chuang R-Y, Venter JC, Hutchison CA, Smith HO. Enzymatic assembly of DNA molecules up to several hundred kilobases. Nature Methods. 2009; 6:343-5.

[235] Wang W, Malcolm BA. Two-stage PCR protocol allowing introduction of multiple mutations, deletions and insertions using QuikChangeTM site-directed mutagenesis. Biotechniques. 1999; 26:680-2.

[236] Chung CT, Niemela SL, Miller RH. One-step preparation of competent Escherichia coli: transformation and storage of bacterial cells in the same solution. Proc Natl Acad Sci U S A. 1989; 86:2172-5.

[237] Tagami S, Yanagida K, Kodama TS, Takami M, Mizuta N, Oyama H, et al. Semagacestat Is a Pseudo-Inhibitor of γ-Secretase. Cell Reports. 2017; 21:259-73.

[238] Bradford MM. A rapid and sensitive method for the quantitation of microgram quantities of protein utilizing the principle of protein-dye binding. Analytical biochemistry. 1976; 72:248-54.

[239] Schägger H, von Jagow G. Tricine-sodium dodecyl sulfate-polyacrylamide gel electrophoresis for the separation of proteins in the range from 1 to 100 kDa. Analytical Biochemistry. 1987; 166:368-79.

[240] Wiltfang J, Arold N, Neuhoff V. A new multiphasic buffer system for sodium dodecyl sulfate-polyacrylamide gel electrophoresis of proteins and peptides with molecular masses 100 000–1000, and their detection with picomolar sensitivity. ELECTROPHORESIS. 1991; 12:352-66.

[241] Towbin H, Staehelin T, Gordon J. Electrophoretic transfer of proteins from polyacrylamide gels to nitrocellulose sheets: procedure and some applications. Proceedings of the National Academy of Sciences. 1979; 76:4350-4.

[242] Trambauer J, Rodríguez Sarmiento RM, Fukumori A, Feederle R, Baumann K, Steiner H. Aβ43-producing PS1 FAD mutants cause altered substrate interactions and respond to γ-secretase modulation. EMBO reports. 2020; 21:e47996.

[243] Kretner B, Trambauer J, Fukumori A, Mielke J, Kuhn PH, Kremmer E, et al. Generation and deposition of Aβ43 by the virtually inactive presenilin-1 L435F mutant contradicts the presenilin loss-of-function hypothesis of Alzheimer's disease. EMBO molecular medicine. 2016; 8:458-65.

[244] Capell A, Saffrich R, Olivo JC, Meyn L, Walter J, Grünberg J, et al. Cellular expression and proteolytic processing of presenilin proteins is developmentally regulated during neuronal differentiation. Journal of neurochemistry. 1997; 69:2432-40.

[245] Citron M, Oltersdorf T, Haass C, McConlogue L, Hung AY, Seubert P, et al. Mutation of the β-amyloid precursor protein in familial Alzheimer's disease increases β-protein production. Nature. 1992; 360:672-4.

[246] Jacobsen H, Reinhardt D, Brockhaus M, Bur D, Kocyba C, Kurt H, et al. The influence of endoproteolytic processing of familial Alzheimer's disease presenilin 2 on Aβ42 amyloid peptide formation. Journal of Biological Chemistry. 1999; 274:35233-9.

[247] Fukumori A, Fluhrer R, Steiner H, Haass C. Three-Amino Acid Spacing of Presenilin Endoproteolysis Suggests a General Stepwise Cleavage of γ-Secretase-Mediated Intramembrane Proteolysis. Journal of Neuroscience. 2010; 30:7853-62.

[248] Klafki HW, Wiltfang J, Staufenbiel M. Electrophoretic separation of βA4 peptides (1-40) and (1-42). Analytical biochemistry. 1996; 237:24-9.

[249] Aguayo-Ortiz R, Dominguez L. Simulating the γ-secretase enzyme: Recent advances and future directions. Biochimie. 2018; 147:130-5.

[250] Dilger J, Fisher L, Haydon D. A critical comparison of electrical and optical methods for bilayer thickness determination. Chemistry and Physics of Lipids. 1982; 30:159-76.

[251] Lew S, Ren J, London E. The effects of polar and/or ionizable residues in the core and flanking regions of hydrophobic helices on transmembrane conformation and oligomerization. Biochemistry. 2000; 39:9632-40.

[252] Adamian L, Liang J. Helix-helix packing and interfacial pairwise interactions of residues in membrane proteins1. Journal of Molecular Biology. 2001; 311:891-907.

[253] White SH, Wimley WC. Membrane protein folding and stability: physical principles. Annual review of biophysics and biomolecular structure. 1999; 28:319-65.

[254] Tedde A, Bartoli A, Piaceri I, Ferrara S, Bagnoli S, Serio A, et al. Novel presenilin 1 mutation (Ile408Thr) in an Italian family with late-onset Alzheimer's disease. Neuroscience letters. 2016; 610:150-3.

[255] Roher AE, Lowenson JD, Clarke S, Woods AS, Cotter RJ, Gowing E, et al. beta-Amyloid-(1-42) is a major component of cerebrovascular amyloid deposits: implications for the pathology of Alzheimer disease. Proceedings of the National Academy of Sciences. 1993; 90:10836-40.

[256] Arber C, Villegas-Llerena C, Toombs J, Pocock JM, Ryan NS, Fox NC, et al. Amyloid precursor protein processing in human neurons with an allelic series of the PSEN1 intron 4 deletion mutation and total presenilin-1 knockout. Brain Communications. 2019; 1:1-10.

[257] Mori K, Okochi M, Tagami S, Nakayama T, Yanagida K, Kodama TS, et al. The production ratios of AICDε51 and Aβ42 by intramembrane proteolysis of βAPP do not always change in parallel. Psychogeriatrics. 2010; 10:117-23.

[258] Cai T, Tomita T. Sequential conformational changes in transmembrane domains of presenilin 1 in Aβ42 downregulation. The Journal of Biochemistry. 2021; 0:1-13.

[259] Moehlmann T, Winkler E, Xia X, Edbauer D, Murrell J, Capell A, et al. Presenilin-1 mutations of leucine 166 equally affect the generation of the Notch and APP intracellular domains independent of their effect on Aβ42 production. Proceedings of the National Academy of Sciences. 2002; 99:8025-30.

[260] Högel P, Götz A, Kuhne F, Ebert M, Stelzer W, Rand KD, et al. Glycine perturbs local and global conformational flexibility of a transmembrane helix. Biochemistry. 2018; 57:1326-37.

[261] Dong H, Sharma M, Zhou H-X, Cross TA. Glycines: role in α-helical membrane protein structures and a potential indicator of native conformation. Biochemistry. 2012; 51:4779-89.

[262] Morley JE, Farr SA, Nguyen AD, Xu F. What is the Physiological Function of Amyloid-Beta Protein? Journal of Nutrition, Health and Aging. 2019; 23:225-6.

[263] Esbjörner EK, Chan F, Rees E, Erdelyi M, Luheshi LM, Bertoncini CW, et al. Direct observations of amyloid β Self-assembly in live cells provide insights into differences in the kinetics of Aβ(1-40) and Aβ(1-42) aggregation. Chemistry and Biology. 2014; 21:732-42.

[264] Hu X, Crick SL, Bu G, Frieden C, Pappu RV, Lee JM. Amyloid seeds formed by cellular uptake, concentration, and aggregation of the amyloid-beta peptide. Proceedings of the National Academy of Sciences of the United States of America. 2009; 106:20324-9.

[265] Kamp F, Winkler E, Trambauer J, Ebke A, Fluhrer R, Steiner H. Intramembrane proteolysis of β-amyloid precursor protein by γ-secretase is an unusually slow process. Biophysical Journal. 2015; 108:1229-37.

[266] Chávez-Gutiérrez L, Bammens L, Benilova I, Vandersteen A, Benurwar M, Borgers M, et al. The mechanism of γ-secretase dysfunction in familial Alzheimer disease. The EMBO journal. 2012; 31:2261-74.

# 7 List of Figures

# 8 List of Tables

# 9 List of Abbreviations

| | |
|---|---|
| * | Statistically significant (unpaired Student's T-test); $p < 0.05$ |
| ** | Statistically significant (unpaired Student's T-test); $p < 0.01$ |
| *** | Statistically significant (unpaired Student's T-test); $p < 0.001$ |
| aa | Amino acids |
| AD | Alzheimer's Disease |
| ADAM | A Disintegrin And Metalloproteinase |
| AICD | APP intracellular domain |
| APH-1 | Anterior Pharynx-defective phenotype 1 |
| ApoE | Apolipoprotein E |
| APP | Amyloid precursor protein |
| APPsw | APP with the "Swedish" mutation K670N/M671NL |
| APS | Ammonium persulfate |
| Aβ | Amyloid-β |
| $Aβ_{11-x}$ | Truncated Aβ peptide after BACE-1 cleavage at the β'-site |
| BACE-1 | β-site APP cleaving enzyme-1 |
| bp | Base pairs |
| Bpa | p-Benzoyl-L-phenylalanine |
| C100/C100-His6 | Recombinant APP-C100-His6 based on C99 with a N-terminal Met |
| C83 | C-terminal fragment of APP generated by α-secretase (see also CTFα) |
| C99 | C-terminal fragment of APP generated by BACE-1 (see also CTFβ) |
| CHAPSO | 3-([3-Cholamidopropyl]dimethylammonio)-2-hydroxy-1-propanesulfonate |
| CHCA | α-Cyano-4-hydroxycinnamic acid |
| cps | Counts per second |
| cryo-EM | Cryo-electron microscopy |
| CTF | Carboxy-terminal fragment |
| CTFα | C-terminal fragment of APP generated by α-secretase |
| CTFβ | C-terminal fragment of APP generated by BACE-1 |
| $dH_2O$ | Deionized water |
| dKO | Double knock-out |
| DMEM | Dulbecco's Modified Eagle Medium |
| DMSO | Dimethyl sulfoxide |
| DNA | Deoxyribonucleic acid |
| dNTP | Deoxyribose nucleoside triphosphate |
| DZNE | German Center for Neurodegenerative Diseases |
| *E. coli* | *Escherichia coli* |
| ECL | Enhanced chemiluminescence |

| | |
|---|---|
| EDTA | Ethylenediaminetetraacetic acid |
| ELISA | Enzyme-linked Immunosorbent Assay |
| ER | Endoplasmic reticulum |
| FAD | Inherited form of AD (Familial Alzheimer's Disease) |
| FCS | Fetal calf serum |
| G418 | Geneticin |
| GA | Gibson assembly |
| GSI/GSIs | γ-Secretase inhibitor(s) |
| GSM/GSMs | γ-Secretase modulator(s) |
| $H_6X$ | Hexahistidine-Xpress epitope-tag |
| HEK293 | Human embryonic kidney 293 cells |
| HEK293/sw | HEK293 cells stably expressing APPsw |
| HEK293/sw PS1/2$^{-/-}$ dKO | HEK293/sw cells with homozygous KO of endogenous PS1 and PS2 |
| HRP | Horseradish peroxidase |
| ICD/ICDs | Intracellular domain(s) |
| iGSM | Inverse GSM |
| IP | Immunoprecipitation |
| IP-MS | Combined immunoprecipitation and mass spectrometry |
| iPSCs | Induced pluripotent stem cells |
| $k_{cat}$ | Catalytic constant |
| $K_m$ | Michaelis constant |
| KO | Knock-out |
| LB | Lysogeny broth |
| LE | Late endosome |
| LYS | Lysosome |
| m/z | Mass-to-charge ratio |
| MALDI-TOF | Matrix-assisted laser desorption/ionization - time of flight |
| MD | Molecular dynamics |
| MEF | Mouse embryonic fibroblast |
| MS | Mass spectrometry |
| n | Sample size |
| n.h. | Non homologous |
| n.s. | Not significant |
| NCT | Nicastrin |
| $NCT_{im}$ | Immature form of NCT |
| $NCT_m$ | Maturated form of NCT |
| NP-40 | Nonidet P40 |
| NTF | Amino-terminal fragment |
| $OD_x$ | Optical density at λ = x nm |

| | |
|---|---|
| p | Two-tailed probability value (unpaired Student's t-test) |
| PAGE | Polyacrylamide gel electrophoresis |
| PAS | Protein A Sepharose |
| PBS | Phosphate-buffered saline |
| PCR | Polymerase chain reaction |
| PDB | Protein database catalogue number |
| PEG 3000 | Polyethylene glycol, 3000 g/mol |
| Pen/Strep | Penicillin/Streptomycin mix |
| PEN-2 | Presenilin enhancer 2 |
| PGS | Protein G Sepharose |
| Pi | Protease inhibitor cocktail |
| PS | Presenilin |
| PS1 | Presenilin 1 |
| PS1/2 | PS variant containing the NTF of PS1 combined with the PS2 CTF |
| PS2 | Presenilin 2 |
| PS2/1 | PS variant containing the NTF of PS2 combined with the PS1 CTF |
| PS2-All-PS1TMDs | PS2 variant with substitutions of all membrane spanning regions by the one of PS1 |
| PS2-CTF-PS1TMDs | PS2 variant with substitutions membrane spanning regions in the CTF by the one of PS1 |
| PS2-NTF-PS1TMDs | PS2 variant with substitutions membrane spanning regions in the NTF by the one of PS1 |
| PS2ρTM | PS2 variant with substitution of the indicated TMDs by the ones of PS1 |
| PVDF | Polyvinylidene fluoride |
| QC | QuikChange mutagenesis |
| RBC | restriction based cloning |
| rpm | Revolutions per minute |
| sAPP | Secreted N-terminal APP fragment |
| sAPPα | sAPP generated by α-secretase |
| sAPPβ | sAPP generated by BACE-1 |
| SDS | Sodium dodecyl sulfate |
| TAE | Tris-acetate/EDTA |
| TBS | Tris-buffered saline |
| TBS-T | TBS containing polysorbate 20 "Tween" |
| TEMED | Tetramethylethylenediamine |
| temp. | Temperature |
| TFA | Trifluoroacetic acid |
| TLN | Telencephalin |
| TMD/TMDs | transmembrane domain(s) |

| | |
|---|---|
| Tris | Tris(hydroxymethyl)aminomethane |
| TSS | Transformation and storage solution |
| TUM | Technical University of Munich |
| U | *Units*, 1 µmol/min substrate turnover |
| UV | Ultraviolet |
| v/v | Volume per volume |
| w/v | Weight per volume |
| WF | Wiltfang |
| xg | Times gravity |
| Zeo | Zeocin |
| λ | Wavelength |

# Publications

Schanzenbach C, **Schmidt FC**, Breckner P, Teese MG, Langosch D. Identifying ionic interactions within a membrane using BLaTM, a genetic tool to measure homo- and heterotypic transmembrane helix-helix interactions. *Scientific Reports.* 7, 43476; (2017).

**Schmidt FC**, Steiner H, Langosch D. Making Swaps Until Activity Drops - Localizing the Different Specific Activity of Presenilin Homologues to Protein Domains. *Biophysical Journal.* 116(3), 425a; (2019).